2019

Analyzing and exploiting biomass thermal deconstruction

Jake Kendall Lindstrom
Iowa State University

Analyzing and exploiting biomass thermal deconstruction

by

Jake Kendall Lindstrom

A dissertation submitted to the graduate faculty

in partial fulfillment of the requirements for the degree of

DOCTOR OF PHILOSOPHY

Major: Mechanical Engineering

Program of Study Committee:
Robert C. Brown, Major Professor
Theodore Heindel
Wenzhen Li
Mark Mba Wright
Brent Shanks

The student author and the program of study committee are solely responsible for the content of this dissertation. The Graduate College will ensure this dissertation is globally accessible and will not permit alterations after a degree is conferred.

Iowa State University
Ames, Iowa
2019

DEDICATION

For Laura Norman, my steadfast partner.

TABLE OF CONTENTS

ACKNOWLEDGMENTS

I have found that mentorship leads to growth more than individual tasks or projects as long as the mentee is somewhat malleable and puts effort into learning. With that in mind, I am particularly grateful to Dr. Robert Brown for accepting me into his group and guiding me throughout graduate school. Furthermore, I am thankful for my committee members—Drs. Theodore Heindel, Wenzhen Li, Mark Mba Wright, and Brent Shanks—whose critique and guidance undoubtedly strengthened this work. I would also like to thank everyone who is a part of the Bioeconomy Institute at Iowa State University, particularly Ryan Smith and Patrick Johnston. Outside of Iowa State University, I appreciate the guidance I have received from exceptional scientists and, for some, their confidence in me that has led to multiple successful collaborations. Each mentor listed here sculpted me into a better researcher and engineer.

I want to express my appreciation and gratitude to ExxonMobil (specifically Ross Mabon), the National Science Foundation, and the Gary & Donna Hoover Endowment. Without their support this work could not have come to fruition.

If you are reading this section and are disappointed you were not included, this is your paragraph. I could not list everyone worthy of acknowledgements, so to avoid failing to mention someone here is a generalized list: my family, friends, running partners, teachers, professors from Grinnell College and Iowa State University, and Laura Norman's and my cat—Oliver.[1]

Lastly, thank you, Laura Norman.

[1] If you see any typos in this dissertation, blame his paws.

ABSTRACT

The study of biomass thermal deconstruction most often focuses on its final products while neglecting the non-volatile condensed phase intermediate species. Furthermore, given the often short reaction durations, time-resolution is also rarely achieved. This dissertation aims to correct these two omissions by developing and utilizing multiple methods of truncated thermal deconstruction of biomass or its constituent biopolymers (namely cellulose). The results demonstrate that final product yields result from the myriad of reactions occurring primarily within the condensed phase intermediate species. Analyzing this overlooked aspect of thermal deconstruction will assist others when building more accurate predictive models. Additionally, once better understood, these reactions can be exploited to produce higher product yields of desired chemicals.

PREFACE

As I started my graduate research, I was tasked with determining if sugar yields from cellulose fast pyrolysis could be increased. Scouring the literature, I could not find any experimental works that suggested feasible methods of improving sugar yields. Furthermore, I could not manipulate published pyrolysis models so they would predict substantially higher sugar yields. I wondered whether this result represented reality or was merely a byproduct of the modeling. I continued thinking along these lines, eventually landing on the one question that would define my entire dissertation, "how do we know what we know?"

I did not ask myself repeatedly, "what do we know?" At that point I had a reasonably firm understanding of the literature, although I was always working to expand it. Instead, I studied the experiments that led to important conclusions within the field. Almost all of the results were produced by examining the starting feedstock and final products. I saw an opening. I resolved to examine the intermediate products directly, instead of deducing what had occurred based on product yields. Immediately after this decision, I realized why others before me had not done it.

Attempting to scrutinize rapidly decomposing non-volatile material at hundreds of degrees Celsius seemed quixotic at best. I realized that analyzing these transient products as they were decomposing posed far too many chemical instrumentation challenges. I took another course, deciding that capturing intermediate products for subsequent analysis would be more feasible. My logic was simple; thermochemical processing requires high temperatures, so after my desired reaction time I can lower the reaction

temperature to stop the reactions prematurely. This principle worked better than I dared hope, and it became my methodology for all of the research in my dissertation.

In this dissertation, chapter one represents my attempt to delineate the cutting edge of thermochemical research. It is reprinted from the second edition of *Thermochemical Processing of Biomass: Conversion into Fuels, Chemicals and Power* where it serves as the theoretical underpinnings for other chapters in the book prepared by other authors with expertise in various topics in thermochemical processing.

Chapter two, published originally in the journal *Green Chemistry*, and chapter three, to be submitted for publication, focus on understanding the condensed phase reactions occurring during cellulose thermal deconstruction. Chapter four, also in preparation for publication in a scientific journal, uses similar techniques to chapter three to assess the early stages of thermal deconstruction of biomass. Chapter five, prepared as a perspective on the field of thermal deconstruction of lignocellulosic biomass, details the oversights that drove me to focus on the question, "how do we know what we know?" Lastly, chapter six summarizes what I have found and gives suggestions for future research.

CHAPTER 1 CONDENSED PHASE REACTIONS DURING THERMAL DECONSTRUCTION OF BIOMASS

Jake K. Lindstrom,[a] Alexander Shaw,[b] Xiaolei Zhang,[b] and Robert C. Brown[a,c]

a- Department of Mechanical Engineering, Iowa State University, Ames, IA, USA

b- School of Mechanical and Aerospace Engineering, Queen's University Belfast, Belfast, BT9 5AH, UK

c- Bioeconomy Institute, Iowa State University, Ames, IA, USA

Chapter and cover reprinted from the 2nd edition of "Thermochemical Processing of Biomass: Conversion into Fuels, Chemicals and Power" *with permission from John Wiley & Sons, Inc.*

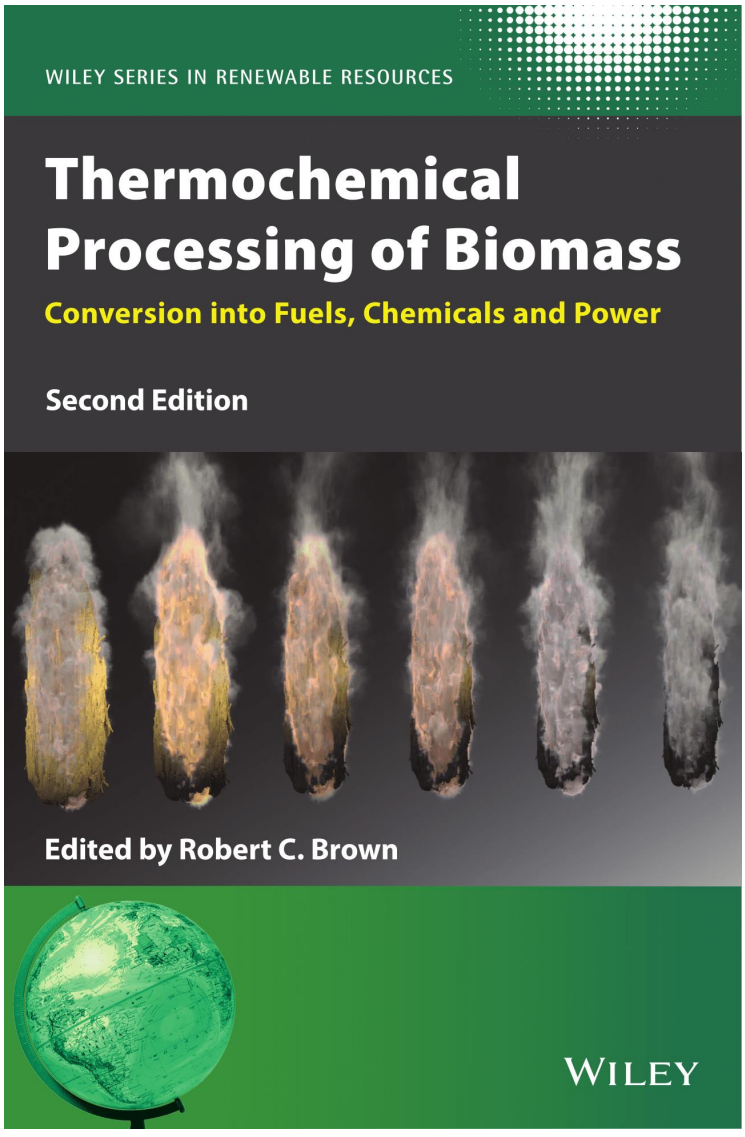

Introduction to Condensed Phase Reactions during Thermal Deconstruction of Biomass

All biomass thermochemical processes begin with depolymerization and decomposition reactions within a solid substrate that release volatile products and typically leave behind carbonaceous solid products. Despite their universal importance, condensed phase (liquid and solid) reactions during thermal deconstruction have received relatively little attention due to the difficulty in directly analyzing these reactions. While external conditions vary widely among thermochemical processes, reactions within the condensed phase are largely similar. Understanding condensed phase reactions can provide insight into the wide range of thermochemical processes.

Six thermochemical processes are discussed in this chapter: torrefaction, slow pyrolysis, solvent liquefaction, fast pyrolysis, gasification, and combustion. With the exception of solvent liquefaction, the operating temperature range is distinct for each process, as shown in Figure 1.1, although these limits can be flexible.

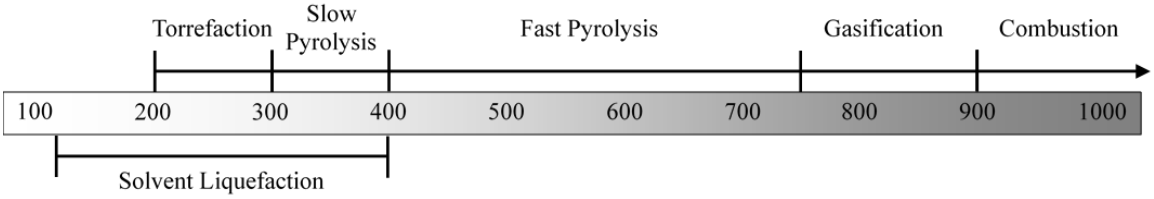

Figure 1.1. Approximate operating temperatures for torrefaction,[1] slow pyrolysis,[2] solvent liquefaction,[3] fast pyrolysis,[2] gasification,[2] and combustion range from 105 °C to greater than 1000 °C. Temperatures shown in Celsius.

Figure 1.2 shows typical yields of solid, liquid, and gas for these thermochemical processes. (Solvent liquefaction is excluded because yields are widely variable depending

upon operating conditions). The trend is clear: higher temperatures favor gaseous products over solid products.

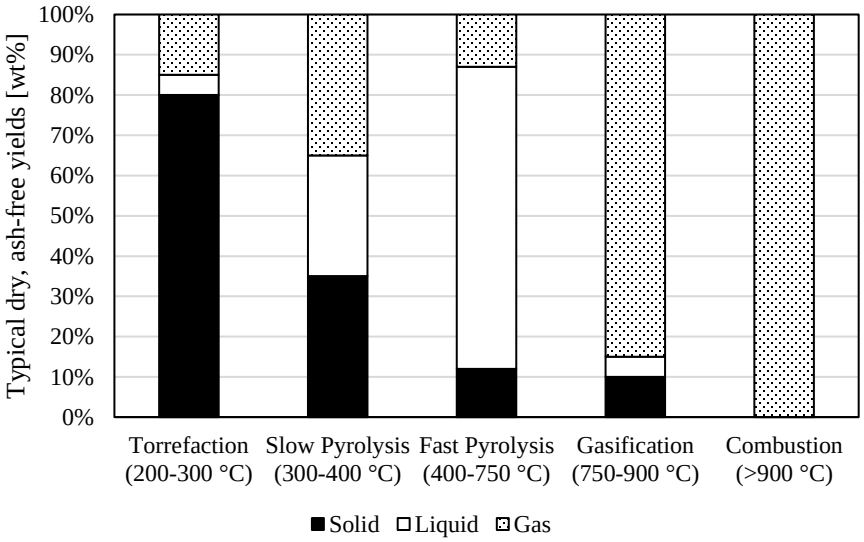

Figure 1.2. As temperature increases, the yield of gas increases and that of carbonaceous solid decreases for a wide range of thermochemical processes. Source: figure produced using data from Bridgwater.[2]

Understanding thermal deconstruction of biomass requires familiarity with biomass composition. Lignocellulosic biomass, the common feedstock for thermochemical processes, typically contains 50-60 wt% structural carbohydrates—namely cellulose and hemicellulose—and 15-40 wt% lignin, with the remaining mass composed of extractives, proteins, ash, etc.[4] This composition can vary significantly among different plant varieties, parts (e.g. stalk versus leaves), and cell wall layers (e.g. primary versus secondary cell wall). Regardless of composition, these components intertwine to form a complex composite structure (Figure 1.3).[5–7]

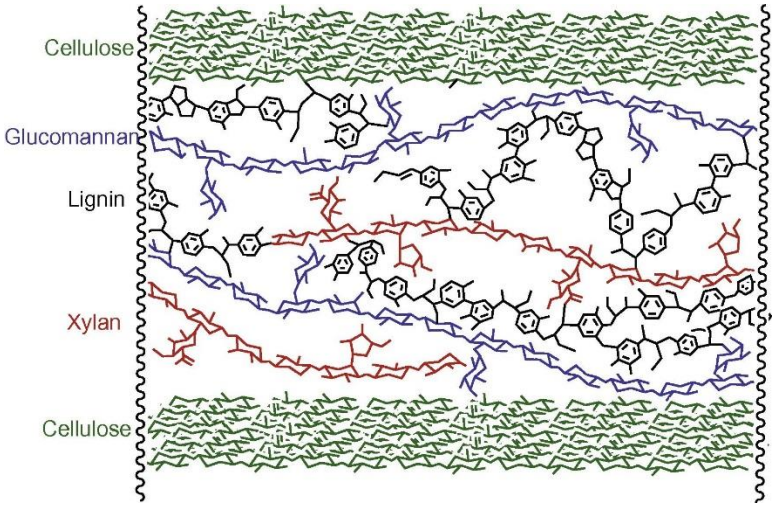

Figure 1.3. This depiction of cellulose, hemicellulose (glucomannan, xylan), and lignin shows some of the difficulty of using an extracted version of the polymer as a model compound. All the components in biomass are interconnected to form a complicated three dimensional structure. Source: figure reproduced from Reference 7, with permission from Elsevier.

This intricate structure complicates chemical and kinetic analysis. As a result, thermal deconstruction of the three main biopolymers is often studied individually. Isolated versions of these polymers and smaller model compounds, such as monomers and dimers, are commonly used despite marked differences from their native forms. There is value in this approach, but correctly applying the results to lignocellulosic biomass can be challenging. For example, thermochemical conversion analysis usually accounts for biomass varieties and, to some extent, plant components, but plant cellular structure is mostly neglected. See Harris and Stone[5] for a comprehensive review of plant cell wall structure and chemistry.

Cellular microstructure plays an underappreciated role in thermochemical processes. Plants evolved to resist physical, chemical, and biological attack making them recalcitrant to deconstruction. Cell structure and arrangement also affect thermal deconstruction. In particular, heat and mass transfer within biomass particles affects product yields. *The Role of Cell Wall Structure in Thermal Deconstruction* examines these effects in more detail.

Accounting for the effects of cellular structure may improve the understanding of thermal deconstruction, but its importance may depend upon scale. For example, random error at the macroscale may overwhelm minute—but real—differences at the micro or nano domains. This error propagation indicates that efforts to model deconstruction at multiple scales are inherently imprecise. Their primary usefulness is providing a qualitative understanding of the overall process.

This chapter explores condensed phase reactions important to thermal deconstruction, first by noting common physical and chemical transformations among different thermochemical processes. This chapter attempts to unify a wide spectrum of thermochemical processes in terms of the fundament thermal deconstruction mechanisms that occur in the condensed phase of biomass.

Thermochemical Processes

Thermal deconstruction of biomass is integral to several kinds of processes for which heat is the driving force of physical and chemical transformations. Many of the most important transformations occur in the condensed phase—with solid biomass depolymerizing and decomposing into liquids, vapors, gases, and solid residue—although secondary reactions of vaporized species can also be important in determining the ultimate yields of products. Despite similarities, thermochemical processes can be categorized according to whether the principle product is gases (combustion and gasification), liquids (pyrolysis and solvent liquefaction), or solids (torrefaction and slow pyrolysis), although they all produce smaller amounts of the other products as well.

Processes Yielding Chiefly Solids

Torrefaction and slow pyrolysis are characterized as producing solids as the principle products, specifically torrefied biomass and charcoal. These carbonaceous solids have applications as solid fuels. Charcoal has also been used as a soil amendment, in which case it is referred to as biochar.

Torrefaction

Torrefaction is the low temperature (200 to 300 °C) partial decomposition of biomass in the absence of oxygen. See Tumuluru *et al.*[1] for an extensive review of biomass torrefaction. Its Latin root word *torrefacio* means *parch* but the transformation involves more than dehydration. Torrefaction converts biomass into a carbonaceous solid fuel, superficially resembling peat or charcoal but with important chemical differences. The resulting fuel, known as torrefied biomass, is typically used as a solid combustion fuel for heat or electricity generation.

Generating torrefied biomass involves slowly heating biomass, which drives out water and other volatile chemicals. These products primarily derive from hemicellulose, which completely decomposes during torrefaction. Lignin and cellulose degrade to a lesser extent because they are more stable than hemicellulose.[1] The reaction temperature most strongly dictates the extent of this degradation.[8]

The products of thermal deconstruction of hemicellulose account for most of the mass and energy loss during torrefaction including the reduction of a significant fraction of the hydrogen and oxygen present in the biomass. Partially removing these elements increases the higher heating value (HHV) of torrefied biomass (Figure 1.4) by transforming it into a more carbonaceous solid fuel (Figure 1.5).

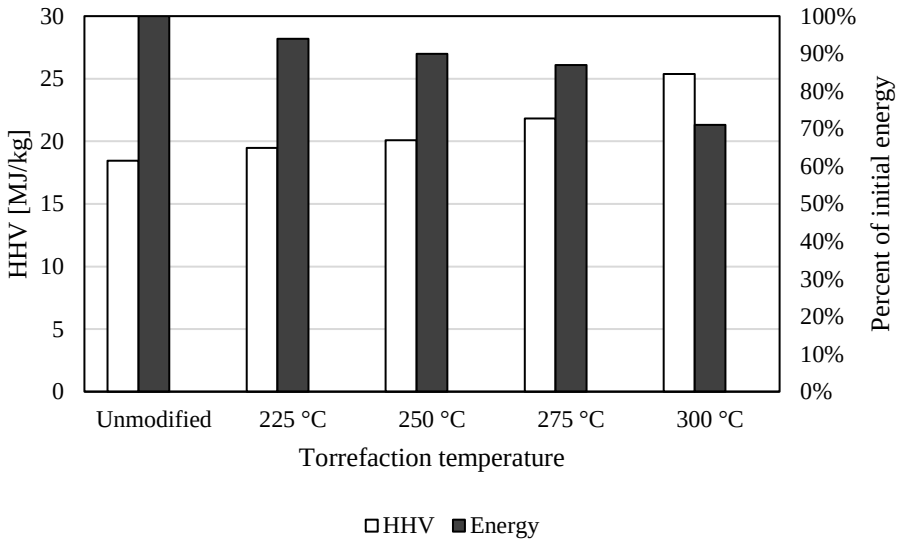

Figure 1.4. The higher heating value (HHV) of torrefied biomass (pine) increases with torrefaction temperature. Source: figure produced using data from Phanphanich and Mani.[9]

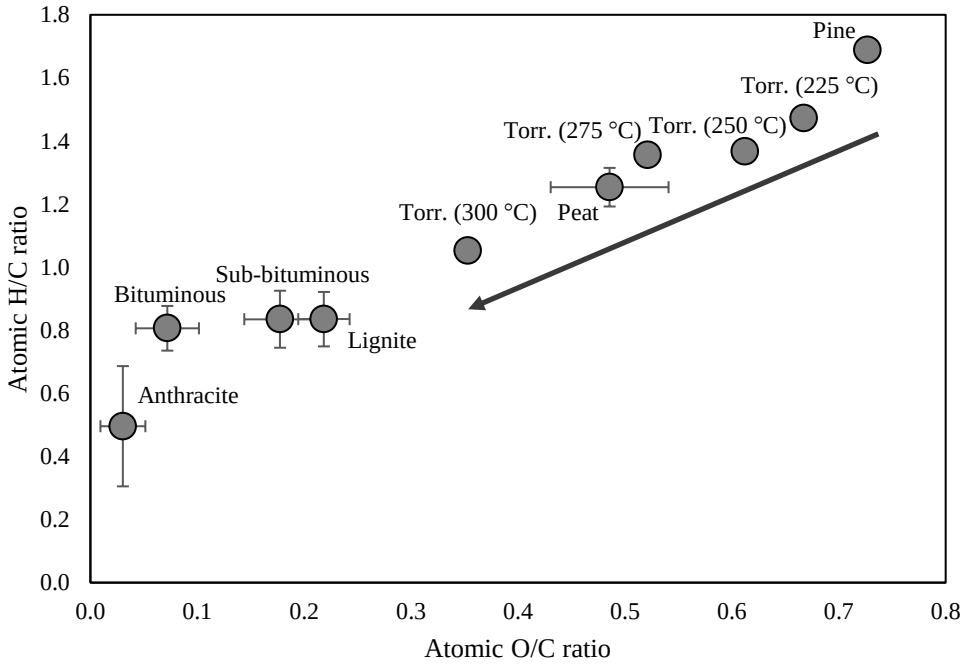

Figure 1.5. As torrefaction temperature increases, lignocellulosic biomass becomes more carbonaceous and similar to peat and coal, as illustrated in this van Krevelen diagram of pine torrefaction.[9] Peat averages and standard deviations were determined from 21 samples in the Phyllis2 database maintained by the Energy Research Centre of the Netherlands.[10] Coal averages and standard deviations were computed after classifying 6573 coal samples from the U.S. Geological Survey COALQUAL[11] database according to ASTM D388-18.[12]

Torrefaction represents relatively limited thermal deconstruction compared to other thermochemical processes as only hemicellulose completely decomposes. Cellulose and lignin decompose to a very limited extent compared to higher temperature processes.

Slow pyrolysis

Slow pyrolysis is the low temperature (300 to 400 °C) thermal deconstruction of biomass under oxygen-starved conditions over the course of hours or even days to form biochar and relatively low molecular weight vapors and non-condensable gases. Derived from the Greek roots *pyro* and *lysis* meaning *fire* and *splitting* respectively, pyrolysis involves all components of the plant cell wall. Slow pyrolysis differs from fast pyrolysis only in heating rate and final reaction temperature although sometimes research on slow pyrolysis is conducted at higher temperatures. The principle product of slow pyrolysis is a solid carbonaceous residue that is commonly called charcoal or biochar.

Humans began producing charcoal from slow pyrolysis thousands of years ago.[13] Cave art is the most enduring and famous evidence of charcoal use, but it also found use as a soil amendment[14] as well as the main component in gunpowder,[15] among other uses. Nevertheless, historically and today, charcoal is primarily used as solid fuel.

Slow reaction rate favors high charcoal yields. The exact chemical mechanisms are not fully understood but low temperatures, gas ventilation rates, and solids residence times are known to increase char yield (Figure 1.6).[16,17]

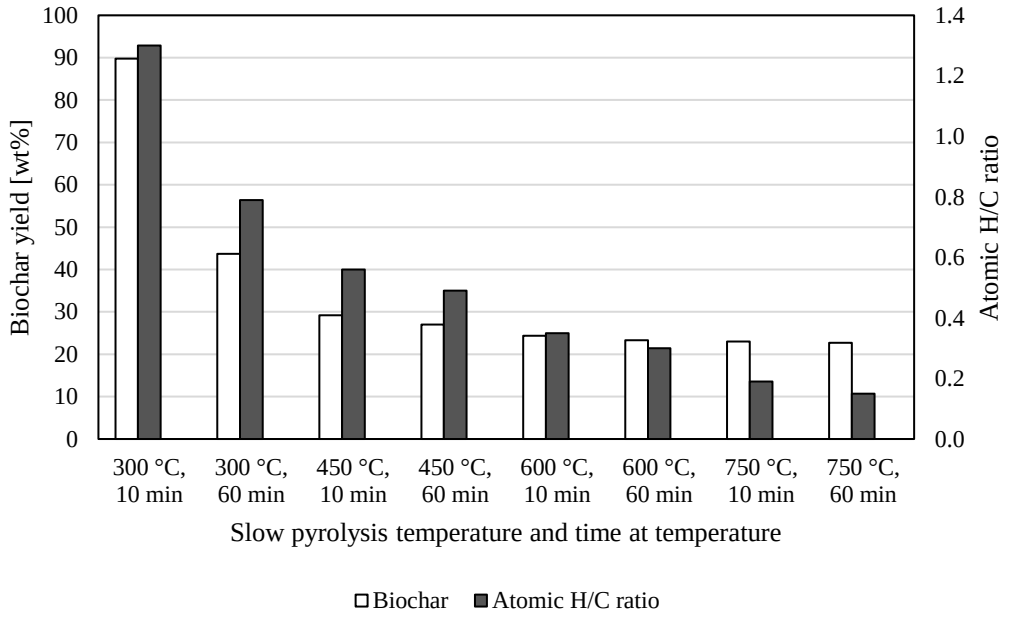

Figure 1.6. Yield and atomic hydrogen to carbon (H/C) ratio for biochar produced during slow pyrolysis both decrease with increasing temperature and reaction time. Source: figure produced using data from Ronsse *et al.*[16]

Heating rate obscures the relationship between temperature and reaction time (Figure 1.7).[18] Two otherwise identical biomass samples heated at different rates to the same final temperature have distinct product yields as a result of the very different spatial and temporal temperature profiles experienced by the samples.

Regardless of heating profile, cellulose and lignin are depolymerized along with hemicellulose during slow pyrolysis. Slow pyrolysis deconstructs biomass to a considerably greater extent than does torrefaction, with charcoal containing a higher carbon content than torrefied biomass and on par with some coals.

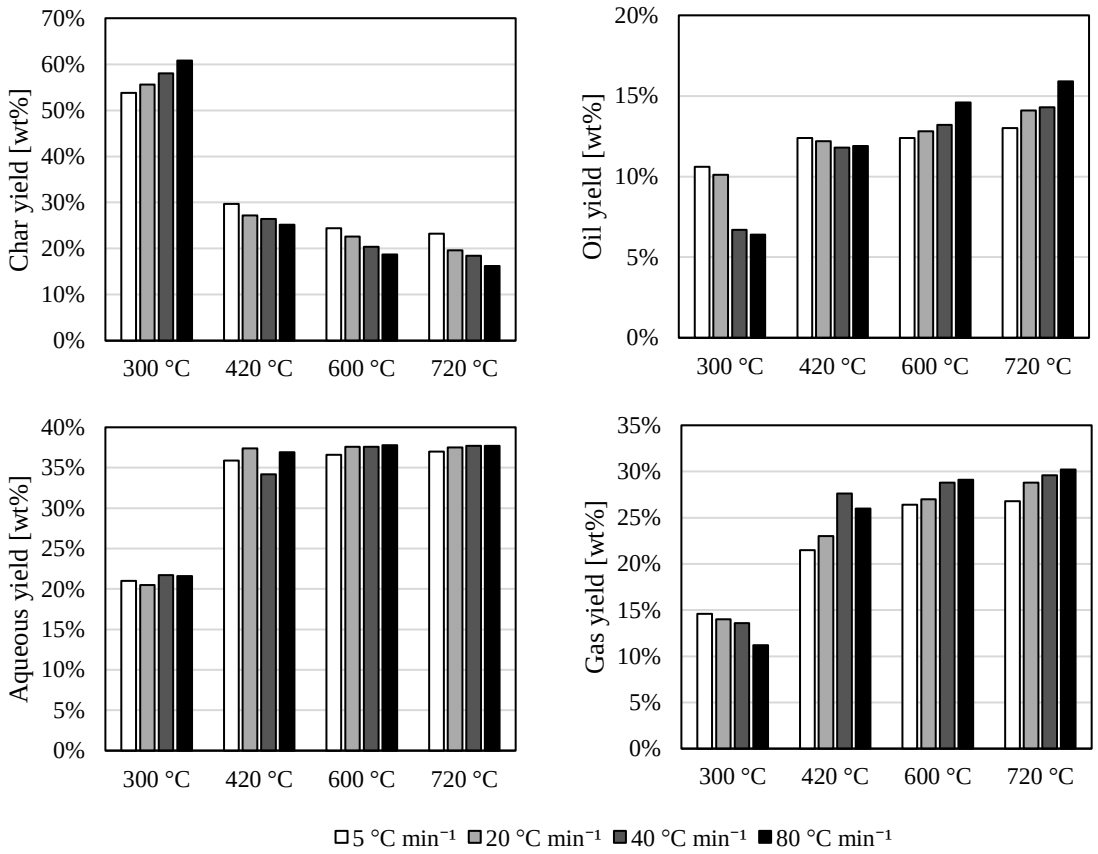

Figure 1.7. Heating rate alters product yields differently at low and high temperatures. Despite this incongruous variable, temperature predicts yields better than heating rate. Source: figure produced using data from Williams and Besler.[18]

Processes Yielding Chiefly Liquids

Processes that generate primarily liquid products—solvent liquefaction and fast pyrolysis—occupy a middle ground between lower temperatures promoting char formation and higher temperatures that promote cracking of vapors into permanent gases. Solvent liquefaction and fast pyrolysis both rapidly depolymerize and deconstruct biomass to yield primarily liquid products of similar chemical composition. The intent of solvent liquefaction is to dissolve or otherwise disperse liquid products into the solvent medium for subsequent recovery as liquid known as bio-oil or bio-crude. Fast pyrolysis

attempts to vaporize liquid products into an inert gas stream as quickly as they are formed, which are subsequently condensed to a liquid known as bio-oil or pyrolysis liquid.

Solvent liquefaction

Solvent liquefaction is the thermal deconstruction of biomass in a solvent at moderate temperatures (105 to 400 °C) and high pressure (2 to 20 MPa).[3] The process generates primarily solubilized products but also gases and solids. Solvent plays several roles including transporting heat to the biomass, dissolving select components of the biomass, dispersing products (preventing their condensation to larger molecules), and changing the thermodynamic environment in favor of certain chemical reactions.

In solvent liquefaction, water, organic solvents, or non-aqueous inorganic solvents (such as concentrated mineral acids) are used as the reaction medium. These solvents perturb the thermodynamic properties of reactants and reaction intermediates, profoundly influencing the final products of thermal deconstruction.[19] In contrast, the gaseous environment of other thermochemical processes only influence heat and mass transport among reactants and products.

Depending on the solvent, intermolecular forces between solvent and biomass affect kinetic parameters but do not necessarily change the reaction mechanism.[20,21] For example, Ghosh *et al.*[21] determined the apparent activation energies for cellulose depolymerization in γ-valerolactone, acetonitrile, and tetrahydrofuran, and showed the activation energies were reduced up to 67% compared to fast pyrolysis of cellulose. In these polar aprotic solvents, product distributions were also strongly dependent on choice of solvent although the kinds of products remained the same.[21]

Furthermore, many protic solvents chemically react with either biomass or its products to form products not otherwise expected from solvent liquefaction. Alcohols, for example, can alkylate solubilized carbohydrates.[22] Water, notably, can hydrolyze glycosidic bonds, forming smaller oligosaccharides or monosaccharides.[23] Shuai *et al.*[24] exploited this phenomena by stabilizing lignin deconstruction products via reactions with formaldehyde, significantly reducing secondary reactions of these products that form intractable carbon-carbon bonds.

The unique opportunity for solvent liquefaction is the potential of solvents to perturb the chemical kinetics of thermal deconstruction and improve product selectivity under mild reaction conditions. This distinct advantage compared to other thermochemical processes is somewhat countervailed by the expense of solvents and difficulties of solvent recovery.

Fast pyrolysis

Fast pyrolysis is the moderately high temperature (400 to 750 °C) thermal deconstruction of organic matter in the absence of oxygen. It produces mainly bio-oil—a viscous, acidic liquid—plus non-condensable gases and char. Depending on process conditions, fast pyrolysis can produce approximately 75 wt% bio-oil.[2] Bio-oil originates from the evaporation or thermal ejection of liquids formed during the thermal deconstruction of biomass polymers. These vapors and aerosols are subsequently condensed or otherwise separated from the non-condensable gas stream, thus exiting the pyrolysis reactor as liquid bio-oil.

Like for all thermochemical processes, temperature is a major determinant of the yield of fast pyrolysis products, as shown in Figure 1.8.[25] The existence of an optimal

temperature for maximum bio-oil yield demonstrates the balance between char formation at lower temperatures and gas generation at higher temperatures.

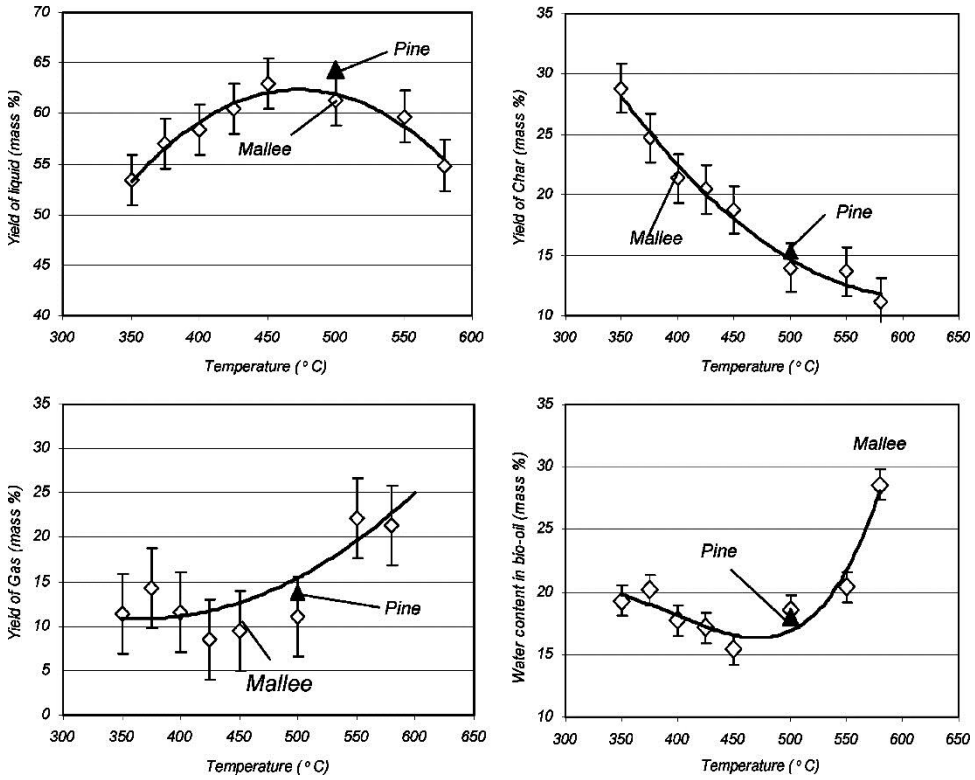

Figure 1.8. The effect of temperature on the yield of solids (char), liquids (bio-oil), gases, and water in the bio-oil from fast pyrolysis of mallee wood. Most notably the liquid yield decreases as secondary reactions begin to play a larger role at higher temperatures. Source: figure reproduced with permission from Reference 25.

Fast pyrolysis is fundamental to combustion and gasification, producing the vapors that are ultimately cracked and/or oxidized into flue gas and producer gas, respectively. Thus, an understanding of fast pyrolysis as a thermal deconstruction process provides insights into the physical and chemical mechanisms of combustion and gasification, as subsequently described.

Processes Yielding Chiefly Gases

Gasification and combustion generate primarily gaseous products. Biomass is aggressively deconstructed into vapors and gases followed by gas-phase cracking and

oxidation reactions to form ideally only permanent gases. The product distributions of gasification and combustion are distinct. The theoretical products of gasification, determined by thermodynamic equilibrium, are mixtures of carbon monoxide (CO), carbon dioxide (CO_2), hydrogen (H_2), methane (CH_4), and small amounts of low molecular weight alkanes and alkenes, with virtually no char or tar present. In practice, chemical equilibrium is difficult to attain and the products include tar and char, the amounts depending upon temperature and reaction time, as well as contaminants such as hydrogen sulfide and hydrogen cyanide. The product stream is sometimes called producer gas although more often referred to as syngas (an abbreviation of *synthesis gas*, indicating its use in catalytic synthesis of fuels and chemicals). The theoretical products of combustion are only CO_2 and water although in practice they usually include small amounts of soot, tar, and nitrogen and sulfur oxides.

Some gasifiers are indirectly heated, using heat exchangers or heat carriers to transport thermal energy into the gasifier. More commonly gasifiers are directly heated, admitting oxygen or air into the reactor where it reacts with biomass or pyrolysis products to provide thermal energy to deconstruct the biomass. Air or oxygen is always supplied to a combustor. Despite operation at different equivalence ratios, the devolatilization products of gasification and combustion are similar before being converted into final products by oxidation reactions (Figure 1.9).

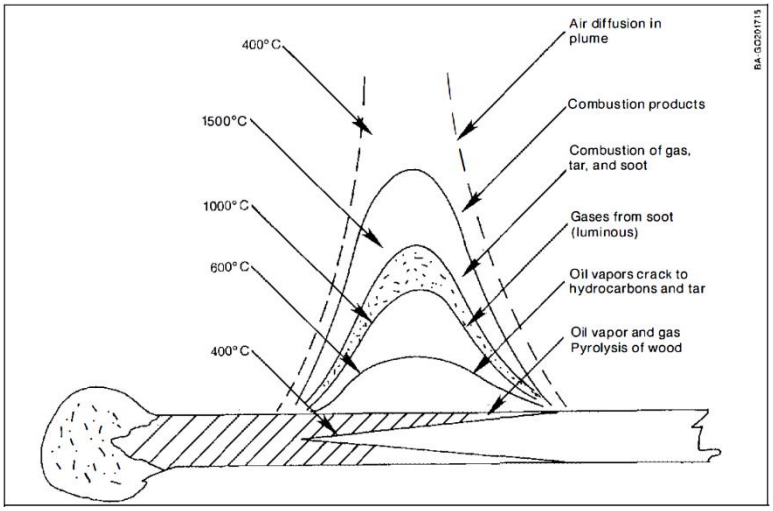

Figure 1.9. This depiction of a wooden match burning illustrates how biomass undergoes pyrolysis, gasification, and then combustion. Figure reproduced from the Solar Energy Research Institute report Handbook of Biomass Downdraft Gasifier Engine Systems.[26]

Gasification

Gasification occurs at temperatures greater than 650 °C, sometimes in the presence of steam and/or oxygen, yielding primarily producer gas but also tar and char. Most biomass gasifiers operate in the range of 750 to 900 °C to prevent ash fouling although in a few instances entrained flow, slagging reactors have been developed, which operate at considerably higher temperatures.[27,28] Devolatilization rapidly releases gases and liquids from the pyrolyzing biomass, which is followed by more gradual secondary reactions in the gas phase.

Gasification undergoes four major stages of thermal deconstruction: heating and drying, pyrolysis, gas-phase reactions, and gas-solid reactions. All thermal deconstruction processes include drying and pyrolysis, which release vapors and gases. The extent of gas-phase and solid-gas reactions are important in determining the ultimate gas composition leaving the gasifier.

The ability to accurately predict product distributions of producer gas, tar, and char from a gasifier is dependent as much on the condensed phase reactions of biomass as

the secondary reactions of tar (condensable vapors), gas, and char. Devolatilization of biomass is very fast compared to the gas-solid reactions of char and the gas-phase reactions of producer gas and tars; thus the immediate products of biomass devolatilization can be considered as reactants for subsequent gas-solid and gas-phase reactions. Whereas most of the relevant gas-solid and gas-phase reaction kinetics are well known, the elementary reactions responsible for condensed phase reactions are poorly understood and usually represented by semi-empirical global reaction mechanisms.

Combustion

Combustion is the high temperature (typically greater than 900 °C) exothermic oxidation of fuel, producing flue gas. The earliest form of bioenergy, humans have used fires from wood combustion as a source of energy for hundreds of thousands of years.[29] Today, this thermal energy is used for a wide range of applications including process heat and electricity generation.

Combustion oxidizes organic compounds into carbon dioxide and water while leaving behind ash from the mineral content in the biomass. Combustion follows four main steps: heating and drying, pyrolysis, flaming combustion, and char combustion. Flaming combustion occurs in a thin flame front surrounding the fuel particle where volatiles diffusing away from the biomass and oxygen from the surrounding air reach a critical equivalence ratio (Figure 1.10). As long as volatiles are being expelled from the biomass, essentially no oxygen reaches the biomass surface. Once devolatilization is complete—usually on the order of a few seconds or less at typical combustion temperatures—oxygen is able to penetrate to the particle surface and commence the gas-solid reaction of char oxidation.

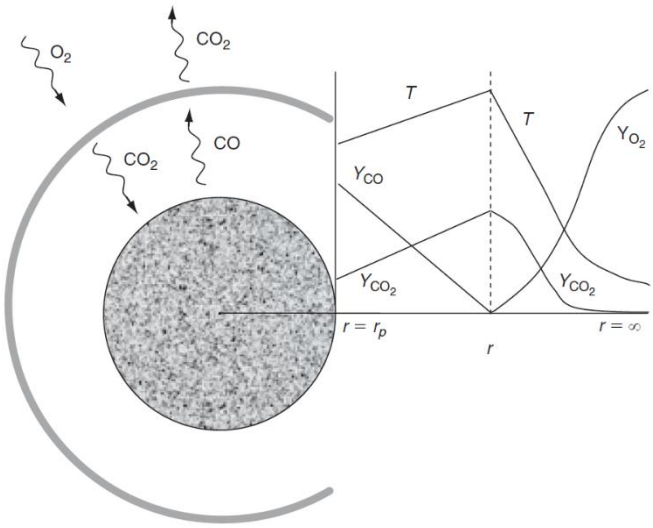

Figure 1.10. Biomass combustion begins with release of volatiles that burn in a thin flame where oxygen diffusing toward the biomass particle reaches a critical equivalence ratio. Source: figure reproduced from Reference 30 with permission from Elsevier.

These last two oxidation steps are similar to the gas-phase and gas-solid reactions that occur during gasification, except that they occur at higher equivalence ratios and temperatures. Ideally, the products of combustion are carbon dioxide and water, and the chemical energy of the reactants has been wholly converted into high temperature thermal energy, which can be used for process heating, steam production, or electric power generation.

Understanding Condensed Phase Reactions

The fact that researchers have broadly neglected the study of the condensed phase reactions that occur during thermal deconstruction reflects the difficulties in directly probing them; however, understanding condensed phase reactions is vital to improving the performance of thermochemical processes. As one example, fast pyrolysis of biomass is well known to produce anhydro-monosaccharides but at much lower yields than expected based on experiments with pure cellulose and hemicellulose. This discrepancy was traced to condensed phase reactions in the pyrolyzing biomass catalyzed by natural-

occurring alkali and alkaline earth metals (AAEM) that fragmented pyranose rings. Understanding this cause led to the development of a biomass pretreatment that passivated AAEM, leading to higher sugar yields.[31,32] (These reactions are discussed further at the end of section *Formation of liquid products* under the heading *Effects of alkali and alkaline earth metals*.) In fact, there has been recent progress in modeling elementary reactions of complex thermal deconstruction reactions,[33–37] an important advance over the use of global reaction mechanisms[38–40] to describe these complex processes. This progress should encourage future experimental studies of condensed phase reactions to validate these models.

Challenges in Investigating Condensed Phase Reactions

Much of the research on thermal deconstruction of biomass has focused on volatile products since these are much easier to access and analyze than the intermediate (and sometimes transient) products that form in the condensed phase. In general, biopolymers are not readily dissolved or volatilized, the basis of many analytical techniques such as by liquid or gas chromatography. Progress in evaluating the thermal deconstruction of biopolymers requires approaches in which large oligomeric products can be detected.

Capturing intermediate products can present significant challenges. Low volatility and short reaction times paired with high temperatures make interrogating condensed phase products difficult. Some experiments have used entrained flow reactors[41,42] or concentrated radiation[43–45] to heat samples rapidly. Both kinds of apparatus are able to rapidly terminate heating by removing the samples from the heated zone or turning off the radiation source although this does not necessarily quench thermal deconstruction

reactions. It is very likely that reactions continue as the intermediate products are slowly cooled. Few fast pyrolysis experiments have been able to both rapidly heat biopolymer samples and rapidly cool condensed phase products, whether studying cellulose[46–48] or lignocellulose.[47,49,50]

Although much of the research on biomass thermal deconstruction has actually employed extracted polysaccharides or lignin, thermal deconstruction of the *ex situ* polymer may depart significantly from the *in situ* polymer because interactions between the biomass components are lost. Tiarks[51] has explicitly demonstrated these differences in experiments with a filament pyrolyzer enclosed within an optically accessible chamber. A powdered sample of technical lignin obtained from enzymatic hydrolysis of cornstover was observed to melt, coalesce into a hemispherical shape, and lose mass through both devolatilization and liquid droplet ejection. However, it was clear that droplet ejection was an artifact of the experimental arrangement, arising from the coalescence of individual lignin particles into a single liquid mass and non-uniform heating of the sample. Rather than forming at the free surface between melted lignin and gas atmosphere, volatiles were generated at the interface of the hot filament and the bottom of the melt. These vapors could only escape by flowing upward through the melt as bubbles, exploding at the free surface and ejecting liquid droplets into the gas flow. In contrast, practical reactors achieve more uniform heating of particles, releasing volatiles directly to the surrounding gas. Furthermore, lignin polymers within actual lignocellulosic biomass are dispersed among the cellulose microfibrils, which is expected to prevent their surface tension-driven coalescence. In fact, although Tiarks[51] observed some evidence of lignin migrating to the surface of biomass fibers during pyrolysis, it

was not sufficient to cause coalescence as observed for extracted lignin. When extracted lignin was mixed with a fumed silica matrix, the lignin was sufficiently dispersed to prevent melted particles from agglomerating during pyrolysis. As shown in Figure 1.11, the resulting film of melted lignin showed only minor ejection phenomena, with most of the mass loss due to vaporization from the melt phase. Tiarks[51] also observed little thermal ejection when pyrolyzing cellulose that was dispersed as small particles along the filament heater of the pyrolyzer, arguing that previous studies reporting this phenomenon suffered from non-uniform heating of the sample.[52,53]

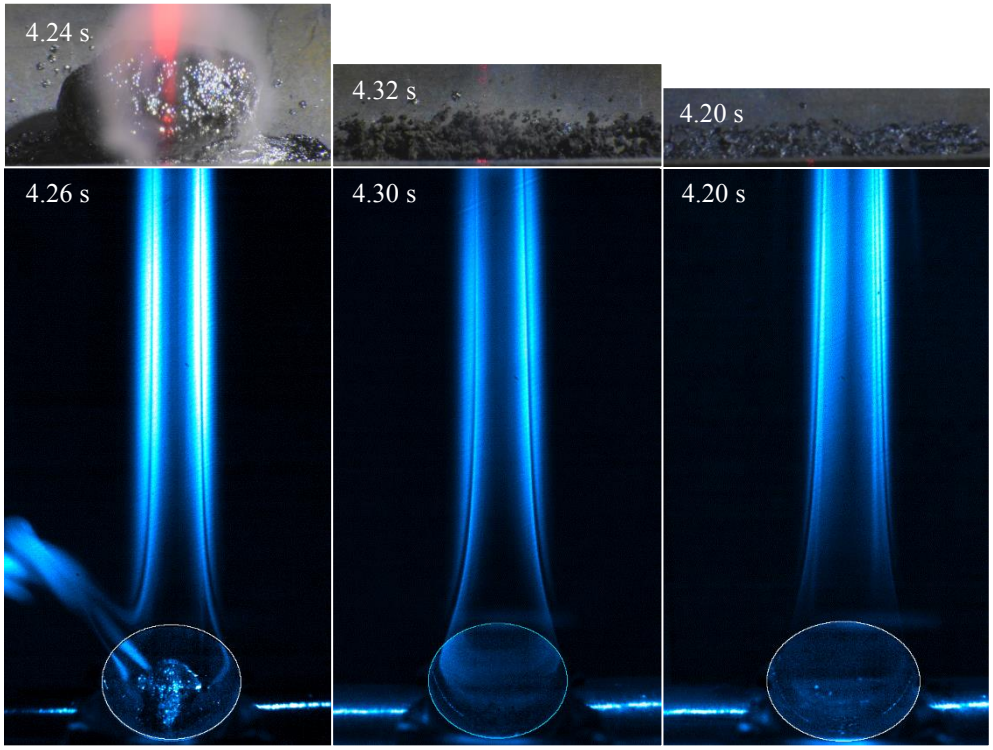

Figure 1.11. Comparing pyrolysis of extracted lignin (left), extracted lignin mixed with silica matrix (center), and red oak (right) demonstrates how thermal ejection is an artifact of particle coalescence and non-uniform heating from below the sample. Source: figure adapted with permission from Tiarks.[51]

Even if extracted polymers behaved like their *in situ* counterparts,[54] most reactors and chemical instruments are ill-suited to examine condensed phase reactions. For instance, extracted cellulose is well known to progress through a liquid intermediate

during fast pyrolysis. (See Lédé's review for a thorough account.)[55] These liquid intermediate products have been identified as anhydro-oligosaccharides.[56] Their maximum degree of polymerization (DP) is typically measured to be around seven;[41,57] however, Lindstrom *et al.*[48] recently identified anhydro-oligosaccharides up to DP 60 from partially pyrolyzed cellulose. More importantly, this work concluded that larger oligomers probably exist but have evaded detection by conventional water-based analyses because they are insoluble in water. This subtle instrumentation issue resulted in theories and models biased toward water-soluble anhydro-oligosaccharides, which is not the full picture.

Present methods for the analysis of biopolymers or their oligomers are relatively unwieldy. To probe specific reactions within biopolymers, model compounds with specific moieties or bonds are often chosen to represent particular areas of interest. Model compound experiments often focus on yields or types of products,[58,59] but more advanced methods, such as isotope labeling,[60–63] are needed for more detailed insights. However, model compound experiments can be confounded by heat and mass transfer limitations, among other problems, so researchers often resort to the well-controlled conditions offered by computational chemistry to provide insights into polymer decomposition.

Computational chemistry and its many approximations are discussed in *Computational methodology*, but a few assumptions are worth noting here. These calculations are often performed as gas phase reactions with the results assumed to hold true for condensed phase reactions. Furthermore, there is significant uncertainty in computed values of kinetic parameters, depending on the nature of the computations. Depending on the level of theory used, these constants can vary significantly. For

example, the commonly used Becke-three parameter-Lee-Yang-Parr (B3LYP) functional is thought to predict pre-exponential factors[33,34] within an order of magnitude and activation energies[64] within ± 4.8 kcal mol^{-1}. Taken together, errors in rate coefficients can be orders of magnitude. Lastly, computational power limitations bias modeling toward smaller molecules.

Biomass thermal deconstruction is not simply the depolymerization of the three main biopolymers in lignocellulosic biomass. It also entails the deconstruction of the lignocellulosic matrix, a structure involving the interaction of cellulose, hemicellulose, and lignin to produce a composite material with its own unique physical properties. Too often, experiments and modeling overlook these interactions, which likely has hindered progress in understanding thermal deconstruction of biomass.

The Role of Cell Wall Structure in Thermal Deconstruction

Cell wall structure plays an important role in the thermal deconstruction of biomass, determining the rate at which heat is conducted into the composite structure of lignocellulosic biomass and the rate mass is transported out of the disintegrating plant material. Thus, two key areas discussed in this section are heat and mass transfer during thermal deconstruction, and the structural breakdown of the plant cell wall.

Lignocellulosic biomass has unusual heat transfer characteristics for a solid material. Conventional heat transfer calculations, mainly the Biot number, demonstrate that the relatively low thermal conductivity of biomass creates thermal gradients in particles (Figure 1.12). However, detailed studies indicate this simple calculation significantly underestimates the actual thermal gradients that occur.[65–68]

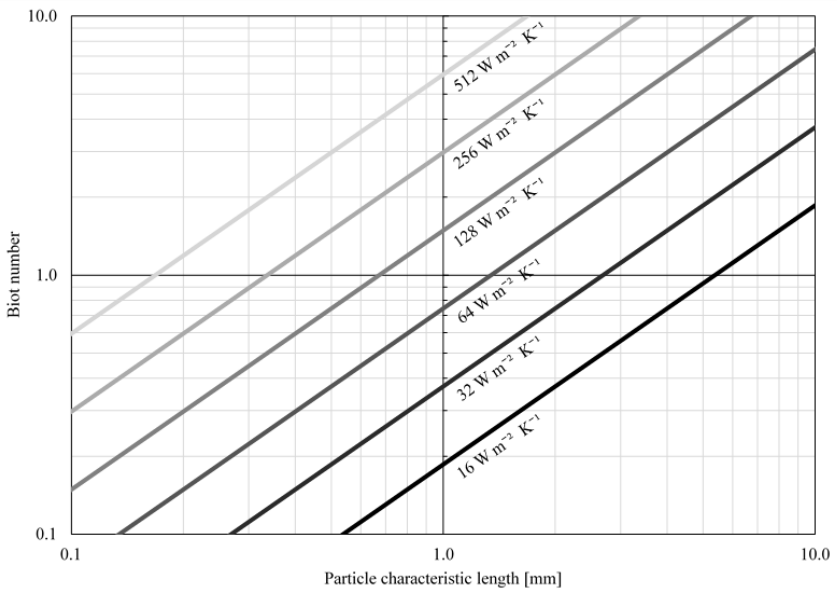

Figure 1.12. Even relatively small biomass particles can develop thermal gradients when subject to high heat transfer. Produced with assistance from Chad A. Peterson using the thermal conductivity of pine.[69,70]

Within biomass particles, asymmetry in the microstructure of biomass dramatically influences heat transfer. Biomass has the highest thermal conductivity through its cell walls axial to their lumina[71] (the interiors of the cells); however, lumina, as well as larger tubes such as xylem, inhibit radial thermal conduction. To examine intraparticle heat and mass transfer more accurately, Ciesielski *et al.*[66] modeled fast pyrolysis of pine and aspen particles with realistic particle, cell wall, and cell lumina dimensions, as measured by multiple microscopy and spectroscopy methods. Accounting for the lumina predicts significantly slower heat transfer, particularly into the cores of particles (Figure 1.13).

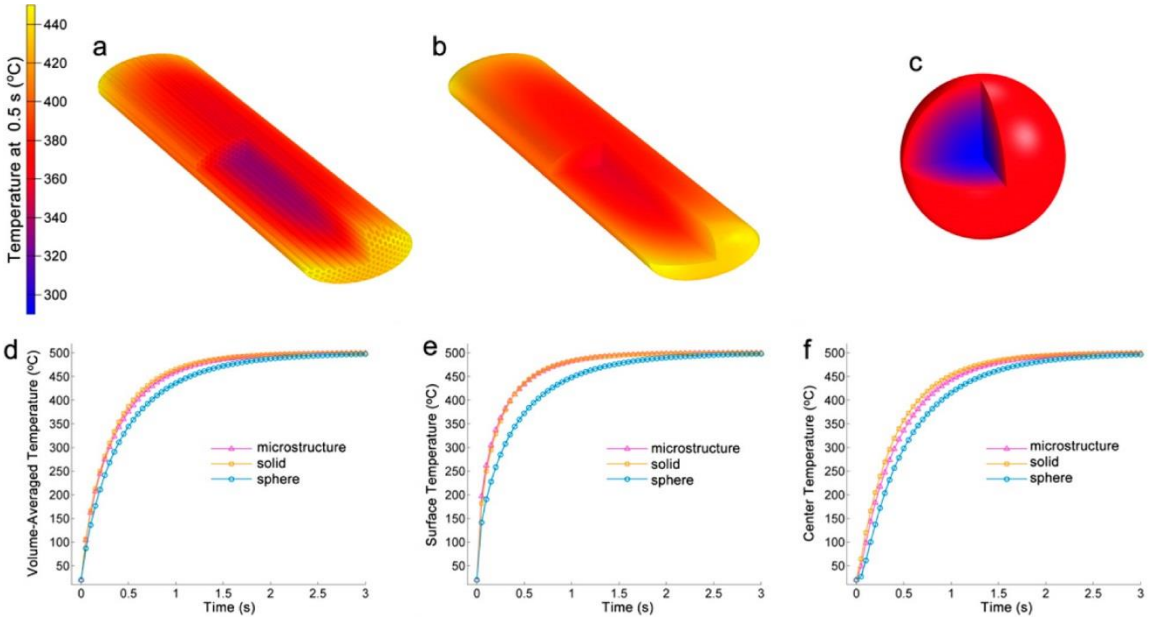

Figure 1.13. Computer simulation of the heating of three biomass particles of similar thermal mass but different structure show markedly dissimilar thermal gradients. Realistic morphology [a] develops larger temperature gradients than particles with the same proportions but without cell lumina [b]. Spherical particles [c], often used for modeling simplicity, have dramatic thermal gradients that do not accurately represent biomass. Source: figure reproduced with permission from Reference 66.

Different biomass species can exaggerate this effect. Using the same realistic biomass models, Pecha *et al.*[68] calculated aspen to have a heat transfer coefficient roughly 20% greater than pine in a laminar flow regime because of their differing microstructures. Understanding these heat transfer effects is essential for realistic modeling. Thermal gradients can alter product yields because reaction rates increase exponentially with temperature.[72,73] Large particles, in particular, are more susceptible to these gradients—as described by the Biot number, which is directly related to particle characteristic length. There are limits to reducing particle size in industrial practice, however, because comminution costs grow exponentially with decreasing particle size.[74]

Other factors have also received limited attention but deserve more thorough investigation. As biomass is heated, moisture is driven out of the particles, and the high specific heat and enthalpy of water vaporization likely exaggerates thermal gradients.

Similarly, volatile product formation and vaporization may slow heat transfer, especially as most condensed phase thermal deconstruction reactions are endothermic.

The diffusion time for volatiles released from biomass particles likely plays a strong role in secondary reactions, which often are responsible for molecules decomposing into non-condensable gases, thus reducing yields of liquid products. While the structure of cell lumina can impede radial heat transfer through particles, it assists mass transfer of volatile products out,[66] so further analysis of this transport phenomena may contribute toward improving liquid yields.

Inclusion of cell morphology in the analysis of transport phenomena is insufficient if it is static. The complex cell wall microstructure breaks down and changes during thermal deconstruction.[42] Haas, Nimlos, and Donohoe saw significant morphological changes when they heated small, thin sections of poplar at approximately 2.5 K s^{-1} under a light microscope with an inert atmosphere.[75] The poplar expanded only in the radial direction (Figure 1.14). (Videos of this expansion are available in the supplemental material of Reference 75.) Cell walls swelled, grew taut, partially converted into volatile products, and then contracted as these products escaped. The final configuration had about 10-15% more lumina area compared to unmodified cell walls due to this expansion and contraction, but more so from the volatile product mass transfer. These changes likely slow heat transfer and increase volatile product mass transfer. Clearly, cell wall structure is important to both the rate and final products of thermal deconstruction of biomass.

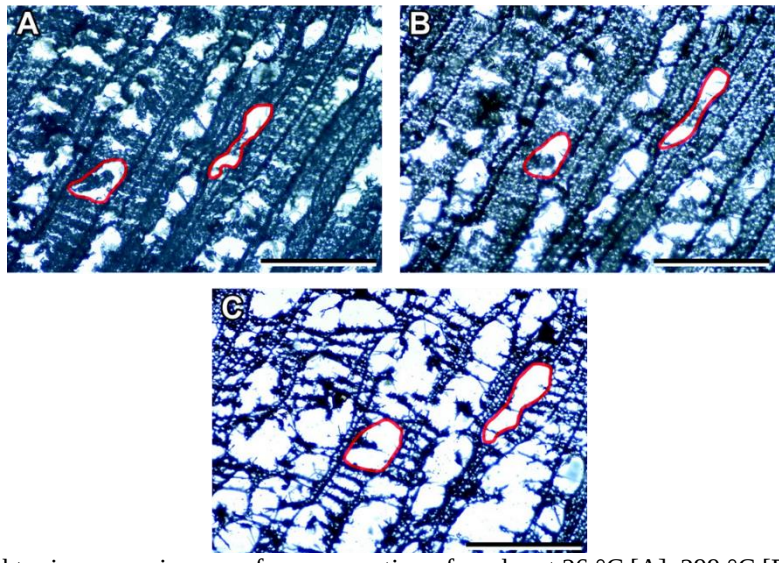

Figure 1.14. Light microscope images of a cross section of poplar at 26 °C [A], 299 °C [B], and 501 °C [C] show how cell walls expand when heated before contracting as volatile products leave. The red outlines surround xylem. Scale bars equal 1 mm. Source: figure reproduced with permission from Reference 75.

Use of Computational Chemistry to Understand Thermal Deconstruction

Computational chemistry has increasingly helped overcome the dearth of experiments on condensed phase reactions. Starting in the mid-2000s, researchers have used computational chemistry in combination with experimental measurements to examine condensed phase reactions. The rise of theoretical methods has allowed researchers to better understand how species evolve during the thermal deconstruction of various kinds of biomass components. Furthermore, the results of theoretical investigations are helping guide experimentalists to tailor reaction conditions, with the aim of achieving greater control over product distribution.

Experiments have revealed hundreds of compounds produced from thermal deconstruction of biomass. A key advantage of computational methodologies is that they allow rapid simulation of a wide range of experimental parameters which would take significantly longer to test in a laboratory. In this way, computational chemistry can be of

great assistance to the experimentalist, as both a guide to potential research avenues and as a time saving tool.

The following text serves as a primer on computational chemistry methods. This overview is followed with a description of key condensed phase reactions that occur during biomass thermal deconstruction, and concludes with a brief discussion of current deficiencies in these methods and suggestions for future computational studies.

Computational methodology

Computational investigations of biomass deconstruction are used to estimate how the energy of a system of reacting molecules evolves over the course of the reaction. For instance, the difference in energy between the pyranose and furanose forms of glucose indicates which structure is more stable. Calculating the energy of a lignin model compound and its decomposition products can determine whether the reaction proceeds endothermically or exothermically. The prediction of reaction mechanisms and their associated enthalpies is a common undertaking and allows for researchers to understand the reasons why certain products are favored under different experimental conditions.

The Hartree-Fock (HF) method, an early computational approach to describing molecular systems, was never widely applied toward the study of biomass deconstruction. HF does not account explicitly for the Coulombic repulsion of individual electrons, termed the electron correlation, and instead works only with an averaged repulsion. Owing to this fact, the energy obtained using the HF method converges to a value that is always above the true ground state energy, at a point known as the HF limit. Due to this overestimation, improvements dubbed post-Hartree-Fock were introduced to include electron correlation. One such example shown to be highly accurate is the

coupled cluster method. This method is useful in biomass deconstruction investigations in areas such as modeling the decomposition of glucose and fructose molecules.[76]

An alternative to HF based methods is density functional theory (DFT), which has seen widespread use in the field of biomass conversion. In DFT, the energy of the system is calculated as a function of electronic density. For purposes of this description, it is sufficient to note that DFT makes approximations to account for electronic quantum mechanics, namely the Born-Oppenheimer approximation. This has resulted in a hierarchy of methods ranging in complexity from a local density approximation (LDA) to the double hybrid methods. Some of the most popular methods fall into the hybrid and meta-hybrid categories. One that has seen significant application for biomass deconstruction studies over the course of the last decade is the Becke-three parameter-Lee-Yang-Parr (B3LYP) functional.[77–80] The speed of the B3LYP functional and its prediction of accurate geometries has led to its use in modeling a range of phenomena including degradation of cellulose, hemicellulose, and lignin.[81–83] More recently, the Minnesota family of functionals from Zhao and Truhlar[84,85] has gained popularity in the biomass field and is regularly encountered in the literature, while use of the aforementioned B3LYP method is increasingly less common.

DFT is used to calculate the energy of reactants and products for a reaction. Transition state theory (TST) is used to understand the mechanism by which a reaction occurs, and traditional TST posits that a reaction proceeds from reactant to product via a transition state complex. Using TST, a complicated mechanism can be divided into a number of elementary reactions, with each step proceeding through a transition state

complex. Figure 1.15 illustrates the energy change for a hypothetical substitution reaction.

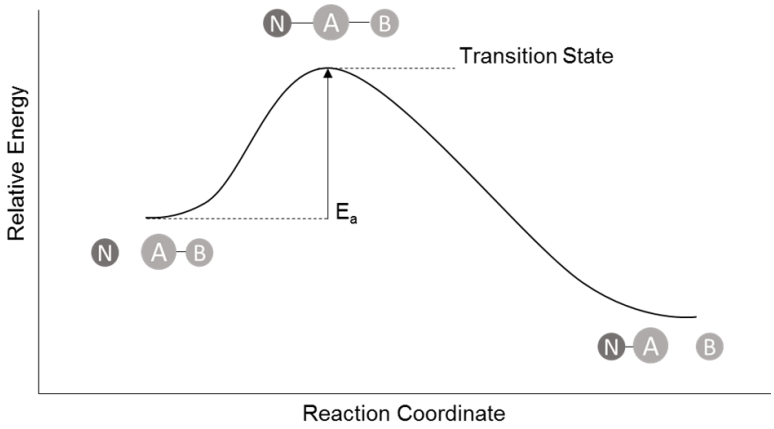

Figure 1.15. This reaction coordinate diagram demonstrates a generic substitution reaction, highlighting the position of the transition state.

As this simplified example shows, computational chemistry has the potential to provide insights not possible through experimentation techniques; however, despite accounting for quantum details, the information and conclusions derived are imperfect. The reaction intermediates, mechanisms, and slew of products predicted by computational chemistry seem definite, but like all computer models, the accuracy of results depend on the assumptions about mechanisms and boundary conditions.

Formation of liquid products

Thermal deconstruction of solid biomass can produce solids, liquids, vapors, and gases as primary products. The elevated temperatures of thermal deconstruction quickly vaporize most liquid products although there is evidence that a small amount may also escape as aerosol.[51,52,86] In the case of fast pyrolysis, the desire is to quickly sweep these vapors from the reactor and cool them into liquid products. At sufficiently high temperatures and long residence times, these vapors crack or dehydrate by secondary reactions into gases and char, although this is not the focus of this section.

Cellulose conversion reactions

Levoglucosan, as the major product of the thermal deconstruction of cellulose, has attracted substantial attention in computational studies of biomass pyrolysis. Experimental studies have shown fast pyrolysis of pure cellulose produces approximately 60 wt% levoglucosan under optimal conditions,[87] although the presence of alkali and alkaline earth metals in lignocellulosic biomass catalyzes pyranose ring fragmentation which can dramatically reduce this yield.[88]

Cellulose thermal deconstruction experiments, however, like others using isolated biopolymers, are fraught with confounding variables. The cellulose source and isolation method impacts the material significantly. Drying the cellulose irreparably alters the structure,[89] and the resulting cellulose crystalline allomorphs, as well as the degree of crystallinity, may influence experimental outcomes.[90,91] However, attempting to model reactions of cellulose consisting of many thousands of connected glucose monomers would be impractical. Instead, early computational researchers supposed that glucopyranose, the monomeric unit of cellulose, was a suitable model compound for their computational studies. In particular, several groups investigated how levoglucosan could arise from glucopyranose through a dehydration and ring forming mechanism based on a single transition state.[81,92–94]

The problem with modeling the formation of levoglucosan from glucopyranose is the assumption that other monomers in the polysaccharide chain do not influence the process. In fact, depolymerization of cellulose to form levoglucosan entails breaking glycosidic bonds between adjacent pyranose rings, so these bonds should be included in simulations of thermal deconstruction. An example is the study of Zhang *et al.*[95] who

determined energy requirements for homolytic and heterolytic breakage of the glycosidic bond in cellobiose, a glucose dimer. Although the homolytic route was found to be significantly more favorable in terms of bond dissociation energy, the energy requirement of 79 kcal mol^{-1} was still large, suggesting this may not be the most likely route for levoglucosan formation.

An alternative route to cellulose depolymerization proposed by Mayes and Broadbelt employed a low energy concerted mechanism,[96] illustrated in Figure 1.16. The glycosidic bonds between pyranose units in the cellulose chain are cleaved to produce anhydro-oligosaccharides, as has been observed experimentally.[41,48,57] Subsequent cleavage at the terminal glycosidic linkage of an anhydro-oligosaccharide yields levoglucosan. This route provides the lowest energy mechanism for levoglucosan formation from cellulose. Zhang *et al.*[97] compared these three possible levoglucosan formation mechanisms in a dry gaseous atmosphere and verified that homolytic cleavage has a substantially higher energy barrier than their proposed levoglucosan chain-end mechanism.

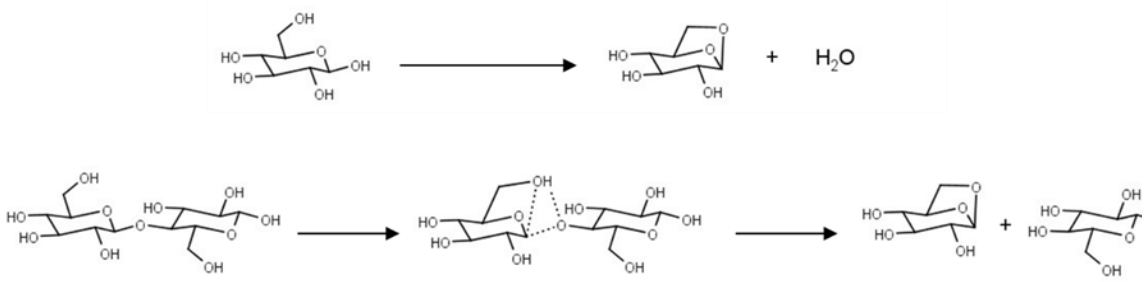

Figure 1.16. Top: Formation of levoglucosan from glucopyranose in a single step reaction. Bottom: Simplified representation of Mayes and Broadbelt's chain-end mechanism for levoglucosan formation.[96]

Cellulose, and its subsequent anhydro-oligosaccharides, break into increasingly small anhydro-oligosaccharides. Because levoglucosan forms from terminal monomers,

the relative abundance of these monomers controls the rate of levoglucosan formation. As a result, cellulose produces very little levoglucosan before it has substantially depolymerized.[35,48] Levoglucosan and many less valuable, lower molecular weight products primarily derive from low DP anhydro-oligosaccharides.

After levoglucosan is formed, it can decompose into lower molecular weight molecules, especially as reaction temperature increases.[98] Such secondary reactions may help explain differences observed experimentally in liquid product yields. Zhang *et al.*[99] evaluated the decomposition pathways for levoglucosan and concluded that dehydration has a lower energy barrier compared to C-C or C-O bond breaking, suggesting it dominates secondary reactions of levoglucosan decomposition.

Assary and Curtiss suggested that levoglucosenone (LGO) can be formed from the double dehydration of levoglucosan; however, the thermal stability of levoglucosan and the high activation energy required for the reaction discourage this as a feasible route.[92] Lu and co-workers suggest an alternative mechanism in which LGO forms from cellulose through a chain-end mechanism similar to that for levoglucosan formation.[100] This hypothesis is supported by experimental work in which pyrolysis of cellobiose produced more LGO than did pyrolysis of glucose.[87]

Hydroxymethyl furfural (HMF) is another important product of biomass thermal deconstruction. Based on its chemical formula, HMF requires two dehydration reactions to derive from glucopyranose. A concerted mechanism of formation from cellulose has been considered, but the high energy requirements render this route unfeasible.[101] Correspondingly, two formation mechanisms from glucopyranose have been proposed, both initiated through an opening of the pyran ring and subsequent dehydrative

cyclization to yield the furanose form of the sugar.[81,93] Between these two proposed mechanisms, the order of the elementary steps differ but the energy barriers are very similar.

Furthermore, experimental work has shown that pyrolysis of fructose produced greater amounts of HMF than did glucose, indicating that glucose-fructose tautomerization proposed by previous work may be more likely. Mayes and co-workers[102] compared multiple routes for HMF formation in a comprehensive study and found that tautomerization prior to dehydration was the most energetically favorable pathway.

While it is reasonable to expect furfural (FF) to form following removal of the hydroxymethyl group from HMF, the energy barrier for this reaction is very high.[103] Alternatively it has been suggested that the formation of FF and HMF are competitive with one another and that a Grob-fragmentation could be a significant low-energy step for removal of the hydroxymethyl group.[104]

The multitude of reactions forming these small molecules are well suited for computational chemistry; however, they still require firm experimental evidence. For example, thermohydrolysis, a depolymerization reaction that generates a glucose molecule, has been proposed.[33,35] By this theory, the glucose produced via thermohydrolysis degrades into many lower molecular weight products. This reaction has not been experimentally validated for cellulose, even though it can predict final product yields very accurately.[33,35] Experiments examining the solid and liquid phase intermediate products during cellulose pyrolysis have not found anywhere close to the

amount of glucose these models predict.[48,105,106] Reactions, such as thermohydrolysis, should be experimentally validated if possible.

Hemicellulose conversion reactions

Thermal deconstruction of hemicellulose typically leads to a variety of small, oxygenated products with relatively low sugar and anhydrosugar yields, such as xylose and anhydroxylopyranose.[107] Studies on the deconstruction of hemicellulose are less numerous than cellulose, most likely owing to the greater variability in products and monosaccharides within the polymer. Experimental studies are typically performed on extracted hemicelluloses,[107–109] but computational chemistry is perhaps better suited.[36] Hemicellulose, unlike cellulose, is a branched heteropolymer composed of pentoses, hexoses, hexuronic acids, and acetyl groups.[110] A standard structure or composition cannot be defined as it differs among biomass species,[110] stages of plant growth,[111,112] and even cell wall layers.[113] Nevertheless, the prevalence of xylose in hemicelluloses—and not in cellulose—means that it is often chosen as a model compound for investigation.

The formation of FF from xylose appears to be more straightforward than its formation from glucose. Wang *et al.*[114] suggest the process involves a pyranose ring opening, removing two hydroxy groups, and then forming a five membered furan ring. The energy barriers in this conversion can be greatly reduced by explicitly including a water molecule in the computations.[114] Just as Seshadri and Westmoreland[94] found that hydroxyl groups promote glucose deconstruction, xylose conversion to FF may be assisted by water as well as other small, oxygenated chemicals surrounding hemicellulose. Similar routes have been proposed for other monosaccharides found in hemicelluloses, such as arabinose.[82]

By molecular weight, FF is one of the larger products produced from hemicellulose deconstruction, but many small chain carboxylic acid, ketone, and aldehyde type species are also derived through degradation of hemicellulose saccharides.[82,115–117] Hemicellulose thermally degrades more easily than cellulose and lignin,[1] which explains the pervasiveness of these small chemicals in the liquid fractions of thermochemical processing methods. Likely in part due to relative instability and low economic value of its products, hemicellulose has not received as much study as cellulose or lignin, although it has recently garnered more attention.[36,109]

Lignin conversion reactions

Lignin thermal deconstruction generally produces large amounts of phenolic monomers and oligomers, as well as non-condensable gases and char.[118] Studying these lignin deconstruction reactions is perhaps more difficult than for cellulose or hemicellulose because of the large number of potential products. Like the other main biopolymers, extracting lignin from biomass can significantly modify the structure.[119–121] Lignin structure varies dramatically among plant species[122] and even within the same plant at different times during its growth.[123,124] Unlike cellulose or hemicellulose, lignin is highly crosslinked with an apparently random structure, leading to its well-known recalcitrance.[122,125]

To avoid these complications, researchers often employ model compounds to study lignin deconstruction. Models of lignin deconstruction are rarely based on elementary reaction mechanisms, instead employing simple lumped parameter models. With lignin's complexity, experiments typically only provide product yields from isolated lignin[118,126] or changes in bond prevalence before and after heating,[127] not

specific reaction pathways or mechanisms. Model compounds are necessary for more detailed reaction and kinetic study toward the eventual goal of a comprehensive model.[37]

Phenethyl phenyl (PPE) is frequently employed as a model compound to investigate fragmentation of β-O-4 ether linkages, one of the most prevalent bonds in lignin. The relatively simple structure of PPE is convenient for computational studies while accounting for the influence of aromatic groups on important structural effects in lignin deconstruction. More comprehensive information on lignin deconstruction reactions can be found in Kawamoto.[128]

Homolytic reactions are thought to dominate lignin deconstruction, but concerted mechanisms may also play a role. Jarvis *et al.*[129] found strong experimental evidence for concerted mechanisms at temperatures below 1,000 °C but at higher temperatures homolytic pathways appear to be more thermodynamically favorable. Huang *et al.*[83] narrowed the likely concerted reactions to retro-ene fragmentation[130] and Maccoll elimination.[131] Elder and Beste[132] further analyzed these reactions with computational chemistry, determining that retro-ene fragmentation presents the most favorable low-temperature pathway. Many other lignin model compounds are also likely to degrade via concerted reactions at low temperatures and homolysis at higher temperatures,[133] although there are exceptions. For example, 1-(4-methoxyphenyl)-2-(2-methoxyphenoxy) ethanol, a synthesized lignin dimer model compound, likely reverses this temperature trend.[134]

These findings highlight the complexity of condensed phase reactions during lignin thermal deconstruction. Small changes in the substituents attached to aromatic rings within lignin can greatly alter the degradation reaction rates and even the type of

decomposition reactions. Owing to the diversity of aromatic substituent groups in lignin, these reactions warrant further investigation.

Evolution of water

The production of water during biomass deconstruction impacts the properties of the products, oftentimes necessitating removal prior to utilizing the products in specific applications (for instance, if they are to be used as liquid fuels). The concentration of water in liquid products is often very high (typically 20 wt%),[25] so it is important to understand how biomass deconstruction reactions generate water. Many works show water arising from the removal of hydroxyl groups from cellulose and hemicellulose monomers,[93,102,103,115,117] suggesting that the presence of water in deconstruction products is most likely unavoidable.

Effects of alkali and alkaline earth metals

Biomass contains notable amounts of alkali and alkaline earth metals (AAEM), with potassium and calcium being noteworthy elements. The presence of AAEM can have a catalytic effect on deconstruction reactions.[32,88] Notably, the yield of sugars decreases with increasing presence of AAEM because other degradation reactions dominate. In a comprehensive study, Mayes *et al.*[135] examined the effect of sodium cations on a wide range of reactions that occur during glucose pyrolysis. Their findings suggested that rate coefficients were increased considerably for a majority of the reaction pathways though not all.[135] Importantly, the presence of a sodium ion did not alter the mechanisms of the various reaction pathways, leading to generation of the same products but in different concentrations. These computational findings agree with their

experimental results. In another work, potassium was modeled for comparison to sodium and similar catalytic trends were observed for both ions.[136]

Notably, this trend can be reversed by passivating the AAEM with stoichiometric quantities of mineral acids.[32,88] Most likely, thermally stable salts form between the conjugate bases and AAEM, preventing their catalytic action.

Formation of gaseous products

Compared to the hundreds of chemicals in the liquid products of thermochemical processing, gas composition is fairly simple.[18,137–139] It has been proposed that CO and CO_2 arise through decarbonylation and decarboxylation reactions, respectively.[140] CO can be formed from lignin through decarbonylation of benzaldehyde type moieties, while decarboxylation of benzoic acid derivatives leads to CO_2 formation. The formation of CO has a significantly higher energy barrier than for the formation of CO_2, in agreement with pyrolysis experiments, where CO_2 is formed in greater quantities than CO.[18,34,137–139]

Methane is thought to evolve from homolytic cleavage of methyl groups from the ends of methoxy functionalities in lignin, as shown in Figure 1.17.[141] The resulting methyl radical is then converted to methane by combining with an unbound hydrogen atom. This route, while feasible, is highly speculatively and requires significant energy to overcome the homolysis barrier. An alternative route requires the methoxy group be located ortho to a hydroxy group, enabling a concerted reaction to occur in which the methyl group sequesters the neighboring phenolic hydrogen, liberating methane and leaving two adjacent carbonyl type groups attached to the ring. This route is considerably more energetically facile than the homolytic route.

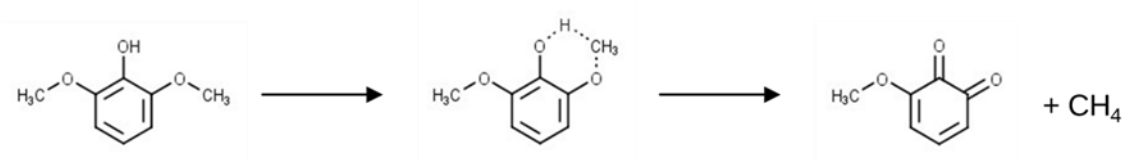

Figure 1.17. One potential route for methane formation from lignin is homolytic cleavage of methyl groups from the ends of methoxy functionalies as illustrated here for the model lignin compound syringol.[141]

Char formation

Theoretical investigations into the formation of char and carbonaceous materials during thermal deconstruction of biomass are limited. Many theories have been proposed as to why these compounds form, but studies do not provide a direct link to mechanisms of polycyclic aromatic species formation. In high temperature thermal deconstruction processes, such as fast pyrolysis and gasification, char is often an unwanted side product formed from the dehydration of more desirable product molecules. A greater understanding of char formation mechanisms is essential to reducing its formation. Once understood, these mechanisms can be used to help tailor thermal decomposition to minimize char production and increase the output of more valuable organic compounds.

Computational studies of large scale polymers

Over the past decade, the application of computational methods to study thermal deconstruction of biomass has expanded greatly. Ever advancing computational power has led to an increase in the complexity of model systems, and, as a result, a greater range of mechanisms may be investigated to account for the experimentally observed products.

In some instances, computational work is expanding beyond small model compounds and investigating large scale polymers. These studies are beginning to bridge the gap between chemistry and materials science—a vital step.[142–146] A continuation of this trend may lead to detailed research on larger polymeric species of lignin, or perhaps

facilitate the modeling of intermolecular interactions between polymer chains to more accurately capture the chemistry of decomposition reactions.

Conclusions

All thermochemical processes are closely related. Often distinctions among them are the result of imposed definitions, not the reactions themselves. Examining condensed phase biomass thermal deconstruction reactions shows that the processes—with the exception of solvent liquefaction—merely occupy different positions on a continuum of reaction times and temperatures. Despite varying temperatures, heating rates, and reaction times, the different methodologies for thermochemical processing of biomass are fundamentally similar.

This relationship can be exploited to probe difficult to analyze reactions. For example, the relative strength of bonds can be determined with slow heating rate and low temperature processes, such as torrefaction and slow pyrolysis. These conclusions should be verified at higher heating rates and temperatures but they provide a sound basis for further work. Additionally, volatile products from fast pyrolysis could be used as a starting point for gasification and combustion studies.

This exploitation is possible because the similarities are more than parallels; they are often the same reactions. On the other hand, overreliance on these comparisons invites error. Relative reaction rates change with temperature, and these differences can grow as intermediate product concentrations and subsequent condensed phase reaction rates shift. Within reason, the condensed phase reactions during thermal deconstruction can act as powerful tools for suggesting answers to research questions or point to new avenues of study.

References

(1) Tumuluru, J. S.; Sokhansanj, S.; Hess, J. R.; Wright, C. T.; Boardman, R. D. A Review on Biomass Torrefaction Process and Product Properties for Energy Applications. *Ind. Biotechnol.* **2011**, *7* (5), 384–401.

(2) Bridgwater, A. V. Review of Fast Pyrolysis of Biomass and Product Upgrading. *Biomass and Bioenergy* **2012**, *38*, 68–94.

(3) Haverly, M. R. An Experimental Study on Solvent Liquefaction, Iowa State University, 2016.

(4) Kenney, K. L.; Smith, W. A.; Gresham, G. L.; Westover, T. L. Understanding Biomass Feedstock Variability. *Biofuels* **2013**, *4* (1), 111–127.

(5) Harris, P. J.; Stone, B. A. Chemistry and Molecular Organization of Plant Cell Walls. In *Biomass Recalcitrance: Deconstructing the Plant Cell Wall for Bioenergy*; Himmel, M. E., Ed.; Blackwell Publishing, 2008; pp 61–93.

(6) Henriksson, G. Lignin. In *Wood Chemistry and Wood Biotechnology*; Ek, M., Gellerstedt, G., Henriksson, G., Eds.; Walter de Gruyter: Berlin, New York, 2009; pp 121–145.

(7) Oinonen, P.; Zhang, L.; Lawoko, M.; Henriksson, G. On the Formation of Lignin Polysaccharide Networks in Norway Spruce. *Phytochemistry* **2015**, *111*, 177–184.

(8) Tumuluru, J. S.; Kremer, T.; Wright, C. T.; Boardman, R. D. Proximate and Ultimate Compositional Changes in Corn Stover during Torrrefaction Using Thermogravimetric Analyzer and Microwaves. *Am. Soc. Agric. Biol. Eng. Annu. Int. Meet.* **2012**, *2*.

(9) Phanphanich, M.; Mani, S. Impact of Torrefaction on the Grindability and Fuel Characteristics of Forest Biomass. *Bioresour. Technol.* **2011**, *102* (2), 1246–1253.

(10) Phyllis2, Database for Biomass and Waste https://phyllis.nl/ (accessed Jan 8, 2019).

(11) Palmer, C. A.; Oman, C. L.; Park, A. J.; Luppens, J. A. The U.S. Geological Survey Coal Quality (COALQUAL) Database Version 3.0. *United States Geol. Surv. Data Ser.* **2015**, *975*, 1–43.

(12) *ASTM Standard D388, 2018, "Standard Classification of Coals by Rank";* ASTM International: West Conshohocken, PA, 2018.

(13) Antal, M. J.; Grønli, M. The Art, Science, and Technology of Charcoal Production. *Ind. Eng. Chem. Res.* **2003**, *42* (8), 1619–1640.

(14) Denevan, W. M. A Bluff Model of Riverine Settlement in Prehistoric Amazonia. *Ann. Assoc. Am. Geogr.* **1996**, *86* (4), 654–681.

(15) Gray, E.; Marsh, H.; McLaren, M. A Short History of Gunpowder and the Role of Charcoal in Its Manufacture. *J. Mater. Sci.* **1982**, *17* (12), 3385–3400.

(16) Ronsse, F.; van Hecke, S.; Dickinson, D.; Prins, W. Production and Characterization of Slow Pyrolysis Biochar: Influence of Feedstock Type and Pyrolysis Conditions. *GCB Bioenergy* **2013**, *5* (2), 104–115.

(17) Brown, R. C.; del Campo, B.; Boateng, A. A.; Garcia-Perez, M.; Mašek, O. Fundamentals of Biochar Production. In *Biochar for Environmental Management: Science, Technology and Implementation*; Lehmann, J., Joseph, S., Eds.; Taylor & Francis Group: London, U.K., 2015; pp 39–61.

(18) Williams, P. T.; Besler, S. The Influence of Temperature and Heating Rate on the Slow Pyrolysis of Biomass. *Renew. Energy* **1996**, *7* (3), 233–250.

(19) Shuai, L.; Luterbacher, J. Organic Solvent Effects in Biomass Conversion Reactions. *ChemSusChem* **2016**, *9* (2), 133–155.

(20) Kawamoto, H.; Hatanaka, W.; Saka, S. Thermochemical Conversion of Cellulose in Polar Solvent (Sulfolane) into Levoglucosan and Other Low Molecular-Weight Substances. *J. Anal. Appl. Pyrolysis* **2003**, *70*, 303–313.

(21) Ghosh, A.; Brown, R. C.; Bai, X. Production of Solubilized Carbohydrate from Cellulose Using Non-Catalytic, Supercritical Depolymerization in Polar Aprotic Solvents. *Green Chem.* **2016**, *18* (4), 1023–1031.

(22) Ishikawa, Y.; Saka, S. Chemical Conversion of Cellulose as Treated in Supercritical Methanol. *Cellulose* **2001**, *8*, 189–195.

(23) Mellmer, M. A.; Martin Alonso, D.; Luterbacher, J. S.; Gallo, J. M. R.; Dumesic, J. A. Effects of γ-Valerolactone in Hydrolysis of Lignocellulosic Biomass to Monosaccharides. *Green Chem.* **2014**, *16* (11), 4659–4662.

(24) Shuai, L.; Amiri, M. T.; Questell-Santiago, Y. M.; Héroguel, F.; Li, Y.; Kim, H.; Meilan, R.; Chapple, C.; Ralph, J.; Luterbacher, J. S. Formaldehyde Stabilization Facilitates Lignin Monomer Production during Biomass Depolymerization. *Science (80-.).* **2016**, *354* (6310), 329–333.

(25) Garcia-Perez, M.; Wang, X. S.; Shen, J.; Rhodes, M. J.; Tian, F.; Lee, W. J.; Wu, H.; Li, C. Z. Fast Pyrolysis of Oil Mallee Woody Biomass: Effect of Temperature on the Yield and Quality of Pyrolysis Products. *Ind. Eng. Chem. Res.* **2008**, *47* (6), 1846–1854.

(26) Reed, T. B.; Das, A. *Handbook of Biomass Downdraft Gasifier Engine Systems*; Golden, Colorado, 1988.

(27) van der Drift, A.; Boerrigter, H.; Coda, B.; Cieplik, M. K.; Hemmes, K. *Entrained Flow Gasification of Biomass: Ash Behaviour, Feeding Issues, and System Analyses*; 2004.

(28) Chhiti, Y.; Kemiha, M. Thermal Conversion of Biomass, Pyrolysis and Gasification : A Review. *Int. J. Eng. Siences* **2013**, *2* (3), 75–85.

(29) Gowlett, J. A. J. The Discovery of Fire by Humans: A Long and Convoluted Process. *Philos. Trans. R. Soc. B Biol. Sci.* **2016**, *371* (1696), 20150164.

(30) Glassman, I.; Yetter, R. A.; Glumac, N. G. Combustion of Nonvolatile Fuels. In *Combustion*; Elsevier Inc., 2014; pp 477–536.

(31) Kuzhiyil, N.; Dalluge, D.; Bai, X.; Kim, K. H.; Brown, R. C. Pyrolytic Sugars from Cellulosic Biomass. *ChemSusChem* **2012**, *5* (11), 2228–2236.

(32) Dalluge, D. L.; Daugaard, T.; Johnston, P.; Kuzhiyil, N.; Wright, M. M.; Brown, R. C. Continuous Production of Sugars from Pyrolysis of Acid-Infused Lignocellulosic Biomass. *Green Chem.* **2014**, 4144–4155.

(33) Vinu, R.; Broadbelt, L. J. A Mechanistic Model of Fast Pyrolysis of Glucose-Based Carbohydrates to Predict Bio-Oil Composition. *Energy Environ. Sci.* **2012**, *5* (12), 9808–9826.

(34) Zhou, X.; Nolte, M. W.; Mayes, H. B.; Shanks, B. H.; Broadbelt, L. J. Experimental and Mechanistic Modeling of Fast Pyrolysis of Neat Glucose-Based Carbohydrates. 1. Experiments and Development of a Detailed Mechanistic Model. *Ind. Eng. Chem. Res.* **2014**, *53* (34), 13274–13289.

(35) Zhou, X.; Nolte, M. W.; Shanks, B. H.; Broadbelt, L. J. Experimental and Mechanistic Modeling of Fast Pyrolysis of Neat Glucose-Based Carbohydrates. 2. Validation and Evaluation of the Mechanistic Model. *Ind. Eng. Chem. Res.* **2014**, *53* (34), 13290–13301.

(36) Zhou, X.; Li, W.; Mabon, R.; Broadbelt, L. J. A Mechanistic Model of Fast Pyrolysis of Hemicellulose. *Energy Environ. Sci.* **2018**, *11* (5), 1240–1260.

(37) Yanez, A. J.; Natarajan, P.; Li, W.; Mabon, R.; Broadbelt, L. J. Coupled Structural and Kinetic Model of Lignin Fast Pyrolysis. *Energy & Fuels* **2018**, *32* (2), 1822–1830.

(38) Diebold, J. P. A Unified, Global Model for the Pyrolysis of Cellulose. *Biomass and Bioenergy* **1994**, *7* (1–6), 75–85.

(39) Burnham, A. K.; Zhou, X.; Broadbelt, L. J. Critical Review of the Global Chemical Kinetics of Cellulose Thermal Decomposition. *Energy & Fuels* **2015**, *29* (5), 2906–2918.

(40) Ranzi, E.; Debiagi, P. E. A.; Frassoldati, A. Mathematical Modeling of Fast Biomass Pyrolysis and Bio-Oil Formation. Note I: Kinetic Mechanism of Biomass Pyrolysis. *ACS Sustain. Chem. Eng.* **2017**, *5* (4), 2867–2881.

(41) Piskorz, J.; Majerski, P.; Radlein, D.; Vladars-Usas, A.; Scott, D. S. Flash Pyrolysis of Cellulose for Production of Anhydro-Oligomers. *J. Anal. Appl. Pyrolysis* **2000**, *56* (2), 145–166.

(42) Thompson, L. C.; Ciesielski, P. N.; Jarvis, M. W.; Mukarakate, C.; Nimlos, M. R.; Donohoe, B. S. Estimating the Temperature Experienced by Biomass Particles during Fast Pyrolysis Using Microscopic Analysis of Biochars. *Energy & Fuels* **2017**, *31* (8), 8193–8201.

(43) Boutin, O.; Ferrer, M.; Lédé, J. Flash Pyrolysis of Cellulose Pellets Submitted to a Concentrated Radiation: Experiments and Modelling. *Chem. Eng. Sci.* **2002**, *57*, 15–25.

(44) Lédé, J.; Blanchard, F.; Boutin, O. Radiant Flash Pyrolysis of Cellulose Pellets: Products and Mechanisms Involved in Transient and Steady State Conditions. *Fuel* **2002**, *81* (10), 1269–1279.

(45) Liu, Q.; Wang, S.; Wang, K.; Guo, X.; Luo, Z.; Cen, K. Mechanism of Formation and Consequent Evolution of Active Cellulose during Cellulose Pyrolysis. *Acta Physico-Chimica Sin.* **2008**, *24* (11), 1957–1963.

(46) Krumm, C.; Pfaendtner, J.; Dauenhauer, P. J. Millisecond Pulsed Films Unify the Mechanisms of Cellulose Fragmentation. *Chem. Mater.* **2016**, *28*, 3108–3114.

(47) Lindstrom, J. K.; Ciesielski, P. N.; Johnston, P. A.; Peterson, C. A.; Gable, P.; Brown, R. C. Thermal Deconstruction Opens Biomass for Acid Hydrolysis to Monomeric Sugars. In *AIChE Annual Meeting*; Minneapolis, MN, 2017.

(48) Lindstrom, J. K.; Proano-Aviles, J.; Johnston, P. A.; Peterson, C. A.; Stansell, J. S.; Brown, R. C.; Johnston, P. A.; Brown, R. C. Competing Reactions Limit Levoglucosan Yield during Fast Pyrolysis of Cellulose. *Green Chem.* **2019**, *21*, 178–186.

(49) Gable, P.; Brown, R. C. Effect of Biomass Heating Time on Bio-Oil Yields in a Free Fall Fast Pyrolysis Reactor. *Fuel* **2016**, *166*, 361–366.

(50) Maduskar, S.; Facas, G. G.; Papageorgiou, C.; Williams, C. L.; Dauenhauer, P. J. Five Rules for Measuring Biomass Pyrolysis Rates: Pulse-Heated Analysis of Solid Reaction Kinetics of Lignocellulosic Biomass. *ACS Sustain. Chem. Eng.* **2018**, *6* (1), 1387–1399.

(51) Tiarks, J. A. Investigation of Fundamental Transport and Physicochemical Phenomena in Lignocellulosic Fast Pyrolysis, Iowa State University, 2018.

(52) Teixeira, A. R.; Mooney, K. G.; Kruger, J. S.; Williams, C. L.; Suszynski, W. J.; Schmidt, L. D.; Schmidt, D. P.; Dauenhauer, P. J. Aerosol Generation by Reactive Boiling Ejection of Molten Cellulose. *Energy Environ. Sci.* **2011**, *4*, 4306.

(53) Teixeira, A. R.; Gantt, R.; Joseph, K. E.; Maduskar, S.; Paulsen, A. D.; Krumm, C.; Zhu, C.; Dauenhauer, P. J. Spontaneous Aerosol Ejection: Origin of Inorganic Particles in Biomass Pyrolysis. *ChemSusChem* **2016**, *9* (11), 1322–1328.

(54) Zhang, J.; Choi, Y. S.; Yoo, C. G.; Kim, T. H.; Brown, R. C.; Shanks, B. H. Cellulose–Hemicellulose and Cellulose–Lignin Interactions during Fast Pyrolysis. *ACS Sustain. Chem. Eng.* **2015**, *3* (2), 293–301.

(55) Lédé, J. Cellulose Pyrolysis Kinetics: An Historical Review on the Existence and Role of Intermediate Active Cellulose. *J. Anal. Appl. Pyrolysis* **2012**, *94*, 17–32.

(56) Radlein, D. S.; Grinshpun, A.; Piskorz, J.; Scott, D. S. On the Presence of Anhydro-Oligosaccharides in the Sirups from the Fast Pyrolysis of Cellulose. *J. Anal. Appl. Pyrolysis* **1987**, *12* (1), 39–49.

(57) Lin, Y.-C.; Cho, J.; Tompsett, G. A.; Westmoreland, P. R.; Huber, G. W. Kinetics and Mechanism of Cellulose Pyrolysis. *J. Phys. Chem. C* **2009**, *113* (46), 20097–20107.

(58) Chu, S.; Subrahmanyam, A. V; Huber, G. W. The Pyrolysis Chemistry of a β-O-4 Type Oligomeric Lignin Model Compound. *Green Chem.* **2013**, *15* (1), 125–136.

(59) Kim, K. H.; Bai, X.; Brown, R. C. Pyrolysis Mechanisms of Methoxy Substituted α-O-4 Lignin Dimeric Model Compounds and Detection of Free Radicals Using Electron Paramagnetic Resonance Analysis. *J. Anal. Appl. Pyrolysis* **2014**, *110*, 254–263.

(60) Paine, J. B.; Pithawalla, Y. B.; Naworal, J. D.; Thomas, C. E. Carbohydrate Pyrolysis Mechanisms from Isotopic Labeling Part 1: The Pyrolysis of Glycerin: Discovery of Competing Fragmentation Mechanisms Affording Acetaldehyde and Formaldehyde and the Implications for Carbohydrate Pyrolysis. *J. Anal. Appl. Pyrolysis* **2007**, *80* (2), 297–311.

(61) Paine, J. B.; Pithawalla, Y. B.; Naworal, J. D. Carbohydrate Pyrolysis Mechanisms from Isotopic Labeling Part 2. The Pyrolysis of D-Glucose: General Disconnective Analysis and the Formation of C1 and C2 Carbonyl Compounds by Electrocyclic Fragmentation Mechanisms. *J. Anal. Appl. Pyrolysis* **2008**, *82* (1), 10–41.

(62) Degenstein, J. C.; Murria, P.; Easton, M.; Sheng, H.; Hurt, M.; Dow, A. R.; Gao, J.; Nash, J. J.; Agrawal, R.; Delgass, W. N.; et al. Fast Pyrolysis of 13C-Labeled Cellobioses: Gaining Insights into the Mechanisms of Fast Pyrolysis of Carbohydrates. *J. Org. Chem.* **2015**, *80* (3), 1909–1914.

(63) Hutchinson, C. P.; Lee, Y. J. Evaluation of Primary Reaction Pathways in Thin-Film Pyrolysis of Glucose Using 13C Labeling and Real-Time Monitoring. *ACS Sustain. Chem. Eng.* **2017**, *5* (10), 8796–8803.

(64) Lynch, B. J.; Fast, P. L.; Harris, M.; Truhlar, D. G. Adiabatic Connection for Kinetics. *J. Phys. Chem. A* **2000**, *104* (21), 4811–4815.

(65) Bahng, M. K.; Donohoe, B. S.; Nimlos, M. R. Application of an Fourier Transform-Infrared Imaging Tool for Measuring Temperature or Reaction Profiles in Pyrolyzed Wood. *Energy & Fuels* **2011**, *25* (1), 370–378.

(66) Ciesielski, P. N.; Crowley, M. F.; Nimlos, M. R.; Sanders, A. W.; Wiggins, G. M.; Robichaud, D.; Donohoe, B. S.; Foust, T. D. Biomass Particle Models with Realistic Morphology and Resolved Microstructure for Simulations of Intraparticle Transport Phenomena. *Energy & Fuels* **2015**, *29* (1), 242–254.

(67) Wiggins, G. M.; Ciesielski, P. N.; Daw, C. S. Low-Order Modeling of Internal Heat Transfer in Biomass Particle Pyrolysis. *Energy & Fuels* **2016**, *30* (6), 4960–4969.

(68) Pecha, M. B.; Garcia-Perez, M.; Foust, T. D.; Ciesielski, P. N. Estimation of Heat Transfer Coefficients for Biomass Particles by Direct Numerical Simulation Using Microstructured Particle Models in the Laminar Regime. *ACS Sustain. Chem. Eng.* **2017**, *5* (1), 1046–1053.

(69) Austin, L. W.; Eastman, C. W. On the Relation between Heat Conductivity and Density in Some of the Common Woods. *Wisconsin Acad. Sci. Arts, Lett.* **1900**, 539–543.

(70) Mason, P. E.; Darvell, L. I.; Jones, J. M.; Williams, A. Comparative Study of the Thermal Conductivity of Solid Biomass Fuels. *Energy & Fuels* **2016**, *30* (3), 2158–2163.

(71) Forest Products Laboratory. *Wood Handbook: Wood as an Engineering Material*; Madison, Wisconsin, 2010; Vol. FPL–GTR–19.

(72) Pan, Y.; Kong, S.-C. Simulation of Biomass Particle Evolution under Pyrolysis Conditions Using Lattice Boltzmann Method. *Combust. Flame* **2017**, *178*, 21–34.

(73) Pan, Y.; Kong, S.-C. Predicting Effects of Operating Conditions on Biomass Fast Pyrolysis Using Particle-Level Simulation. *Energy & Fuels* **2017**, *31* (1), 635–646.

(74) Himmel, M. E.; Tucker, M.; Baker, J.; Rivard, C.; Oh, K.; Grohmann, K. Comminution of Biomass: Hammer and Knife Mills. *Biotechnol. Bioeng. Symp.* **1986**, *15* (15), 39–58.

(75) Haas, T. J.; Nimlos, M. R.; Donohoe, B. S. Real-Time and Post-Reaction Microscopic Structural Analysis of Biomass Undergoing Pyrolysis. *Energy & Fuels* **2009**, *23* (7), 3810–3817.

(76) Assary, R. S.; Curtiss, L. A. Comparison of Sugar Molecule Decomposition through Glucose and Fructose: A High-Level Quantum Chemical Study. *Energy & Fuels* **2012**, *26* (2), 1344–1352.

(77) Vosko, S. H.; Wilk, L.; Nusair, M. Accurate Spin-Dependent Electron Liquid Correlation Energies for Local Spin Density Calculations: A Critical Analysis. *Can. J. Phys.* **1980**, *58* (8), 1200–1211.

(78) Becke, A. D. Density-functional Thermochemistry. III. The Role of Exact Exchange. *J. Chem. Phys.* **1993**, *98* (7), 5648–5652.

(79) Lee, C.; Yang, E.; Parr, R. R. G.; Yang, W.; Parr, R. R. G. Development of the Colle-Salvetti Correlation Energy Formula into a Functional of the Electron Density. *Phys. Rev. B* **1988**, *37* (2), 785–789.

(80) Stephens, P. J.; Devlin, F. J.; Chabalowski, C. F.; Frisch, M. J. Ab Initio Calculation of Vibrational Absorption and Circular Dichroism Spectra Using Density Functional Force Fields. *J. Phys. Chem.* **1994**, *98* (45), 11623–11627.

(81) Huang, J.; Liu, C.; Wei, S.; Huang, X.; Li, H. Density Functional Theory Studies on Pyrolysis Mechanism of β-d-Glucopyranose. *J. Mol. Struct. THEOCHEM* **2010**, *958* (1–3), 64–70.

(82) Wang, S.; Ru, B.; Lin, H.; Luo, Z. Degradation Mechanism of Monosaccharides and Xylan under Pyrolytic Conditions with Theoretic Modeling on the Energy Profiles. *Bioresour. Technol.* **2013**, *143*, 378–383.

(83) Huang, X.; Liu, C.; Huang, J.; Li, H. Theory Studies on Pyrolysis Mechanism of Phenethyl Phenyl Ether. *Comput. Theor. Chem.* **2011**, *976* (1–3), 51–59.

(84) Zhao, Y.; Truhlar, D. G. The M06 Suite of Density Functionals for Main Group Thermochemistry, Thermochemical Kinetics, Noncovalent Interactions, Excited States, and Transition Elements: Two New Functionals and Systematic Testing of Four M06-Class Functionals and 12 Other Function. *Theor. Chem. Acc.* **2008**, *120* (1–3), 215–241.

(85) Zhao, Y.; Truhlar, D. G. Density Functional for Spectroscopy: No Long-Range Self-Interaction Error, Good Performance for Rydberg and Charge-Transfer States, and Better Performance on Average than B3LYP for Ground States. *J. Phys. Chem. A* **2006**, *110* (49), 13126–13130.

(86) Dedic, C.; Tiarks, J. A.; Sanderson, P. D.; Brown, R. C.; Michael, J. B.; Meyer, T. R. Optical Diagnostic Techniques for Investigation of Biomass Pyrolysis. In *Fourth International Conference on Thermochemical Biomass Conversion Science*; Chicago, IL, 2015.

(87) Patwardhan, P. R.; Satrio, J. A.; Brown, R. C.; Shanks, B. H. Product Distribution from Fast Pyrolysis of Glucose-Based Carbohydrates. *J. Anal. Appl. Pyrolysis* **2009**, *86* (2), 323–330.

(88) Patwardhan, P. R.; Satrio, J. A.; Brown, R. C.; Shanks, B. H. Influence of Inorganic Salts on the Primary Pyrolysis Products of Cellulose. *Bioresour. Technol.* **2010**, *101* (12), 4646–4655.

(89) Atalla, R. H.; Brady, J. W.; Matthews, J. F.; Ding, S.-Y.; Himmel, M. E. Structures of Plant Cell Wall Celluloses. In *Biomass Recalcitrance: Deconstructing the Plant Cell Wall for Bioenergy*; Himmel, M. E., Ed.; Wiley, 2008; pp 188–210.

(90) Zhang, J.; Nolte, M. W.; Shanks, B. H. Investigation of Primary Reactions and Secondary Effects from the Pyrolysis of Different Celluloses. *ACS Sustain. Chem. Eng.* **2014**, *2* (12), 2820–2830.

(91) Mukarakate, C.; Mittal, A.; Ciesielski, P. N.; Budhi, S.; Thompson, L.; Iisa, K.; Nimlos, M. R.; Donohoe, B. S. Influence of Crystal Allomorph and Crystallinity on the Products and Behavior of Cellulose during Fast Pyrolysis. *ACS Sustain. Chem. Eng.* **2016**, *4* (9), 4662–4674.

(92) Assary, R. S.; Curtiss, L. A. Thermochemistry and Reaction Barriers for the Formation of Levoglucosenone from Cellobiose. *ChemCatChem* **2012**, *4* (2), 200–205.

(93) Wang, S.; Guo, X.; Liang, T.; Zhou, Y.; Luo, Z. Mechanism Research on Cellulose Pyrolysis by Py-GC/MS and Subsequent Density Functional Theory Studies. *Bioresour. Technol.* **2012**, *104*, 722–728.

(94) Seshadri, V.; Westmoreland, P. R. Concerted Reactions and Mechanism of Glucose Pyrolysis and Implications for Cellulose Kinetics. *J. Phys. Chem. A* **2012**, *116* (49), 11997–12013.

(95) Zhang, X.; Li, J.; Yang, W.; Blasiak, W. Formation Mechanism of Levoglucosan and Formaldehyde during Cellulose Pyrolysis. *Energy & Fuels* **2011**, *25* (8), 3739–3746.

(96) Mayes, H. B.; Broadbelt, L. J. Unraveling the Reactions That Unravel Cellulose. *J. Phys. Chem. A* **2012**, *116* (26), 7098–7106.

(97) Zhang, X.; Yang, W.; Dong, C. Levoglucosan Formation Mechanisms during Cellulose Pyrolysis. *J. Anal. Appl. Pyrolysis* **2013**, *104*, 19–27.

(98) Nimlos, M. R.; Evans, R. J. Levoglucosan Pyrolysis. *Fuel Chem. Div. Prepr.* **2002**, *47* (1), 393.

(99) Zhang, X.; Yang, W.; Blasiak, W. Thermal Decomposition Mechanism of Levoglucosan during Cellulose Pyrolysis. *J. Anal. Appl. Pyrolysis* **2012**, *96*, 110–119.

(100) Lu, Q.; Zhang, Y.; Dong, C.; Yang, Y.-P.; Yu, H. The Mechanism for the Formation of Levoglucosenone during Pyrolysis of β-d-Glucopyranose and Cellobiose: A Density Functional Theory Study. *J. Anal. Appl. Pyrolysis* **2014**, *110* (1), 34–43.

(101) Zhang, Y.; Liu, C.; Chen, X. Unveiling the Initial Pyrolytic Mechanisms of Cellulose by DFT Study. *J. Anal. Appl. Pyrolysis* **2015**, *113*, 621–629.

(102) Mayes, H. B.; Nolte, M. W.; Beckham, G. T.; Shanks, B. H.; Broadbelt, L. J. The Alpha-Bet(a) of Glucose Pyrolysis: Computational and Experimental Investigations of 5-Hydroxymethylfurfural and Levoglucosan Formation Reveal Implications for Cellulose Pyrolysis. *ACS Sustain. Chem. Eng.* **2014**, *2* (6), 1461–1473.

(103) Zhang, Y.; Liu, C.; Xie, H. Mechanism Studies on β-d-Glucopyranose Pyrolysis by Density Functional Theory Methods. *J. Anal. Appl. Pyrolysis* **2014**, *105*, 23–34.

(104) Wang, M.; Liu, C.; Xu, X.; Li, Q. Theoretical Investigation on the Carbon Sources and Orientations of the Aldehyde Group of Furfural in the Pyrolysis of Glucose. *J. Anal. Appl. Pyrolysis* **2016**, *120*, 464–473.

(105) Liu, D.; Yu, Y.; Wu, H. Evolution of Water-Soluble and Water-Insoluble Portions in the Solid Products from Fast Pyrolysis of Amorphous Cellulose. *Ind. Eng. Chem. Res.* **2013**, *52* (36), 12785–12793.

(106) Gong, X.; Yu, Y.; Gao, X.; Qiao, Y.; Xu, M.; Wu, H. Formation of Anhydro-Sugars in the Primary Volatiles and Solid Residues from Cellulose Fast Pyrolysis in a Wire-Mesh Reactor. *Energy & Fuels* **2014**, *28* (8), 5204–5211.

(107) Patwardhan, P. R.; Brown, R. C.; Shanks, B. H. Product Distribution from the Fast Pyrolysis of Hemicellulose. *ChemSusChem* **2011**, *4* (5), 636–643.

(108) Werner, K.; Pommer, L.; Broström, M. Thermal Decomposition of Hemicelluloses. *J. Anal. Appl. Pyrolysis* **2014**, *110*, 130–137.

(109) Zhou, X.; Li, W.; Mabon, R.; Broadbelt, L. J. A Critical Review on Hemicellulose Pyrolysis. *Energy Technol.* **2017**, *5* (1), 216.

(110) Holtzapple, M. T. Hemicelluloses. In *Encyclopedia of Food Sciences and Nutrition*; Caballero, B., Ed.; Elsevier, 2003; pp 3060–3071.

(111) Bikova, T.; Treimanis, A. Solubility and Molecular Weight of Hemicelluloses from Alnus Incana and Alnus Glutinosa. Effect of Tree Age. *Plant Physiol. Biochem.* **2002**, *40* (4), 347–353.

(112) Kurata, Y.; Mori, Y.; Ishida, A.; Nakajima, M.; Ito, N.; Hamada, M.; Yamashita, K.; Fujiwara, T.; Tonosaki, M.; Katayama, Y. Variation in Hemicellulose Structure and Assembly in the Cell Wall Associated with the Transition from Earlywood to Latewood in Cryptomeria Japonica. *J. Wood Chem. Technol.* **2018**, *38* (3), 254–263.

(113) Meier, H. General Chemistry of Cell Walls and Distribution of the Chemical Constituents across the Walls. In *The Formation of Wood in Forest Trees*; Zimmerman, M. H., Ed.; Elsevier, 1964; pp 137–151.

(114) Wang, M.; Liu, C.; Li, Q.; Xu, X. Theoretical Insight into the Conversion of Xylose to Furfural in the Gas Phase and Water. *J. Mol. Model.* **2015**, *21* (11), 296.

(115) Huang, J.; He, C.; Wu, L.; Tong, H. Theoretical Studies on Thermal Decomposition Mechanism of Arabinofuranose. *J. Energy Inst.* **2017**, *90* (3), 372–381.

(116) Lu, Q.; Tian, H. Y.; Hu, B.; Jiang, X. Y.; Dong, C. Q.; Yang, Y. P. Pyrolysis Mechanism of Holocellulose-Based Monosaccharides: The Formation of Hydroxyacetaldehyde. *J. Anal. Appl. Pyrolysis* **2016**, *120*, 15–26.

(117) Huang, J.; He, C.; Wu, L.; Tong, H. Thermal Degradation Reaction Mechanism of Xylose: A DFT Study. *Chem. Phys. Lett.* **2016**, *658*, 114–124.

(118) Patwardhan, P. R.; Brown, R. C.; Shanks, B. H. Understanding the Fast Pyrolysis of Lignin. *ChemSusChem* **2011**, *4* (11), 1629–1636.

(119) Kim, J. Y.; Oh, S.; Hwang, H.; Kim, U. J.; Choi, J. W. Structural Features and Thermal Degradation Properties of Various Lignin Macromolecules Obtained from Poplar Wood (Populus Albaglandulosa). *Polym. Degrad. Stab.* **2013**, *98* (9), 1671–1678.

(120) Katahira, R.; Elder, T. J.; Beckham, G. T. A Brief Introduction to Lignin Structure. In *Lignin Valorization: Emerging Approaches*; Beckham, G. T., Ed.; Royal Society of Chemistry: London, UK, 2018; pp 1–20.

(121) Houtman, C. Lessons Learned from 150 Years of Pulping Wood. In *Lignin Valorization: Emerging Approaches*; Beckham, G. T., Ed.; Royal Society of Chemistry: London, UK, 2018; pp 62–73.

(122) Ragauskas, A. J.; Beckham, G. T.; Biddy, M. J.; Chandra, R.; Chen, F.; Davis, M. F.; Davison, B. H.; Dixon, R. A.; Gilna, P.; Keller, M.; et al. Lignin Valorization: Improving Lignin Processing in the Biorefinery. *Science (80-.).* **2014**, *344* (6185), 1246843–1246843.

(123) Rencoret, J.; Gutierrez, A.; Nieto, L.; Jimenez-Barbero, J.; Faulds, C. B.; Kim, H.; Ralph, J.; Martinez, A. T.; del Rio, J. C. Lignin Composition and Structure in Young versus Adult Eucalyptus Globulus Plants. *Plant Physiol.* **2011**, *155* (2), 667–682.

(124) Grabber, J. H. How Do Lignin Composition, Structure, and Cross-Linking Affect Degradability? A Review of Cell Wall Model Studies. *Crop Sci.* **2005**, *45* (3), 820.

(125) Li, M.; Pu, Y.; Ragauskas, A. J. Current Understanding of the Correlation of Lignin Structure with Biomass Recalcitrance. *Front. Chem.* **2016**, *4*, 45.

(126) Jiang, G.; Nowakowski, D. J.; Bridgwater, A. V. Effect of the Temperature on the Composition of Lignin Pyrolysis Products. *Energy & Fuels* **2010**, *24* (8), 4470–4475.

(127) Kim, J.-Y.; Hwang, H.; Oh, S.; Kim, Y.-S.; Kim, U.-J.; Choi, J. W. Investigation of Structural Modification and Thermal Characteristics of Lignin after Heat Treatment. *Int. J. Biol. Macromol.* **2014**, *66*, 57–65.

(128) Kawamoto, H. Lignin Pyrolysis Reactions. *J. Wood Sci.* **2017**, *63* (2), 117–132.

(129) Jarvis, M. W.; Daily, J. W.; Carstensen, H.-H.; Dean, A. M.; Sharma, S.; Dayton, D. C.; Robichaud, D. J.; Nimlos, M. R. Direct Detection of Products from the Pyrolysis of 2-Phenethyl Phenyl Ether. *J. Phys. Chem. A* **2011**, *115* (4), 428–438.

(130) Hoffmann, H. M. R. The Ene Reaction. *Angew. Chemie Int. Ed. English* **1969**, *8* (8), 556–577.

(131) Maccoll, A. Heterolysis and the Pyrolysis of Alkyl Halides in the Gas Phase. *Chem. Rev.* **1969**, *69* (1), 33–60.

(132) Elder, T.; Beste, A. Density Functional Theory Study of the Concerted Pyrolysis Mechanism for Lignin Models. *Energy & Fuels* **2014**, *28* (8), 5229–5235.

(133) Huang, J.; Liu, C.; Wu, D.; Tong, H.; Ren, L. Density Functional Theory Studies on Pyrolysis Mechanism of β-O-4 Type Lignin Dimer Model Compound. *J. Anal. Appl. Pyrolysis* **2014**, *109*, 98–108.

(134) Chen, L.; Ye, X.; Luo, F.; Shao, J.; Lu, Q.; Fang, Y.; Wang, X.; Chen, H. Pyrolysis Mechanism of β-O-4 Type Lignin Model Dimer. *J. Anal. Appl. Pyrolysis* **2015**, *115*, 103–111.

(135) Mayes, H. B.; Nolte, M. W.; Beckham, G. T.; Shanks, B. H.; Broadbelt, L. J. The Alpha-Bet(a) of Salty Glucose Pyrolysis: Computational Investigations Reveal Carbohydrate Pyrolysis Catalytic Action by Sodium Ions. *ACS Catal.* **2015**, *5* (1), 192–202.

(136) Zhang, Y.; Liu, C. A New Horizon on Effects of Alkalis Metal Ions during Biomass Pyrolysis Based on Density Function Theory Study. *J. Anal. Appl. Pyrolysis* **2014**, *110* (1), 297–304.

(137) Prins, M. J.; Ptasinski, K. J.; Janssen, F. J. J. G. Torrefaction of Wood. Part 2. Analysis of Products. *J. Anal. Appl. Pyrolysis* **2006**, *77* (1), 35–40.

(138) Mullen, C. A.; Boateng, A. A.; Goldberg, N. M.; Lima, I. M.; Laird, D. A.; Hicks, K. B. Bio-Oil and Bio-Char Production from Corn Cobs and Stover by Fast Pyrolysis. *Biomass and Bioenergy* **2010**, *34* (1), 67–74.

(139) Abdoulmoumine, N.; Kulkarni, A.; Adhikari, S. Effects of Temperature and Equivalence Ratio on Pine Syngas Primary Gases and Contaminants in a Bench-Scale Fluidized Bed Gasifier. *Ind. Eng. Chem. Res.* **2014**, *53* (14), 5767–5777.

(140) Liu, C.; Huang, J.; Huang, X.; Li, H.; Zhang, Z. Theoretical Studies on Formation Mechanisms of CO and CO2 in Cellulose Pyrolysis. *Comput. Theor. Chem.* **2011**, *964* (1), 207–212.

(141) Huang, J.; Liu, C.; Tong, H.; Li, W.; Wu, D. A Density Functional Theory Study on Formation Mechanism of CO, CO2 and CH4 in Pyrolysis of Lignin. *Comput. Theor. Chem.* **2014**, *1045*, 1–9.

(142) Beckham, G. T.; Matthews, J. F.; Peters, B.; Bomble, Y. J.; Himmel, M. E.; Crowley, M. F. Molecular-Level Origins of Biomass Recalcitrance: Decrystallization Free Energies for Four Common Cellulose Polymorphs. *J. Phys. Chem. B* **2011**, *115* (14), 4118–4127.

(143) Matthews, J. F.; Himmel, M. E.; Crowley, M. F. Conversion of Cellulose Iα to Iβ via a High Temperature Intermediate (I-HT) and Other Cellulose Phase Transformations. *Cellulose* **2012**, *19* (1), 297–306.

(144) Bu, L.; Himmel, M. E.; Crowley, M. F. The Molecular Origins of Twist in Cellulose I-Beta. *Carbohydr. Polym.* **2015**, *125*, 146–152.

(145) Matthews, J. F.; Bergenstråhle, M.; Beckham, G. T.; Himmel, M. E.; Nimlos, M. R.; Brady, J. W.; Crowley, M. F. High-Temperature Behavior of Cellulose I. *J. Phys. Chem. B* **2011**, *115* (10), 2155–2166.

(146) Payne, C. M.; Himmel, M. E.; Crowley, M. F.; Beckham, G. T. Decrystallization of Oligosaccharides from the Cellulose Iβ Surface with Molecular Simulation. *J. Phys. Chem. Lett.* **2011**, *2* (13), 1546–1550.

CHAPTER 2 COMPETING REACTIONS LIMIT LEVOGLUCOSAN YIELD DURING FAST PYROLYSIS OF CELLULOSE

Jake K. Lindstrom,[a] Juan Proano-Aviles,[a,b] Patrick A. Johnston,[c] Chad A. Peterson,[a] Jackson S. Stansell,[c] Robert C. Brown[a,c]

a- Department of Mechanical Engineering, Iowa State University, Ames, IA 50011, USA

b- Universidad San Francisco de Quito, Quito, Ecuador

c- Bioeconomy Institute, Iowa State University, Ames, IA 50011, USA

Article reprinted from Green Chemistry with permission from the Royal Society of Chemistry.

Abstract

Efforts to understand the reaction mechanisms of cellulose pyrolysis have been stymied by short reaction times and difficulties in probing the condensed phase of cellulose intermediate products. Using time-resolved yields of both volatile and non-volatile products of pyrolysis, we demonstrate that cracking reactions generate anhydro-oligosaccharides while subsequent reactions produce levoglucosan from these anhydro-oligosaccharides. Eventually, cracking of anhydro-oligosaccharides is eclipsed by levoglucosan-producing reactions. These reactions compete with other reactions that produce light oxygenates and non-condensable gases. The relative reaction rates in this competition limit levoglucosan yields from cellulose pyrolysis to approximately 60 wt%.

Keywords

Anhydro-oligosaccharides, Cellulose, Depolymerization, Levoglucosan, Pyrolysis

Introduction

Thermal deconstruction of lignocellulosic biomass, by processes such as fast pyrolysis and solvent liquefaction, is a promising approach for producing renewable fuels

and chemicals.[1] In the ideal manifestation of thermal deconstruction, heat provides the energy to crack the biopolymers making up lignocellulose into monomers and dimers.[2,3] In particular, cellulose yields predominantly the anhydro-monosaccharide levoglucosan (1,6-anhydro-β-D-glucopyranose) and anhydro-disaccharides, such as cellobiosan.[4,5] In practice, cellulose also yields less desirable aldehydes, ketones, carboxylic acids, and furans[5,6] from the fragmentation of pyranose rings.[7–11]

The non-sugar products of polysaccharide thermal deconstruction are in part the product of reactions catalyzed by naturally occurring alkali and alkaline earth metals (AAEM) in lignocellulosic biomass[12] or metal contamination in poorly prepared polysaccharide samples.[3] These metals serve as strong ring-fragmentation catalysts,[2] likely due to ion-dipole forces altering reaction rate coeffecients.[13] Careful purification of polysaccharide samples or passivation of AAEM in lignocellulosic biomass can overcome this effect; however, even in the absence of AAEM and performed under well-controlled laboratory conditions, anhydro-monosaccharide yields from pyrolysis still appear to be limited to approximately 60 wt% from cellulose.[4]

Understanding the fundamental mechanisms of polysaccharide thermal deconstruction is important in designing reactors that maximize yields of simple sugars. Although pyrolysis of cellulose has been studied since the late 19th century, no consensus exists on the reactions responsible for the thermal depolymerization of this relatively simple polysaccharide.[14] In the 1960s, experiments showed that cellulose passes through a liquid state during pyrolysis, termed “active cellulose,” before further decomposing to vapor products.[14] In 1987, Radlein *et al.*[15] identified the liquid intermediate products as anhydro-oligosaccharides. (For an extensive account, see Lédé’s historical review.[14])

More recent experiments have reached general agreement that this liquid intermediate consists of anhydro-oligosaccharides consisting of relatively few monomeric units.[15–21] Cellulose and its derivative anhydro-oligosaccharides differ in two ways: degree of polymerization (DP) and the structure of a terminal monomer (Figure 2.1). Cellulose typically contains thousands of monomers[22] while the maximum measured DP of anhydro-oligosaccharides is usually no more than 7.[14,16,23] However, it should be noted that a recent study identified anhydro-oligosaccharides with DP up to 18.[18] Another difference is that cellulose is terminated by reducing and non-reducing ends while anhydro-oligosaccharides have anhydro and non-reducing ends. Cleavage of this anhydro-end monomer from an anhydro-oligosaccharide is expected to yield levoglucosan although the non-reducing end is also suspected to yield levoglucosan.[24,25]

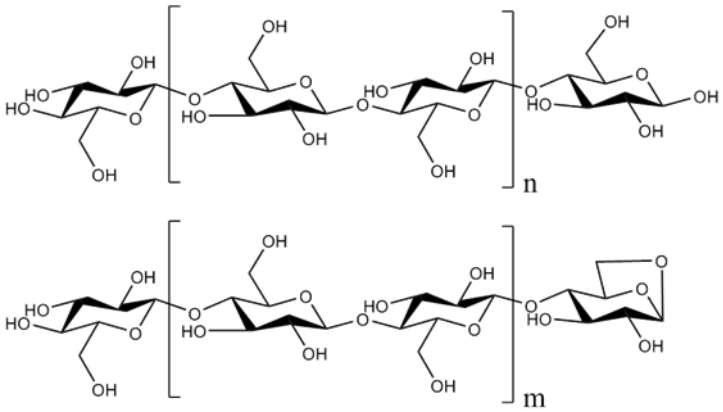

Figure 2.1. Cellulose (top) is terminated by reducing and non-reducing ends. In contrast, the anhydro-oligosaccharides (bottom) resulting from cellulose thermal depolymerization are terminated by an anhydro-end and non-reducing end.

Originally thought to be the product of heterolytic fission, pyrolytic depolymerization of cellulose and its oligomers is now widely accepted to be a concerted reaction that breaks a mid-chain glycosidic bond (not at either end of the chain) to produce two anhydro-oligosaccharides fragments.[24,26] This so-called cracking reaction

(also known as initiation) is thought to occur at purely random locations along the chain. Fragmentation at either of the extreme ends of the chain (terminal glycosidic bonds) is thought to be distinct from cracking and is characterized as either a levoglucosan-producing reaction (LPR) or a degradation reaction (DR).

Computational chemistry has provided recent guidance in understanding fragmentation reactions.[6,8,24,26,27] Although a number of LPRs have been identified,[24,26] the most likely appear to produce levoglucosan from the anhydro-end and non-reducing end of anhydro-oligosaccharides. Computational studies suggest these two LPRs have identical reaction rates.[24,25] On the other hand, Mayes and Broadbelt propose LPRs rates to be slower than cracking reactions at typical pyrolysis temperatures, although this difference lies within the margin of error.[24]

Degradation reactions constitute a diversity of reactions that form light oxygenates and non-condensable gases. The mechanisms of DRs are varied but most are pericylic reactions, likely catalyzed by hydroxyl groups on adjacent molecules.[8] Agarwal *et al.*[28] suggest that DRs are generally less thermodynamically favorable than LPRs.

Broadbelt *et al.* theorize that the majority of light oxygenates come from glucose molecules produced by thermohydrolysis reactions.[10,11,25] Thermohydrolysis entails a water molecule hydrolyzing a terminal glycosidic bond resulting in a glucose molecule and an oligosaccharide that is one monomer shorter than the original. The water for thermohydrolysis is assumed to be generated by monomer dehydration reactions.[10] Their mechanistic model predicts thermohydrolysis can occur more than twice as frequently as other reactions.[11] Furthermore, they calculate thermohydrolysis yields as high as 18 wt% glucose during the course of cellulose depolymerization, which represents 60 wt% of the

condensed phase products at that point in the reaction.[11] Despite the importance of this glucose-producing reaction to the success of the computational model in predicting levoglucosan yields, there has yet to be experimental verification of glucose as a significant reaction intermediate during cellulose pyrolysis.[15,18,19,29]

Efforts to experimentally explore the fundamental reactions of biomass pyrolysis are challenged by difficulties in analyzing short-lived intermediate products in the condensed phase. Accordingly, most experimental studies have focused on analyzing vapor products as they are volatilized from pyrolyzing biomass. Because anhydro-oligosaccharides are non-volatile, this approach to studying pyrolysis overlooks these important intermediate products.[30,31] The short-lived nature of intermediate products and the predominance of experimental methods that only detect volatile products bias studies away from the condensed phase.

The lifetime of short-lived intermediates can be prolonged by slowly heating samples, improving the prospects of sampling them from the condensed phase, but this methodology has dubious relevance to fast pyrolysis. For example, several authors have generated anhydro-oligosaccharides by gradually heating levoglucosan, hypothesizing that anhydro-oligosaccharides only form this way and not directly from cellulose. Using low heating rates conditions, typically less than 200 °C min^{-1} (3.33 °C s^{-1}),[32–34] levoglucosan, hampered by low volatility,[30] slowly evaporates leaving it susceptible to polymerization into anhydro-oligosaccharides. This gradual temperature increase provides levoglucosan additional time to repolymerize compared to typical fast pyrolysis time scales. Zhang *et al.*[35] tested this theory by attempting to pyrolyze levoglucosan in a Frontier Laboratories micropyrolyzer, which at 500 °C has a heating rate of

approximately 10,800 °C min^{-1} (180 °C s^{-1}).[36] The levoglucosan did not pyrolyze; instead it merely vaporized, indicating levoglucosan repolymerizes too slowly to be relevant to the time scales of fast pyrolysis.

Experiments using high heating rates, although they complicate intermediate product sampling, show that cellulose produces anhydro-oligosaccharides. Flash pyrolysis, in this case using a radiant heat source, can be easily terminated by turning off the radiation source.[16,23] Only the thermal mass of the cellulose and the platform holding it remain, which are often quite small, allowing for somewhat rapid cooling. These experiments[14,16,23] demonstrate that anhydro-oligosaccharides of DP 2-7 readily form directly from cellulose at a variety of temperatures. Recent work using other kinds of pyrolysis reactors that partially-pyrolyze cellulose have detected up to DP 18 anhydro-oligosaccharides, as measured by ion chromatography.[18,19] Although more than double the size of previously detected oligomers, compared to cellulose they are still relatively small. The detection of only low DP anhydro-oligosaccharides is likely due to instrumentation limits, not the absence of larger oligomers, as is discussed later in this paper.

In 2016, Dauenhauer's group, with the goal of rapidly truncating pyrolysis reactions, developed a reactor termed PHASR that both rapidly heats and cools small samples, typically thin films.[37] In 2018, they tested multiple hypotheses to see if they could increase levoglucosan yields from cellulose pyrolysis.[38] Using their PHASR they reported surprisingly low levoglucosan yields: approximately 8 wt% from cellulose pyrolysis.[38] In contrast, Frontier Laboratories micropyolyzers produce the highest repeatable levoglucosan yields from cellulose pyrolysis, around 60 wt%.[3,5,36] The reason

for this discrepancy is likely due to differences in sample preparation rather than differences in heating rate as claimed.[39] Thin film cellulose samples, typically a few micron thick,[35,40] form lumps when applied unevenly which leads to additional char formation and catalytic degradation of monomers.[35] This effect explains why some thin film samples produce low levoglucosan yields while powdered cellulose consistently produces higher yields.

Using a thin film of cellulose with the PHASR, Dauenhauer's group suggests that anhydro-oligosaccharides only form after cellulose is heated above 467 °C;[37,41] however, anhydro-oligosaccharides have been previously reported from incomplete cellulose pyrolysis performed at temperatures below 467 °C.[15,18,19,29] Confounding the issue, most of their experiments[37,41] used α-cyclodextrin (which has a DP of six) as a surrogate for cellulose (which has a DP of thousands).[22] While α-cyclodextrin may produce some volatile products at the same rate as thin film cellulose samples,[42] it cannot mimic cellulose transforming into large oligomers—a key step. Furthermore the levoglucosan yield from α-cyclodextrin, 24 wt%,[40] falls substantially short of that typically produced from powdered cellulose, approximately 60 wt%.[3,5,36] Studies focused on understanding cellulose depolymerization are likely to have more success with powdered cellulose in high heating rate reactors with proven records of producing high levoglucosan yields.

Cellulose decomposition into large oligomers and then into increasingly smaller products can be described by a logistic function, a class of ordinary differential equations with a sigmoidal solution.[43,44] These models were developed for thermal decomposition of solid, inorganic material, which can seem very dissimilar from large organic polymers; however, they describe similar phenomena: nucleation and growth. Cracking is analogous

to nucleation—a starting point for another reaction—while LPRs represent growth of decomposition product. For example, the Prout-Tompkins model,[45,46] which was developed to understand the decomposition of potassium permanganate during heating,[45] has since been applied to and closely fits cellulose pyrolysis under low heating rate conditions.[47–49] Other related solid decomposition models such as the Šesták-Berggren[50] model also fit cellulose pyrolysis.[44,48] These models, among others, were developed to understand two-step solid thermal decomposition, and appear to work well for cellulose pyrolysis[43] but have not been applied to high heating rate experiments or directly correlated to specific products.

With the goal of resolving the mechanism of anhydro-oligosaccharide and levoglucosan formation from cellulose, we examined the time evolution of both volatile and non-volatile products during fast pyrolysis of cellulose. We present the first time-resolved measurements of levoglucosan and anhydro-oligosaccharides. We correlate evolution of levoglucosan from cellulose with other volatile products. These data suggest that the yield of levoglucosan from cellulose thermal deconstruction is limited by competition between LPRs and DRs.

Materials and Methodologies

Frontier EGA/PY 3030 D micropyrolyzer

A Frontier EGA/PY 3030 D micropyrolyzer was used for the Controlled Pyrolysis Duration (CPD)-Quench reactor and Short Column (SC)-Flame Ionization Detector (FID). Proano-Aviles *et al.*[36] determined the heating rates in this micropyrolyzer at 400 and 500 °C are 140 and 180 °C s^{-1}, respectively. As sample temperature cannot be directly measured, temperatures indicated are always furnace temperature in subsequent

descriptions and discussions. The interface, a heater at the bottom of the micropyrolyzer which typically contacts a gas chromatograph inlet, was maintained at 400 °C to prevent product condensation.

All pyrolysis experiments were conducted with Sigmacell Type 50 cellulose from Sigma Aldrich. The cellulose was analyzed by High Performance Liquid Chromatography (HPLC) to check for the presence of levoglucosan: none was detected.

Samples for experiments with the CPD-Quench reactor were 500 ± 10 μg, which is small enough to avoid mass transfer issues.[4,35,36] The samples for the SC-FID tests were 75 ± 25 μg. The cellulose particles were approximately 50 μm diameter. The weight average DP was 1,871, as measured by the National Renewable Energy Laboratory[35] which is typical for cellulose. Importantly, the cellulose was derived from softwood pulps. Other sources, such as bacteria, have differently sized and shaped cellulose microfibrils and are poorly representative of lignocellulosic biomass.[51]

Controlled Pyrolysis Duration-Quench reactor

Condensed phase products from fast pyrolysis of cellulose were recovered from a custom-built CPD-Quench analytical pyrolysis system based on a Frontier PY-3030 D micropyrolyzer. This apparatus allows cellulose to be pyrolyzed during well-controlled reaction times with recovery of volatile products and almost instantaneous quenching of condensed phase material including reactant (cellulose) and products (oligosaccharides and monosaccharides). As illustrated in Figure 2.2, this reactor consists of a micropyrolyzer, a condenser to collect vapor products continuously, and a quench vessel that collects intermediate products existing as condensed phases after the prescribed pyrolysis duration.

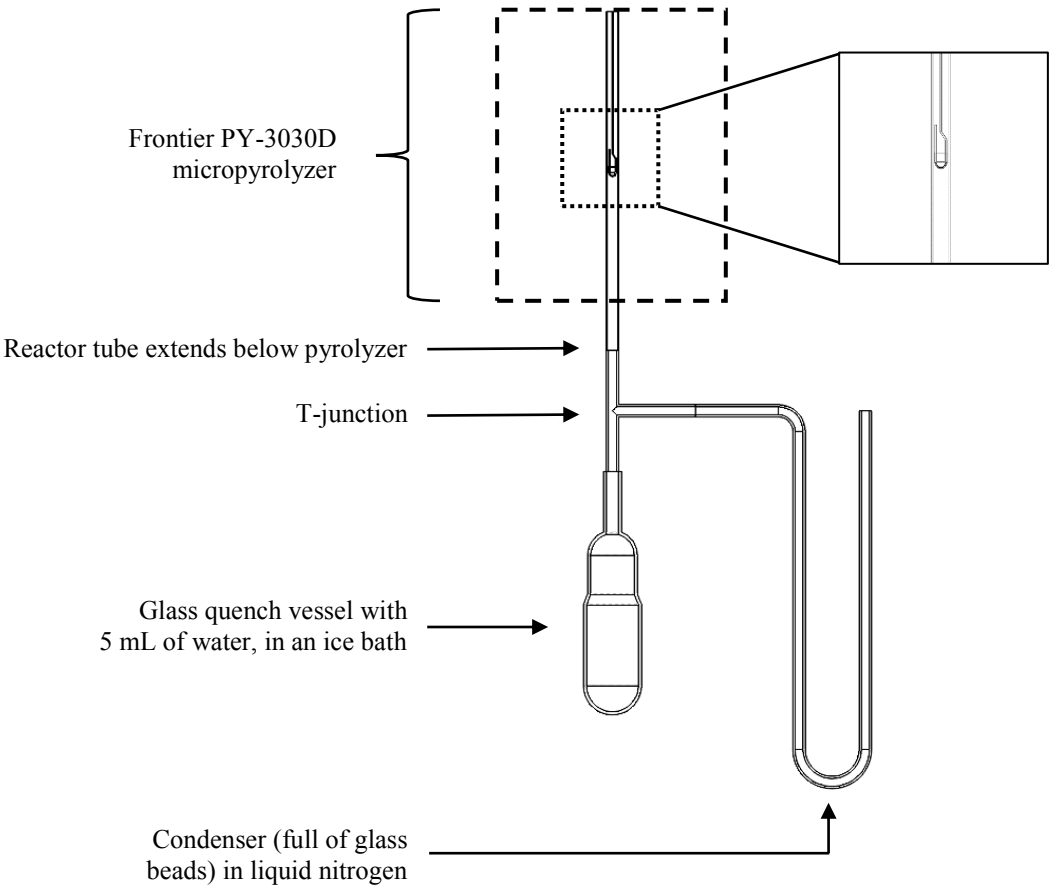

Figure 2.2. The CPD-Quench apparatus captures both volatile and condensed phase products of cellulose pyrolysis after prescribed reaction durations. The Swagelok T-junction and connector to the glass quench vessel are roughly depicted for clarity.

Experiments began by heating the Frontier micropyrolyzer to the desired pyrolysis temperature followed by purging the reactor tube with helium carrier gas at 100 mL min^{-1} for two minutes to remove oxygen. To initiate pyrolysis, an automatically controlled linear actuator rapidly inserted a short, stainless steel sample cup containing the cellulose sample into the furnace section of the micropyrolyzer. Vapors released from the pyrolyzing cellulose were swept into the condenser which is cooled by liquid nitrogen. The condenser contained 3 mL of 1 mm diameter borosilicate glass spheres to increase surface area so all the products were captured. At the end of the prescribed pyrolysis time, the sample holder was dropped into a quench vessel containing chilled

water. Condensed phase material in the sample holder cooled at rates estimated to be hundreds of degrees Celsius per second, rapidly quenching pyrolysis reactions. Up to thirty sequential trials of 500 μg samples were performed to accumulate sufficient condensed phase and volatile samples for chemical analysis. This repetition was also advantageous because it effectively produced an average of the pyrolysis experiments for each test point, reducing the impact of random error.

The 6 mm OD, 5 mm ID 316 stainless steel tubing used for the reactor tube and condenser was deactivated by SilcoTek's SilcoNert 1000 to prevent unwanted catalytic reactions. A custom heating jacket, made by Briskheat and controlled by an Oakton Temp 9000 Advanced Thermocouple Controller, heated the part of the reactor tube extending below the micropyrolyzer, the T-junction, and the horizontal part of the condenser to 400 °C. A brass Swagelok union tee composed the T-junction, and a stainless steel Swagelok Ultra-Torr adapter connected to a glass tube coupled to the glass flask by a conically tapered ground glass joint. For overall clarity, the Briskheat heater and Swagelok parts are omitted from Figure 2.2.

The solvent and condensed phase material caught in the quench vessel and the liquid in the condenser were transferred to lightweight PTFE beaker liners from Welch Fluorocarbon to facilitate weighing on a microbalance (Mettler Toledo XP6). Water in the samples was evaporated in a vacuum oven before determining the mass of each product stream using a microbalance.

To verify the samples were dried completely, the samples were each divided into two subsamples. One of these was analyzed for moisture content via thermogravimetric analysis using a Mettler Toledo TGA/DSC 1. The other was separately dissolved in water

and analyzed by HPLC and Gel Filtration Chromatography (GFC). This procedure was performed in duplicate for each experiment.

Short Column-Flame Ionization Detector

In order to measure the rate of volatile species production, a Varian GC-FID was slightly modified to create the SC-FID, first described in Proano-Aviles *et al.*[36] Instead of using a standard 30 or 60 m column, an Agilent Technologies FS, Deactivated, Hi-Temp- 0.250 mm x 5 m column was cut to 0.50 m and kept at 400 °C to prevent product condensation. The GC inlet with a Frontier PY-3030 D micropyrolyzer was connected by the shortened column to the FID, allowing time-resolved signal analysis. Unlike an analytical GC column, this short column does not separate chemical species but simply serves as a transfer line from the micropyrolyzer to the FID. Although the apparatus configured in this way does not allow identification of individual chemical species, it provides time resolution of the FID signal generated collectively from carbon-containing species volatilized from the cellulose sample.

To maximize heat transfer and advection, a small cellulose sample was pyrolyzed on a small hook in a Frontier PY-3030 D micropyrolyzer mounted to the GC inlet. To prepare the sample for pyrolysis, a cellulose-water slurry was applied to the bottom of a hook normally used to hold the pyrolysis cup. The water in the slurry was evaporated overnight in a vacuum oven, leaving cellulose attached to the bottom of the hook. The hook was weighed before slurry addition and after drying to determine the sample mass. Additional details of this procedure are found in Proano-Aviles *et al.*[36]

Reaction modeling

SC-FID data was fit to the equations described in detail by Burnham.[43,44] In particular the extended Prout-Tompkins model[46,52] (ePT) (Equation 2.1) was used, where α represents conversion. The sigmoid-shaped solution to this equation is appropriate for two-step processes such as crystal nucleation and growth and organic polymer decomposition. Specifically, the ePT was fit to the data by adjusting values of k, m, and n in Equation 2.1.[53] Single step models[43,44] were also considered, but were abandoned because of their poor fit to the experimental data.

$$\frac{d\alpha}{dt} = k\alpha^m(1-\alpha)^n \qquad \text{(Equation 2.1)}$$

To compare to the ePT model, the SC-FID data had to be transformed. All data transformations were performed in *Python 3*.[54] These manipulations converted FID signal [pV] over time [s] into normalized reaction rate and conversion, respectively. These steps, completed separately for each temperature, aid comparing disparate reaction rates and time scales.

The first step involved truncating the SC-FID data. Without this abbreviation the data points before and after pyrolysis would bias and subsequently over-fit the model toward low and high conversions. Furthermore, FID signal and noise is always positive, so the integral of the FID data (the next transformation) would always have a positive slope, thereby never appearing to reach complete conversion. To determine consistently when pyrolysis begins and ends, the first derivative of the FID signal [pV s^{-1}] (dS_{FID}/dt) was taken piecewise between each data point. The cutoff magnitude for dS_{FID}/dt was set at one percent of the maximum of dS_{FID}/dt. Data before and after this cutoff (excluding

the change in sign as the reaction slows down) was ignored for subsequent transformations and curve fitting.

This truncated data set underwent multiple straightforward transformations. It was integrated piecewise at each data point, representing the accumulation of volatile pyrolysis products. The integrated data were transformed to conversion (alpha) by normalizing the accumulation with respect to the maximum integrated FID signal. The piecewise derivative was taken separately for alpha and time, and then change in alpha was divided by change in time to create the reaction rate. The reaction rate was normalized by its maximum value. The models were fit to normalized reaction rate and conversion with *SciPy* using the Levenburg-Marquardt damped least squares algorithm.

HPLC

A Dionex UltiMate® 3000 HPLC with a Refractive Index (RI) detector and two Bio-Rad® Aminex HPX-87P columns in series was used to quantify levoglucosan from the CPD-Quench. The method is described in depth by Yong *et al.*[55] and Dalluge *et al.*[56]

GFC

A Dionex UltiMate® 3000 HPLC with a RI detector and two Agilent Technologies PL aquagel-OH 20 columns in series was used to identify cellulose oligomers from the CPD-Quench. An Agilent Technologies PL aquagel-OH guard protected the two columns. The columns were kept at 25 °C with a 0.800 mL min^{-1} flow rate of 18.2 MΩ cm^{-1} deionized water as the eluent for analysis. The GFC with Chromeleon® software was calibrated using an Agilent Technologies Pullulan Polysaccharide Calibration Kit with the peak average molecule weights: 180, 667, 5,900, 9,600, and 21,100. The anhydro-oligosaccharide structure was further confirmed with

standards of cellobiosan purchased from Carbosynth LLC, and cellotriosan, cellotetraosan, and cellopentaosan from LC Scientific Inc. (now known as Synthose Inc.)

Results and Discussion

Anhydro-oligosaccharide formation

The condensed phase products from the CPD-Quench show oligomeric products form in the first few seconds of pyrolysis. The Pullulan polysaccharide calibration does not fit these products, indicating they are not conventional oligosaccharides. Rather, they are anhydro-oligosaccharides, with their identity confirmed by low DP anhydro-oligosaccharide standards. Their retention times differ from conventional oligosaccharides due to non-size-exclusion effects arising from their differing end-structure. GFC shows the presence of a wide range of DPs but their intensity markedly decreases for anhydro-oligosaccharides with DP greater than 7 (Figure 2.3). However, in the present experiments, this decline is likely due to the inverse relationship between anhydro-oligosaccharide DP and their solubility in water[57] rather than the absence of larger oligosaccharides in the condensed phase products. For the same reason, instrumentation, such as HPLC, using water as an eluent cannot reliably detect anhydro-oligosaccharides larger than DP 7. However, extending our exponential trend line suggests that anhydro-oligosaccharides with DP of approximately 60 should be visible using GFC near or at room temperature, which is more than triple the highest previously reported DP for anhydro-oligosaccharides.[18] Despite the inability to determine the entire range of anhydro-oligosaccharides with GFC, the presence of anhydro-oligosaccharides with DP values two and three orders of magnitude lower than the starting cellulose DP indicates very rapid depolymerization.

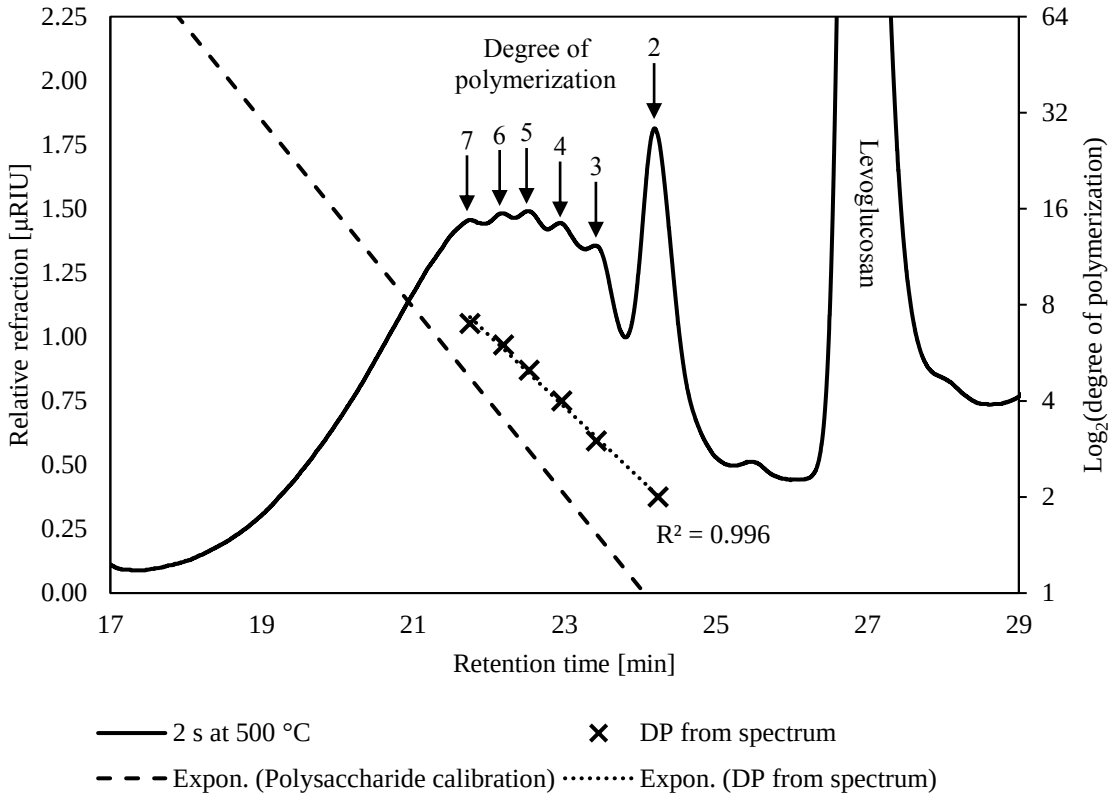

Figure 2.3. Anhydro-oligosaccharides are visible in the GFC spectrum from the condensed products after two seconds of pyrolysis at 500 °C. The exponential trendline created using the DP visible on the spectrum, and their respective retention times, has a high coefficient of determination (0.996) indicating all the visible peaks are homologous anhydro-oligosaccharides.

Also noteworthy was the absence of glucose in either the condensed or volatile products. Broadbelt's mechanistic model predicts up to approximately 18 wt% glucose on a cellulose basis, 60 wt% of the condensed phase.[11] This amount of glucose is well within the detection limits of the HPLC and GFC methodologies used on products from the CPD-Quench apparatus. This conspicuous absence of glucose calls into question the importance of thermohydrolysis in explaining the depolymerization mechanism of cellulose during fast pyrolysis.

The presence of anhydro-oligosaccharides, however, does not reveal whether they originated from depolymerized cellulose or repolymerized levoglucosan. Cellulose could

have depolymerized from its non-reducing end producing levoglucosan and eventually yielding small anhydro-oligosaccharides. Furthermore, the condensed phase contains levoglucosan, as shown in Figure 2.3, which could have formed exclusively from the non-reducing end followed by its repolymerization to anhydro-oligosaccharides—all without recourse to cracking reactions. However, low DP anhydro-oligosaccharides appear before significant amounts of levoglucosan form, as shown in Figure 2.4. The presence of significant levoglucosan in the condensed phase would be expected if levoglucosan repolymerization were responsible for the presence of small anhydro-oligosaccharides.

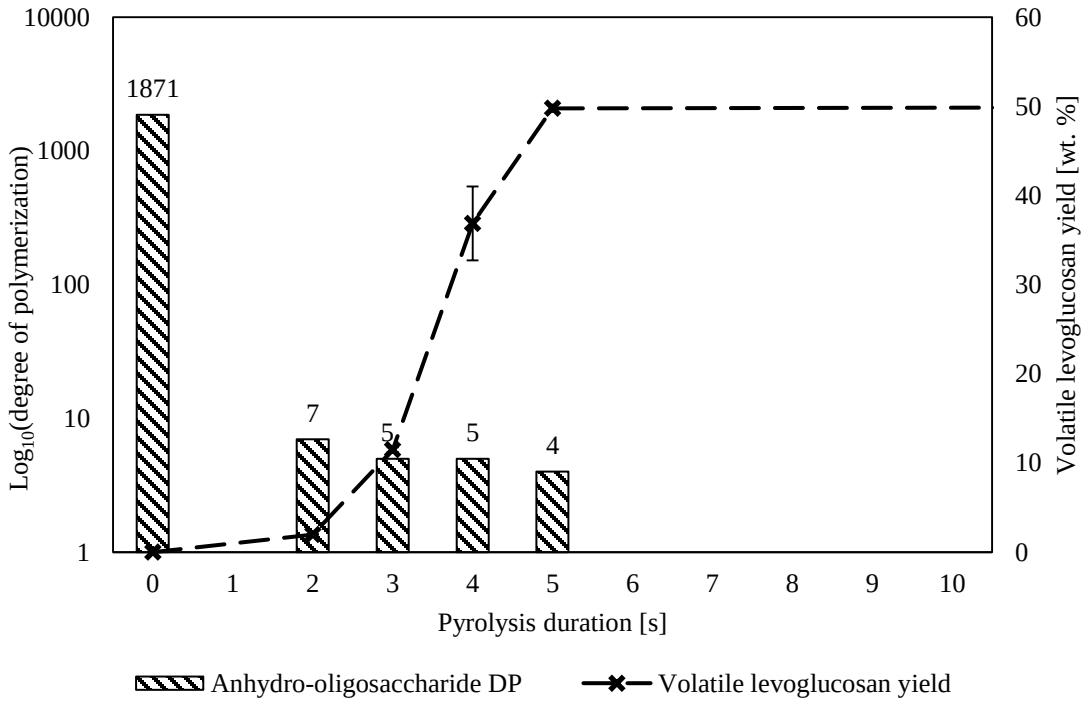

Figure 2.4. The DP of cellulose rapidly decreased ahead of any significant levoglucosan production, indicating extensive cracking of cellulose before substantial levoglucosan was produced. The DPs listed are the highest water-soluble anhydro oligosaccharides that can be directly detected by GFC. The DP of the cellulose before pyrolysis was measured by the National Renewable Energy Laboratory.[35] The longest pyrolysis duration, 300 s, was omitted for clarity but produced 54.4 wt% levoglucosan. Pyrolysis temperature was 500 °C.

The delay in the appearance of levoglucosan compared to the depolymerization of cellulose into small anhydro-oligosaccharides suggests that the initial rate of cracking is much faster than levoglucosan generation from end-chain LPRs. This result should not be surprising considering the plethora of potential cracking sites in long-chain anhydro-oligosaccharides (equal to DP minus two) compared to the small number of sites for end-chain reactions (two per anhydro-oligosaccharide molecule regardless of DP). Quantification of this phenomena is the subject of a future computational study.

Subsequent LPRs

The SC-FID was used to explore the role of LPRs in the rate of levoglucosan production from cellulose. This instrument allows high frequency data collection (10 Hz) on devolatilized pyrolysis products, although at the cost of not being able to individually resolve product species. Thus, there is the question whether the SC-FID signal correlates with levoglucosan, representing about 60 wt% of volatile products,[4,35,36] or is also confounded by the effect of the other 40 wt% of products. To evaluate this question, the FID response was integrated with time to estimate the amount of accumulated products over the course of an experiment. This data was plotted against mass yield of volatilized levoglucosan as determined from the analysis of volatile products from the CPD-Quench under identical experimental conditions. As shown in Figure 2.5, the correlation between volatile levoglucosan as determined in CPD-Quench experiments with the integrated FID signal is excellent, with coefficient of determination of 0.993. The close correlation suggests that the ratio of rates for LPRs and DRs are constant over the course of pyrolysis. It also indicates that the FID signal can serve as a proxy for levoglucosan production rate during pyrolysis and be used for ePT modeling.

.

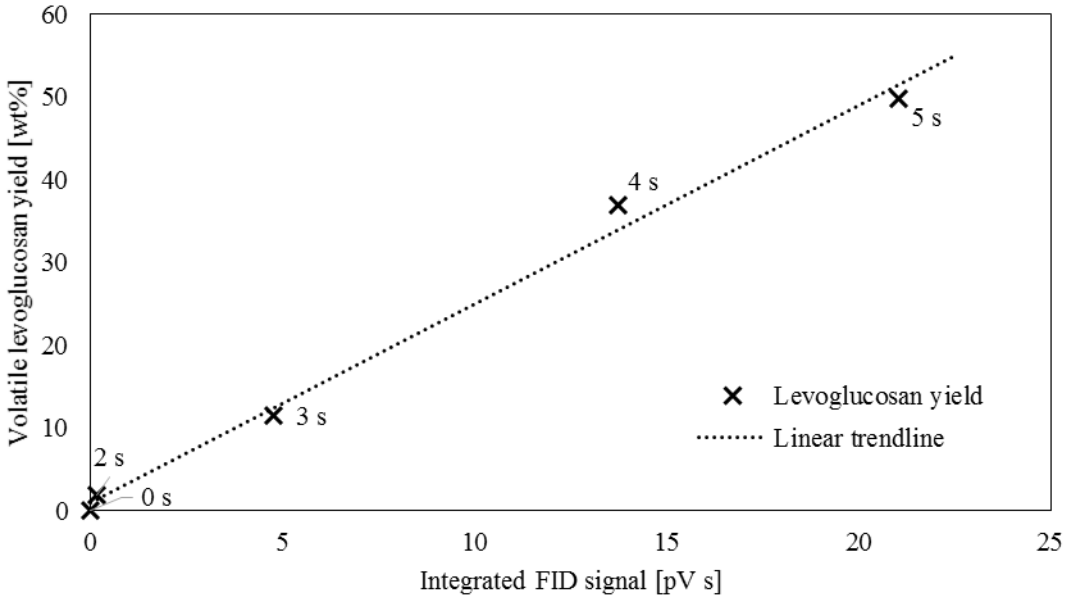

Figure 2.5. The average volatile levoglucosan yield from the CPD-Quench reactor plotted against the FID signal integrated with respect to time (both reactors at 500 °C) closely match (linear fit with a coefficient of determination of 0.993), showing that the FID signal can be used as a proxy for levoglucosan production. Pyrolysis time, in seconds, is indicated at each point.

As described in the Materials and Methodologies section, time-resolved FID data was transformed into normalized reaction rates and conversions (α) for pyrolysis experiments performed at three temperatures (433, 467, and 500 °C). The experimental data presented in this way (Figure 2.6) clearly illustrates LPRs accelerating at low conversions (α less than 0.2 to 0.4, depending upon temperature) followed by decelerating reaction rate for higher conversions. Higher temperatures favor higher conversions before LPRs begins to slow down. The period of rapid increase in the rate of volatile evolution corresponds to LPRs overtaking cracking reactions. However, both cracking and LPRs occur at all pyrolysis temperatures tested, contrary to the theory of Dauenhauer *et al.*[37,41] that cracking only occurs at pyrolysis temperatures above 467 °C. If this were the case, then normalized reaction rate should be constant with respect to conversion for the two experiments plotted in Figure 2.6 at temperatures 433 and 467

°C,[43] which is clearly not the case. The presence of both cracking and LPRs independent of temperature is quantified below in the discussion on fitting the experimental data to the ePT model.

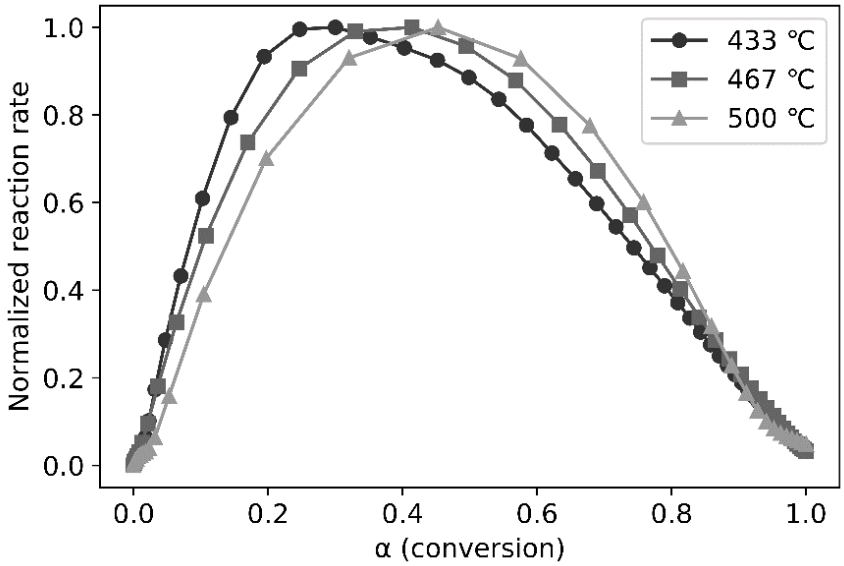

Figure 2.6. The normalized reaction rates plotted against conversion (α) clearly demonstrate an acceleration period (with a positive slope) followed by a deceleration phase (with a negative slope). In conjunction these zones indicate the consecutive dominance of cracking then LPRs.

As shown in Figure 2.7, the ePT model closely fits the experimental data, confirming a two-step reaction consisting of cracking followed by LPRs (and DRs). The skewness and constants derived from fitting these equations to the SC-FID data (Figure 2.7) show the first reaction, cracking, initially occurs more frequently than LPRs. The peak reaction rate occurs at higher conversion for increasing temperatures. This shift is unsurprising as reaction rates accelerate with higher temperatures.

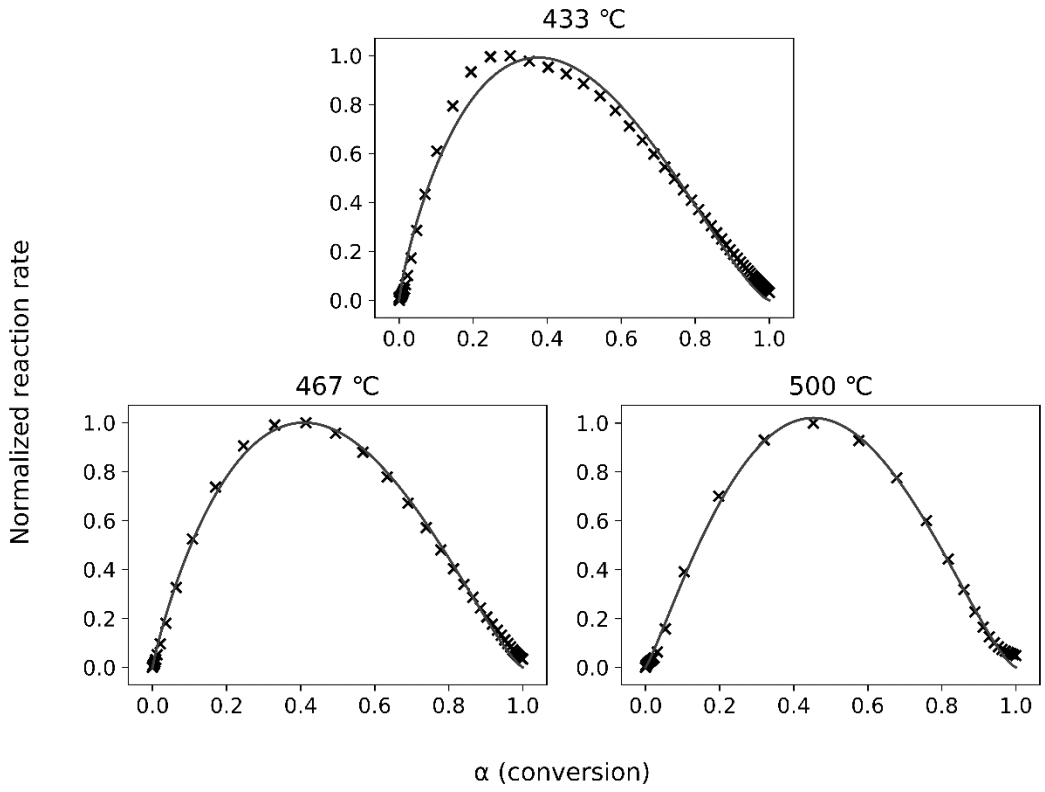

Temperature [°C]	k	m	n	Root-mean-square error
433	4.27	0.830	1.38	0.0440
467	4.43	0.900	1.30	0.0240
500	5.98	1.16	1.40	0.0225

Figure 2.7. The ePT model (lines) closely fits the transformed SC-FID data (crosses). The root-mean-square errors show good fit for all tested temperatures.

These results confirm previous global kinetic analyses that support the two-step scheme.[44] Past work conducted at low heating rates provided important insight into these reactions but did not show if the reaction scheme holds true at higher heating rates more representative of large scale pyrolyzers. This work bridges that gap.

Conclusions

Cellulose exhibits two distinct reaction regimes—cracking then levoglucosan production—during fast pyrolysis at 433, 467, and 500 °C. The competition between

LPRs and DRs limit levoglucosan yields from cellulose pyrolysis to approximately 60 wt%.

Cellulose pyrolysis begins as cracking reactions convert cellulose into anhydro-oligosaccharides, regardless of temperature. Within a few seconds, cellulose with an initial DP of 1,871[35] produces anhydro-oligosaccharides with a DP of less than 60, while in the same time frame, yields very little levoglucosan. Examining the oligosaccharide fragments of cellulose deconstruction is essential for understanding this process, something not possible through surrogates such as α-cyclodextrin. The presence of small anhydro-oligosaccharides from actual polysaccharides cannot be suitably explained without the intervention of cracking reactions that rapidly depolymerize cellulose.

LPRs rely on cracking to create anhydro-oligosaccharides,[24] so increasing the amount of oligomers directly increases LPR rates. This dependence explains the second phase of cellulose pyrolysis: levoglucosan production. The SC-FID plots show cellulose pyrolyzes with the same reaction regimes regardless of temperature, which only changes the reaction rates.

The interplay between these LPRs and a host of DRs limit levoglucosan yields from cellulose to approximately 60 wt%. The DR mechanisms are certainly numerous but do not include thermohydrolysis to a detectable extent. Regardless of their mechanisms, every DR destroys a latent levoglucosan molecule, preventing cellulose from reaching its stoichiometric potential yield of 100 wt% levoglucosan. This prospect could be reached only if no DRs occur. Herein lies the difficulty.

The strong correlation between levoglucosan and less desirable products (light oxygenates and non-condensable gases) indicates an intrinsic link between cracking,

LPRs, and DRs. Cracking creates increasing amounts of progressively smaller anhydro-oligosaccharides where LPRs and DRs compete for each monomer. This competition to utilize these anhydro-oligosaccharides is what limits levoglucosan yields. Understanding the conflict between LPRs and DRs is only possible by studying anhydro-oligosaccharides.

Anhydro-oligosaccharides pose distinct analytical challenges. Foremost, they are short-lived during cellulose pyrolysis, except for cellobiosan which is sometimes observed as a final product.[15] Second, and perhaps the most vexing, they are poorly soluble in water. Cellulose, a polysaccharide with a DP of typically a few thousand, only becomes soluble and possible to analyze with common instrumental techniques after significant depolymerization has decreased its DP by two or three orders of magnitude. Despite these difficulties, the true nature of cellulose pyrolysis can be examined properly only by including the intermediate products.

By analyzing the volatile and non-volatile products, this experimental confirmation of the two-step mechanism improves understanding, assists future modeling, and also invites future study. Cellulose is a complicated material and its pyrolysis is correspondingly chaotic. Future work should integrate experiments that demonstrate the role of anhydro-oligosaccharides, preferably including those with a greater DP than can be analyzed with water as the solvent.

Conflicts of Interest

There are no conflicts to declare.

Acknowledgements

The financial support and guidance from ExxonMobil (ISU Project No. 128056-01), the National Science Foundation (grant numbers 1630404 and 1560012), and the Ecuadorian government through SENESCYT is greatly appreciated. Furthermore, the authors would like express their gratitude to Ross Mabon and Ryan Smith for guidance and useful discussions, Ross D. Mazur and Joshua Otto for experimental support, Eric Lindstrom for editing assistance, and lastly Paul J. H. Tjossem and Mira E. Hall for introducing JKL to the art of electronics.

References

(1) *Thermochemical Processing of Biomass: Conversion into Fuels, Chemicals and Power*; Brown, R. C., Stevens, C., Eds.; Wiley, 2011.

(2) Patwardhan, P. R.; Satrio, J. A.; Brown, R. C.; Shanks, B. H. Influence of Inorganic Salts on the Primary Pyrolysis Products of Cellulose. *Bioresour. Technol.* **2010**, *101* (12), 4646–4655.

(3) Patwardhan, P. R.; Brown, R. C.; Shanks, B. H. Product Distribution from the Fast Pyrolysis of Hemicellulose. *ChemSusChem* **2011**, *4* (5), 636–643.

(4) Patwardhan, P. R.; Satrio, J. A.; Brown, R. C.; Shanks, B. H. Product Distribution from Fast Pyrolysis of Glucose-Based Carbohydrates. *J. Anal. Appl. Pyrolysis* **2009**, *86* (2), 323–330.

(5) Patwardhan, P. R.; Dalluge, D. L.; Shanks, B. H.; Brown, R. C. Distinguishing Primary and Secondary Reactions of Cellulose Pyrolysis. *Bioresour. Technol.* **2011**, *102* (8), 5265–5269.

(6) Mayes, H. B.; Nolte, M. W.; Beckham, G. T.; Shanks, B. H.; Broadbelt, L. J. The Alpha-Bet(a) of Glucose Pyrolysis: Computational and Experimental Investigations of 5-Hydroxymethylfurfural and Levoglucosan Formation Reveal Implications for Cellulose Pyrolysis. *ACS Sustain. Chem. Eng.* **2014**, *2* (6), 1461–1473.

(7) Hutchinson, C. P.; Lee, Y. J. Evaluation of Primary Reaction Pathways in Thin-Film Pyrolysis of Glucose Using 13C Labeling and Real-Time Monitoring. *ACS Sustain. Chem. Eng.* **2017**, *5* (10), 8796–8803.

(8) Seshadri, V.; Westmoreland, P. R. Concerted Reactions and Mechanism of Glucose Pyrolysis and Implications for Cellulose Kinetics. *J. Phys. Chem. A* **2012**, *116* (49), 11997–12013.

(9) Assary, R. S.; Curtiss, L. A. Comparison of Sugar Molecule Decomposition through Glucose and Fructose: A High-Level Quantum Chemical Study. *Energy & Fuels* **2012**, *26* (2), 1344–1352.

(10) Zhou, X.; Nolte, M. W.; Mayes, H. B.; Shanks, B. H.; Broadbelt, L. J. Experimental and Mechanistic Modeling of Fast Pyrolysis of Neat Glucose-Based Carbohydrates. 1. Experiments and Development of a Detailed Mechanistic Model. *Ind. Eng. Chem. Res.* **2014**, *53* (34), 13274–13289.

(11) Zhou, X.; Nolte, M. W.; Shanks, B. H.; Broadbelt, L. J. Experimental and Mechanistic Modeling of Fast Pyrolysis of Neat Glucose-Based Carbohydrates. 2. Validation and Evaluation of the Mechanistic Model. *Ind. Eng. Chem. Res.* **2014**, *53* (34), 13290–13301.

(12) Kuzhiyil, N.; Dalluge, D.; Bai, X.; Kim, K. H.; Brown, R. C. Pyrolytic Sugars from Cellulosic Biomass. *ChemSusChem* **2012**, *5* (11), 2228–2236.

(13) Mayes, H. B.; Nolte, M. W.; Beckham, G. T.; Shanks, B. H.; Broadbelt, L. J. The Alpha-Bet(a) of Salty Glucose Pyrolysis: Computational Investigations Reveal Carbohydrate Pyrolysis Catalytic Action by Sodium Ions. *ACS Catal.* **2015**, *5* (1), 192–202.

(14) Lédé, J. Cellulose Pyrolysis Kinetics: An Historical Review on the Existence and Role of Intermediate Active Cellulose. *J. Anal. Appl. Pyrolysis* **2012**, *94*, 17–32.

(15) Radlein, D. S.; Grinshpun, A.; Piskorz, J.; Scott, D. S. On the Presence of Anhydro-Oligosaccharides in the Sirups from the Fast Pyrolysis of Cellulose. *J. Anal. Appl. Pyrolysis* **1987**, *12* (1), 39–49.

(16) Lédé, J.; Blanchard, F.; Boutin, O. Radiant Flash Pyrolysis of Cellulose Pellets: Products and Mechanisms Involved in Transient and Steady State Conditions. *Fuel* **2002**, *81* (10), 1269–1279.

(17) Lin, Y.-C.; Cho, J.; Tompsett, G. A.; Westmoreland, P. R.; Huber, G. W. Kinetics and Mechanism of Cellulose Pyrolysis. *J. Phys. Chem. C* **2009**, *113* (46), 20097–20107.

(18) Liu, D.; Yu, Y.; Wu, H. Evolution of Water-Soluble and Water-Insoluble Portions in the Solid Products from Fast Pyrolysis of Amorphous Cellulose. *Ind. Eng. Chem. Res.* **2013**, *52* (36), 12785–12793.

(19) Gong, X.; Yu, Y.; Gao, X.; Qiao, Y.; Xu, M.; Wu, H. Formation of Anhydro-Sugars in the Primary Volatiles and Solid Residues from Cellulose Fast Pyrolysis in a Wire-Mesh Reactor. *Energy & Fuels* **2014**, *28* (8), 5204–5211.

(20) Hurt, M. R.; Degenstein, J. C.; Gawecki, P.; Borton II, D. J.; Vinueza, N. R.; Yang, L.; Agrawal, R.; Delgass, W. N.; Ribeiro, F. H.; Kenttämaa, H. I. On-Line Mass Spectrometric Methods for the Determination of the Primary Products of

Fast Pyrolysis of Carbohydrates and for Their Gas-Phase Manipulation. *Anal. Chem.* **2013**, *85* (22), 10927–10934.

(21) Degenstein, J. C.; Hurt, M.; Murria, P.; Easton, M.; Choudhari, H.; Yang, L.; Riedeman, J.; Carlsen, M. S.; Nash, J. J.; Agrawal, R.; et al. Mass Spectrometric Studies of Fast Pyrolysis of Cellulose. *Eur. J. Mass Spectrom.* **2015**, *21* (3), 321–326.

(22) Hallac, B. B.; Ragauskas, A. J. Analyzing Cellulose Degree of Polymerization and Its Relevancy to Cellulosic Ethanol. *Biofuels, Bioprod. Biorefining* **2011**, *5*, 215–225.

(23) Boutin, O.; Ferrer, M.; Lédé, J. Flash Pyrolysis of Cellulose Pellets Submitted to a Concentrated Radiation: Experiments and Modelling. *Chem. Eng. Sci.* **2002**, *57*, 15–25.

(24) Mayes, H. B.; Broadbelt, L. J. Unraveling the Reactions That Unravel Cellulose. *J. Phys. Chem. A* **2012**, *116* (26), 7098–7106.

(25) Vinu, R.; Broadbelt, L. J. A Mechanistic Model of Fast Pyrolysis of Glucose-Based Carbohydrates to Predict Bio-Oil Composition. *Energy Environ. Sci.* **2012**, *5* (12), 9808–9826.

(26) Zhang, X.; Yang, W.; Dong, C. Levoglucosan Formation Mechanisms during Cellulose Pyrolysis. *J. Anal. Appl. Pyrolysis* **2013**, *104*, 19–27.

(27) Zhang, X.; Yang, W.; Blasiak, W. Kinetics of Levoglucosan and Formaldehyde Formation during Cellulose Pyrolysis Process. *Fuel* **2012**, *96*, 383–391.

(28) Agarwal, V.; Dauenhauer, P. J.; Huber, G. W.; Auerbach, S. M. Ab Initio Dynamics of Cellulose Pyrolysis: Nascent Decomposition Pathways at 327 and 600 C. *J. Am. Chem. Soc.* **2012**, *134* (36), 14958–14972.

(29) Wooten, J. B.; Seeman, J. I.; Hajaligol, M. R. Observation and Characterization of Cellulose Pyrolysis Intermediates by 13C CPMAS NMR. A New Mechanistic Model. *Energy & Fuels* **2004**, *18* (1), 1–15.

(30) Oja, V.; Suuberg, E. M. Vapor Pressures and Enthalpies of Sublimation of D-Glucose, d-Xylose, Cellobiose, and Levoglucosan. *J. Chem. Eng. Data* **1999**, *44* (1), 26–29.

(31) Bai, X.; Xue, Y. Transport and Secondary Reactions of Depolymerized/Deconstructed Species. In *Fast Pyrolysis of Biomass: Advances in Science and Technology*; Brown, R. C., Wang, K., Eds.; Royal Society of Chemistry: London, U.K., 2017; pp 57–77.

(32) Kawamoto, H.; Murayama, M.; Saka, S. Pyrolysis Behavior of Levoglucosan as an Intermediate in Cellulose Pyrolysis: Polymerization into Polysaccharide as a Key Reaction to Carbonized Product Formation. *J. Wood Sci.* **2003**, *49* (5), 469–473.

(33) Bai, X.; Johnston, P.; Sadula, S.; Brown, R. C. Role of Levoglucosan Physiochemistry in Cellulose Pyrolysis. *J. Anal. Appl. Pyrolysis* **2013**, *99*, 58–65.

(34) Shoji, T.; Kawamoto, H.; Saka, S. Boiling Point of Levoglucosan and Devolatilization Temperatures in Cellulose Pyrolysis Measured at Different Heating Area Temperatures. *J. Anal. Appl. Pyrolysis* **2014**, *109*, 185–195.

(35) Zhang, J.; Nolte, M. W.; Shanks, B. H. Investigation of Primary Reactions and Secondary Effects from the Pyrolysis of Different Celluloses. *ACS Sustain. Chem. Eng.* **2014**, *2* (12), 2820–2830.

(36) Proano-Aviles, J.; Lindstrom, J. K.; Johnston, P. A.; Brown, R. C. Heat and Mass Transfer Effects in a Furnace-Based Micropyrolyzer. *Energy Technol.* **2017**, *5* (1), 189–195.

(37) Krumm, C.; Pfaendtner, J.; Dauenhauer, P. J. Millisecond Pulsed Films Unify the Mechanisms of Cellulose Fragmentation. *Chem. Mater.* **2016**, *28*, 3108–3114.

(38) Maduskar, S.; Maliekkal, V.; Neurock, M.; Dauenhauer, P. J. On the Yield of Levoglucosan from Cellulose Pyrolysis. *ACS Sustain. Chem. Eng.* **2018**, *6* (5), 7017–7025.

(39) Maduskar, S.; Facas, G. G.; Papageorgiou, C.; Williams, C. L.; Dauenhauer, P. J. Five Rules for Measuring Biomass Pyrolysis Rates: Pulse-Heated Analysis of Solid Reaction Kinetics of Lignocellulosic Biomass. *ACS Sustain. Chem. Eng.* **2018**, *6* (1), 1387–1399.

(40) Mettler, M. S.; Mushrif, S. H.; Paulsen, A. D.; Javadekar, A. D.; Vlachos, D. G.; Dauenhauer, P. J. Revealing Pyrolysis Chemistry for Biofuels Production: Conversion of Cellulose to Furans and Small Oxygenates. *Energy Environ. Sci.* **2012**, *5* (1), 5414–5424.

(41) Zhu, C.; Krumm, C.; Facas, G. G.; Neurock, M.; Dauenhauer, P. J. Energetics of Cellulose and Cyclodextrin Glycosidic Bond Cleavage. *React. Chem. Eng.* **2017**, *2* (2), 201–214.

(42) Mettler, M. S.; Paulsen, A. D.; Vlachos, D. G.; Dauenhauer, P. J. The Chain Length Effect in Pyrolysis: Bridging the Gap between Glucose and Cellulose. *Green Chem.* **2012**, *14* (5), 1284.

(43) Burnham, A. K. Introduction to Chemical Kinetics. In *Global Chemical Kinetics of Fossil Fuels: How to Model Maturation and Pyrolysis*; Springer International Publishing, 2017; pp 25–74.

(44) Burnham, A. K.; Zhou, X.; Broadbelt, L. J. Critical Review of the Global Chemical Kinetics of Cellulose Thermal Decomposition. *Energy & Fuels* **2015**, *29* (5), 2906–2918.

(45) Prout, E. G.; Tompkins, F. C. The Thermal Decomposition of Potassium Permanganate. *Trans. Faraday Soc.* **1944**, *40*, 488–498.

(46) Prout, E. G.; Tompkins, F. C. The Thermal Decomposition of Silver Permanganate. *Trans. Faraday Soc.* **1946**, *42* (9), 468–472.

(47) Capart, R.; Khezami, L.; Burnham, A. K. Assessment of Various Kinetic Models for the Pyrolysis of a Microgranular Cellulose. *Thermochim. Acta* **2004**, *417* (1), 79–89.

(48) Sánchez-Jiménez, P. E.; Pérez-Maqueda, L. A.; Perejón, A.; Pascual-Cosp, J.; Benítez-Guerrero, M.; Criado, J. M. An Improved Model for the Kinetic Description of the Thermal Degradation of Cellulose. *Cellulose* **2011**, *18* (6), 1487–1498.

(49) Mamleev, V.; Bourbigot, S.; Le Bras, M.; Yvon, J. The Facts and Hypotheses Relating to the Phenomenological Model of Cellulose Pyrolysis. Interdependence of the Steps. *J. Anal. Appl. Pyrolysis* **2009**, *84* (1), 1–17.

(50) Šesták, J.; Berggren, G. Study of the Kinetics of the Mechanism of Solid-State Reactions at Increasing Temperatures. *Thermochim. Acta* **1971**, *3* (1), 1–12.

(51) Matthews, J. F.; Beckham, G. T.; Bergenstråhle-Wohlert, M.; Brady, J. W.; Himmel, M. E.; Crowley, M. F. Comparison of Cellulose Iβ Simulations with Three Carbohydrate Force Fields. *J. Chem. Theory Comput.* **2012**, *8* (2), 735–748.

(52) Austin, J. B.; Rickett, R. L. Kinetics Of The Decomposition Of Austenite At Constant Temperature. *Am. Inst. Mining, Metall. Pet. Eng.* **1939**, *135* (8), 396–415.

(53) Jones, E.; Oliphant, T.; Peterson, P. SciPy: Open Source Scientific Tools for Python http://www.scipy.org/.

(54) Pérez, F.; Granger, B. E. IPython: A System for Interactive Scientific Computing Python: An Open and General- Purpose Environment. *Comput. Sci. Eng.* **2007**, *9* (3), 21–29.

(55) Choi, Y. S.; Johnston, P. A.; Brown, R. C.; Shanks, B. H.; Lee, K.-H. Detailed Characterization of Red Oak-Derived Pyrolysis Oil: Integrated Use of GC, HPLC, IC, GPC and Karl-Fischer. *J. Anal. Appl. Pyrolysis* **2014**, *110*, 147–154.

(56) Dalluge, D. L.; Daugaard, T.; Johnston, P.; Kuzhiyil, N.; Wright, M. M.; Brown, R. C. Continuous Production of Sugars from Pyrolysis of Acid-Infused Lignocellulosic Biomass. *Green Chem.* **2014**, 4144–4155.

(57) Goss, E. *Personal Communication, January 22, 2016*.

CHAPTER 3 CELLULOSE SOLID PHASE THERMAL DEPOLYMERIZATION

Jake K. Lindstrom,[a] Patrick A. Johnston,[b] Chad A. Peterson,[a] Preston Gable,[b] Robert C. Brown[a,b]

a- Department of Mechanical Engineering, Iowa State University, Ames, IA 50011, United States

b- Bioeconomy Institute, Iowa State University, Ames, IA 50011, United States

Abstract

Cellulose thermal depolymerization begins as cracking reactions yield anhydro-oligosaccharides. Most previous research to analyze these products could only measure small anhydro-oligosaccharides. We present the first analysis of the full complement of anhydro-oligosaccharide products from rapid thermal depolymerization of cellulose, showing that initial cellulose deconstruction is controlled mainly by relative bond frequency, not relative reaction rates or crystallinity.

Communication body

Fast pyrolysis, gasification, and combustion of biomass are all characterized by rapid thermal depolymerization of plant polymers. Among these thermochemical processes, fast pyrolysis shows the most promise for producing cost-competitive biofuels.[1] Producing sugars, the backbone of the current biofuels industry, presents the most straightforward path for fast pyrolysis biofuels generation. To this end, maximizing sugar yields will be crucial for economic viability.[2]

Cellulose pyrolysis can produce up to 60 wt% levoglucosan, an anhydro-monosaccharide of glucose.[3–5] Understanding the entire deconstruction process should advance any efforts to model it or potentially improve sugar yields, but related works have mostly focused on the volatile products.

Recently, Lindstrom *et al.*[5] provided the first time-resolved data on the volatile and non-volatile products of the fast pyrolysis[6] of cellulose. Cellulose initially depolymerizes into anhydro-oligosaccharides via cracking reactions, which break random mid-chain glycosidic bonds. From these anhydro-oligosaccharides, primarily end-chain reactions generate levoglucosan, light oxygenates, and non-condensable gases.

Moreover, this analysis detected anhydro-oligosaccharides with a degree of polymerization (DP) up to approximately 60,[5] over three times larger than previously detected.[7] Nevertheless, anhydro-oligosaccharides larger than DP 60 may also exist but are insoluble in water, thus avoiding prior detection.

In 1973, Broido *et al.*[8] reported an analysis of water-insoluble anhydro-oligosaccharides from slow pyrolysis of cellulose. With a modified thermogravimetric analyser,[9] cellulose was heated at the relatively slow rate of 5 °C min^{-1} to the desired temperature (up to 225 °C) before cooling.[8] The initial cellulose and its subsequent anhydro-oligosaccharides[§] were nitrated using a concentrated solution of nitric acid, phosphoric acid, and phosphoric pentoxide,[10] and the resulting nitrocellulose was then dissolved into tetrahydrofuran for gel permeation chromatography.[§§] Using polystyrene standards, Broido *et al.*[8] demonstrated that cellulose initially depolymerizes before substantial mass volatilizes. In short, during slow pyrolysis, cellulose undergoes cracking reactions which produce large anhydro-oligosaccharides that continue to crack into ever smaller fragments before significant quantities of volatile products form.

This seminal work by Broido *et al.*[8] garnered fewer than 20 citations in the first 20 years after its publication, despite its relevance to understanding the early stages of pyrolysis.[11] The early work of Broido *et al.*[8] was limited to slow pyrolysis because of the

difficulties of obtaining condensed phase intermediate products under fast pyrolysis conditions. In fact, with few exceptions, experimental data from fast pyrolysis have been obtained after almost complete depolymerization of biomass.[12] Furthermore, most researchers employed analytical techniques presuming carbohydrate products were water soluble;[13–17] however, solubility was recently demonstrated to decline greatly for anhydro-oligosaccharides larger than DP 7.[5]

Herein, we present the first analysis of the full complement of anhydro-oligosaccharides formed in the initial moments of cellulose fast pyrolysis. We have overcome these two limitations by collecting data during the early stages of fast pyrolysis and using analytical methods able to detect large, water-insoluble anhydro-oligosaccharides produced during the initial moments of cellulose thermal deconstruction.

Experiments were performed in a free fall reactor[18] to thermally deconstruct cellulose. This continuously-fed reactor heats Sigmacell Type 50 cellulose particles at hundreds of degrees Celsius per second. After a brief (approximately 1 s) residence in the heated section of the apparatus, feedstock particles exit the reactor and are rapidly quenched in cold nitrogen gas (near -196 °C) to prevent further reaction. Figure 3.1 shows this reactor schematically. The procedure was performed on cellulose with three different reactor temperatures: 375, 400, and 450 °C.

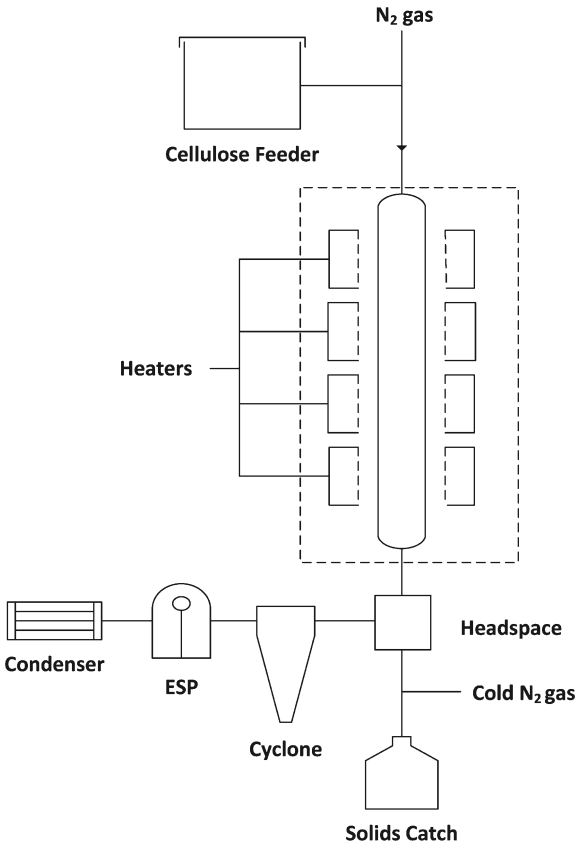

Figure 3.1. This block flow diagram illustrates the free fall reactor used to perform truncated cellulose pyrolysis to investigate the early stages of thermal deconstruction.

The solids from the free fall reactor were imaged using scanning electron microscopy (SEM) and no evidence of droplet formation or other signs of phase changes were observed (Figure 3.2). Like Broido *et al.*[8] investigated with slow pyrolysis, these experiments examine the earliest stages of cellulose rapid thermal deconstruction. Other prior experiments probing cellulose condensed phase intermediates have focused on liquid products;[19] this work solely interrogates solid phase chemistry.

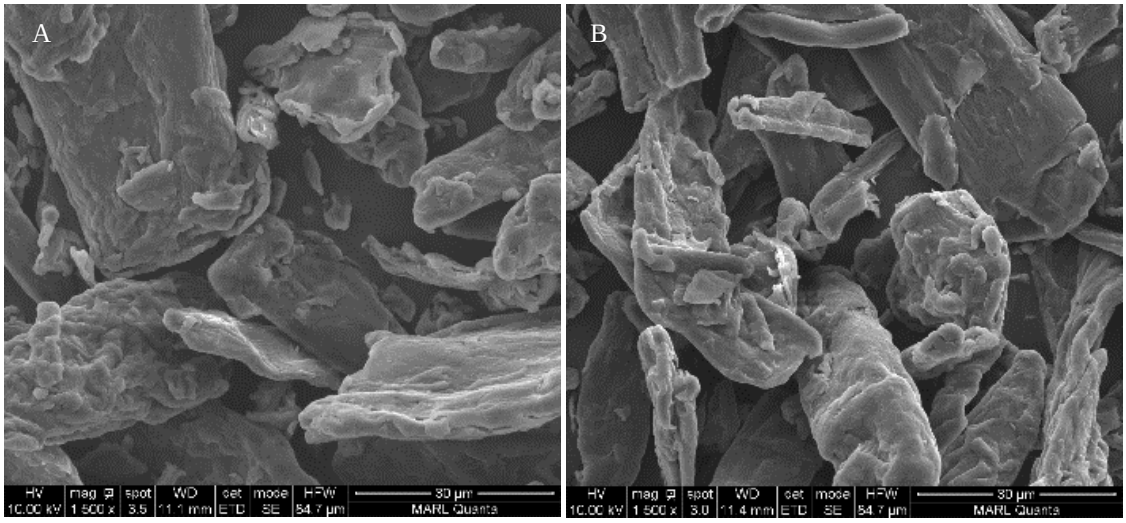

Figure 3.2. SEM images of unmodified (A) and thermally modified cellulose (B) with a reactor temperature of 450 °C demonstrate that even the most extreme conditions tested here did not cause a phase change given the short reaction duration.

The solid phase intermediate products were analyzed with two forms of size-exclusion chromatography (SEC). The first used water as the mobile phase,[5] and the second used a polar organic solvent with lithium chloride (LiCl) to form an exceedingly polar solvent solution (Figure 3.3) suitable for dissolving high molecular weight, water-insoluble anhydro-oligosaccharides.[20–22] The cellulose, thermally deconstructed cellulose, and Pullulan polysaccharide standards,[§§§] were dissolved in dimethylacetamide (DMAc) with 8% LiCl using the procedure described in McCormick.[23] The dissolved samples were then diluted with DMAc to match the 0.5% LiCl-DMAc mobile phase in accordance with Schult *et al.*[24]

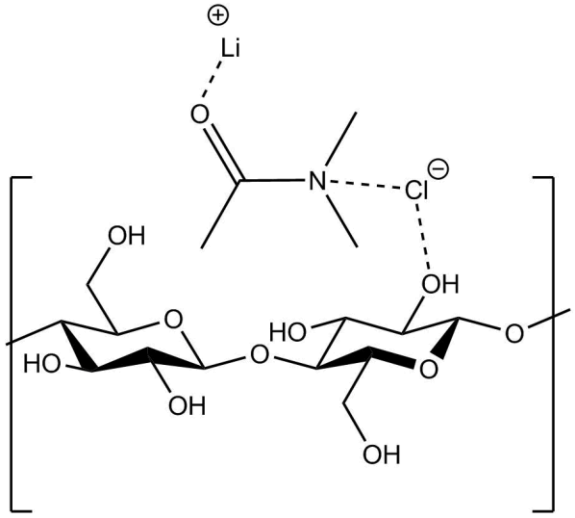

Figure 3.3. LiCl/DMAc likely dissolves cellulose in this type of configuration. The lithium and chloride ions coordinating with DMAc results in an exceptionally polar solvent system. Proposed structure based on McCormick and Hutchinson.[25]

To perform SEC, a Dionex UltiMate® 3000 HPLC (high performance liquid chromatography) was used with a Shodex refractive index (RI) detector and Chromeleon® software. A PolyPore guard column (50 x 7.5 mm) and two PolyPore SEC columns (300 x 7.5 mm) from Agilent Technologies were used in series. The column temperature was held at 70 °C with a flow rate of 0.4 mL min^{-1}.

These analyses, combined with the rapid thermal deconstruction conditions of the free fall reactor, provide the most detailed experimental data on cellulose initial depolymerization to date. The water-based SEC (Figure 3.4) confirms our prior conclusions[5] that low DP anhydro-oligosaccharides form in the initial moments of cellulose fast pyrolysis. As previously noted,[5] the decrease in RI signal for larger anhydro-oligosaccharides is likely due to water solubility limitations.

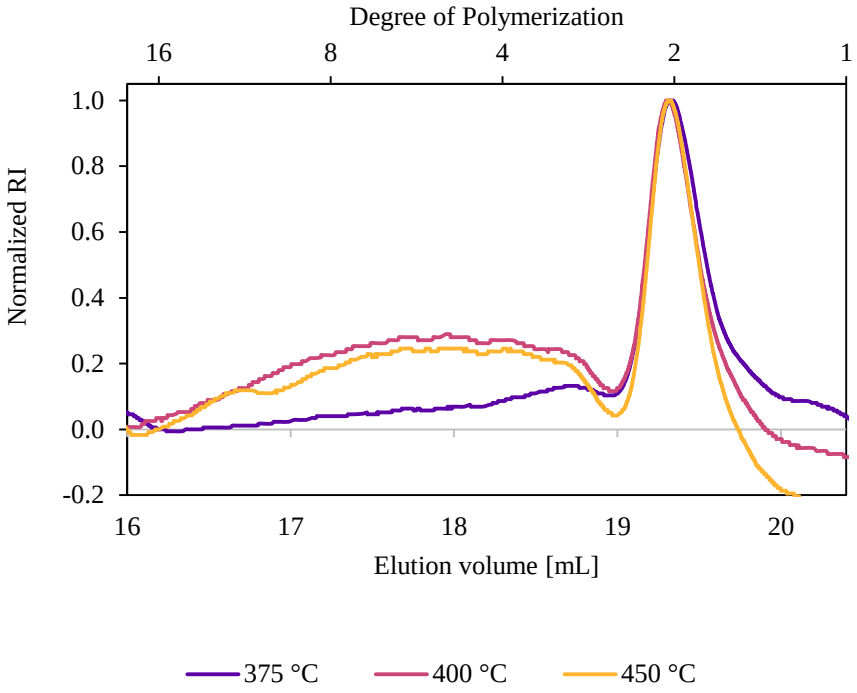

Figure 3.4. All tested free fall temperatures have similar water-soluble anhydro-oligosaccharide products, although water-based SEC can only detect low DP anhydro-oligosaccharides. DP based on retention times reported by Lindstrom *et al.*[5]

Water-insoluble anhydro-oligosaccharides are up to two orders of magnitude longer than their water-soluble counterparts. Figure 3.5A shows the normalized SEC spectra of these anhydro-oligosaccharides. This methodology uses different conditions than in Figure 3.4, so the elution volumes are not comparable. While the chromatographic shift appears slight, even in this early stage of thermal depolymerization the DP has decreased by approximately 18% (Figure 3.5B).

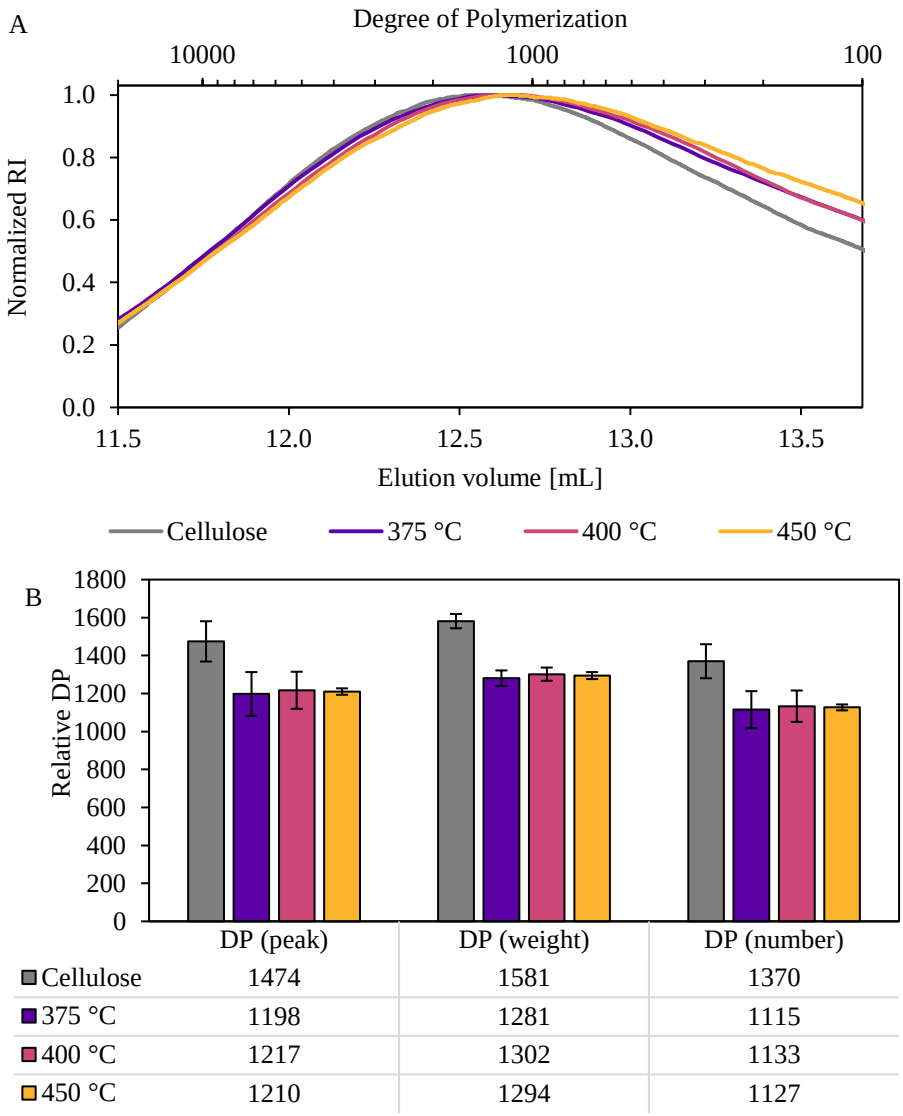

Figure 3.5. The SEC spectra (A) and quantified results (B) demonstrate that all tested reactor temperatures reduced the DP compared to unmodified cellulose.

Both water- and DMAc-based SEC demonstrate that cellulose thermal depolymerization proceeds rapidly via cracking reactions. This analysis corroborates Broido *et al.*[8] and Lindstrom *et al.*,[5] and refutes the theory that cracking reactions only occur above 467 °C.[26,27]

By definition, DP is the main variable during thermal depolymerization, but degree of crystallinity is also often considered due to its potential capability to influence

deconstruction reactions.[28–30] Despite decrystallization activation energies[31] being approximately half that for depolymerization,[32–34] the brief thermal deconstruction in our free fall reactor does not greatly decrystallize cellulose from its native crystal structure, Cellulose-Iβ[29] (Figure 3.6). X-ray diffraction (XRD) experiments determine that cellulose crystallinity index (CI) decreases by 9, 7, and 16% during the approximately 1 s residence time of cellulose in the free fall reactor at reactor temperatures of 375, 400, and 450 °C, respectively.

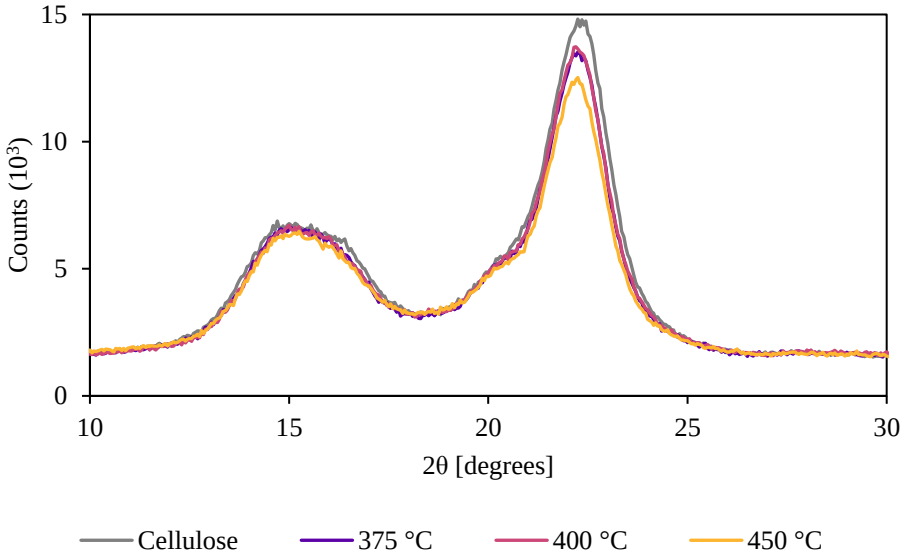

Figure 3.6. Cellulose retains most of its cellulose-Iβ crystalline structure after incomplete thermal deconstruction, as demonstrated by XRD spectra.

Despite the small reduction in CI, crystallinity does not appear to play a major role in cellulose thermal deconstruction. In 1977, Broido and Yow[35] considered a "weak-link mechanism" where cellulose does not crack randomly but rather breaks at more frangible areas of the polymer. Recent computational chemistry supports this theory, deducing that hydroxyl groups from adjacent cellulose sheets within a crystal can lower cracking activation energy.[17,36,37] Nevertheless, our experiments do not reveal multi-modal distributions, which according to Broido and Yow[35] would be evidence of non-

random cracking. This result cannot prove a negative; however, cellulose depolymerization appears independent of crystallinity within this thermally energetic regime. Additionally, the possibility of lower activation energies deserves further study because models using frequently cited cellulose cracking activation energies[33,34] predict large reaction time variations[38] not evident in experiments.[5]

Several computational studies conclude that kinetic rates for depolymerization mechanisms are similar for mid-chain cracking and end-chain levoglucosan production;[33,34] thus something else must account for the initial prevalence of cracking reactions. Activation energies and pre-exponential factors are only part of the rate equation. Concentration, or in this case relative bond frequency, directly influences reaction rates. During the early stages of cellulose thermal depolymerization, relative bond frequency far outweighs minor differences in kinetic parameters between end- and mid-chain reactions. For example, an anhydro-oligosaccharide with a DP of 500 has two end-chain bonds and 497 mid-chain bonds. This probability overwhelmingly favors cracking.

Figure 3.7 illustrates the effect of relative end and mid-chain bond frequency on the progression of cellulose depolymerization. Five ratios of end- over mid-chain reactions are shown, all of which fall within the computational margin of error[39] from Mayes and Broadbelt[33] for these reactions. The exponential shifts in probability from high to low DP expose the inexorable nature of cellulose thermal deconstruction. For initial depolymerization, relative bond frequency is more important than the relative reaction rates.

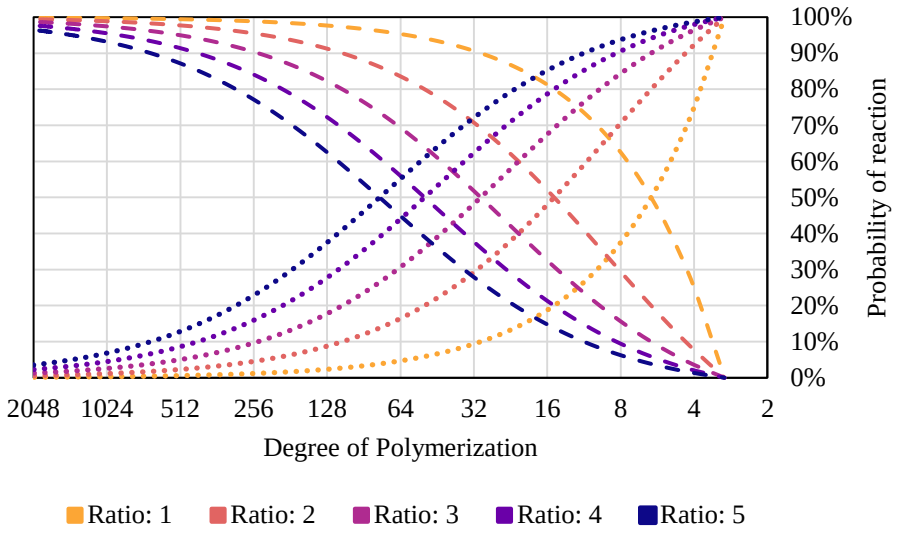

Figure 3.7. Cellulose and anhydro-oligosaccharide DP strongly influences whether cracking or end-chain reactions are more likely to occur. The ratio is defined as the likelihood of a depolymerization reaction occurring in the end over the middle of the chain. Dotted and dashed lines represent the probability of an end- and mid-chain reaction, respectively.

Conclusions

Relative bond frequency drives initial cellulose thermal depolymerization more so than even relatively large differences in reaction rate coefficients. Examining the solid phase thermal depolymerization reactions yields direct evidence that random cracking reactions lower cellulose DP, regardless of temperature. Cellulose crystallinity does not appear to affect this thermal deconstruction. This first analysis of the full complement of intermediate oligomeric products from rapid thermal depolymerization of cellulose, including previously undetected water-insoluble anhydro-oligosaccharides, challenges models that only account for small, water-soluble oligomers.

Conflicts of interest

There are no conflicts to declare.

Acknowledgements

The authors gratefully acknowledge funding from the National Science Foundation (award number: 1630404), U.S. Department of Energy's Office of Energy Efficiency & Renewable Energy (award number: DE-EE0008326), and the Gary and Donna Hoover Endowment. Additionally, the authors appreciate Scott Schlorholtz and Warren Straszheim at the Materials Analysis and Research Laboratory for performing the XRD and SEM experiments, respectively. JKL gratefully recognizes Brent H. Shanks suggesting and discussing the XRD experiments.

Notes and references

§ In 1973, Broido *et al.*[8] surely generated large anhydro-oligosaccharides despite not knowing their exact chemical structure. Only in 1987 did Radlein *et al.*[40] identify anhydro-oligosaccharides as the main intermediate product from cellulose pyrolysis.

§§ Cellulose nitration for chromatography is not used today for two reasons: nitration can hydrolyze cellulose, thus reducing DP,[22] and nitrocellulose is a low explosive, although generally stable.[41]

§§§ Pullulan polysaccharide standards (Agilent Technologies) with the following peak molecular weights [Da] were used to calibrate the SEC: 6,100; 9,600; 21,100; 47,100; 107,000; 200,000; 344,000; and 708,000.

(1) Brown, T. R. Economic Comparison of Various Pathways to Pyrolysis-Based Fuels. In *Fast Pyrolysis of Biomass: Advances in Science and Technology*; Brown, R. C., Wang, K., Eds.; Royal Society of Chemistry: London, U.K., 2017; pp 254–272.

(2) Oudenhoven, S. R. G.; van der Ham, A. G. J.; van den Berg, H.; Westerhof, R. J. M.; Kersten, S. R. A. Using Pyrolytic Acid Leaching as a Pretreatment Step in a Biomass Fast Pyrolysis Plant: Process Design and Economic Evaluation. *Biomass and Bioenergy* **2016**, *95*, 388–404.

(3) Zhang, J.; Choi, Y. S.; Yoo, C. G.; Kim, T. H.; Brown, R. C.; Shanks, B. H. Cellulose–Hemicellulose and Cellulose–Lignin Interactions during Fast Pyrolysis. *ACS Sustain. Chem. Eng.* **2015**, *3* (2), 293–301.

(4) Patwardhan, P. R.; Satrio, J. A.; Brown, R. C.; Shanks, B. H. Product Distribution from Fast Pyrolysis of Glucose-Based Carbohydrates. *J. Anal. Appl. Pyrolysis* **2009**, *86* (2), 323–330.

(5) Lindstrom, J. K.; Proano-Aviles, J.; Johnston, P. A.; Peterson, C. A.; Stansell, J. S.; Brown, R. C. Competing Reactions Limit Levoglucosan Yield during Fast Pyrolysis of Cellulose. *Green Chem.* **2019**, *21* (1), 178–186.

(6) Proano-Aviles, J.; Lindstrom, J. K.; Johnston, P. A.; Brown, R. C. Heat and Mass Transfer Effects in a Furnace-Based Micropyrolyzer. *Energy Technol.* **2017**, *5* (1), 189–195.

(7) Liu, D.; Yu, Y.; Wu, H. Evolution of Water-Soluble and Water-Insoluble Portions in the Solid Products from Fast Pyrolysis of Amorphous Cellulose. *Ind. Eng. Chem. Res.* **2013**, *52* (36), 12785–12793.

(8) Broido, A.; A.C., J.-S.; Ouano, A. C.; Barrall II, E. M. Molecular Weight Decrease in the Early Pyrolysis of Crystalline and Amorphous Cellulose. *J. Appl. Polym. Sci.* **1973**, *17*, 3627–3635.

(9) Weinstein, M. Thermogravimetric Analysis of Ammonia-Swelled Cellulose. *Combust. Sci. Technol.* **1970**, *1* (4), 279–285.

(10) Alexander, W. J.; Mitchell, R. L. Rapid Measurement of Cellulose Viscosity by the Nitration Method. *Anal. Chem.* **1949**, *21* (12), 1497–1500.

(11) Lindstrom, J. K.; Shaw, A.; Zhang, X.; Brown, R. C. Condensed Phase Reactions during Thermal Deconstruction. In *Thermochemical Processing of Biomass: Conversion into Fuels, Chemicals and Power*; Brown, R. C., Ed.; John Wiley and Sons, 2019; pp 17–48.

(12) Zhou, X.; Nolte, M. W.; Shanks, B. H.; Broadbelt, L. J. Experimental and Mechanistic Modeling of Fast Pyrolysis of Neat Glucose-Based Carbohydrates. 2. Validation and Evaluation of the Mechanistic Model. *Ind. Eng. Chem. Res.* **2014**, *53* (34), 13290–13301.

(13) Piskorz, J.; Majerski, P.; Radlein, D.; Vladars-Usas, A.; Scott, D. S. Flash Pyrolysis of Cellulose for Production of Anhydro-Oligomers. *J. Anal. Appl. Pyrolysis* **2000**, *56* (2), 145–166.

(14) Pouwels, A. D.; Eijkel, G. B.; Arisz, P. W.; Boon, J. J. Evidence for Oligomers in Pyrolysates of Microcrystalline Cellulose. *J. Anal. Appl. Pyrolysis* **1989**, *15*, 71–84.

(15) Boutin, O.; Ferrer, M.; Lédé, J. Radiant Flash Pyrolysis of Cellulose—Evidence for the Formation of Short Life Time Intermediate Liquid Species. *J. Anal. Appl. Pyrolysis* **1998**, *47* (1), 13–31.

(16) Lédé, J.; Blanchard, F.; Boutin, O. Radiant Flash Pyrolysis of Cellulose Pellets: Products and Mechanisms Involved in Transient and Steady State Conditions. *Fuel* **2002**, *81* (10), 1269–1279.

(17) Lin, Y.-C.; Cho, J.; Tompsett, G. A.; Westmoreland, P. R.; Huber, G. W. Kinetics and Mechanism of Cellulose Pyrolysis. *J. Phys. Chem. C* **2009**, *113* (46), 20097–20107.

(18) Gable, P.; Brown, R. C. Effect of Biomass Heating Time on Bio-Oil Yields in a Free Fall Fast Pyrolysis Reactor. *Fuel* **2016**, *166*, 361–366.

(19) Lédé, J. Cellulose Pyrolysis Kinetics: An Historical Review on the Existence and Role of Intermediate Active Cellulose. *J. Anal. Appl. Pyrolysis* **2012**, *94*, 17–32.

(20) Dawsey, T. R.; McCormick, C. L. The Lithium Chloride/Dimethylacetamide Solvent for Cellulose: A Literature Review. *J. Macromol. Sci. Part C* **1990**, *30* (3–4), 405–440.

(21) Klemm, D.; Philipp, D.; Heinze, T.; Heinze, U.; Wagenknecht, W. Swelling and Dissolution of Cellulose. In *Comprehensive Cellulose Chemistry*; Wiley-VCH: Weinheim, Germany, 1998; pp 43–82.

(22) Hallac, B. B.; Ragauskas, A. J. Analyzing Cellulose Degree of Polymerization and Its Relevancy to Cellulosic Ethanol. *Biofuels, Bioprod. Biorefining* **2011**, *5*, 215–225.

(23) McCormick, C. L. Novel Cellulose Solutions. 4,278,790, 1981.

(24) Schult, T.; Hjerde, T.; Optun, O. I.; Kleppe, P. J.; Moe, S. Characterization of Cellulose by SEC-MALLS. *Cellulose* **2002**, *9*, 149–158.

(25) McCormick, C. L.; Hutchinson, B. H. Solution Studies of Cellulose in Lithium Chloride and N,N-Dimethylacetamide. *Macromolecules* **1985**, *18* (1529), 2394–2401.

(26) Krumm, C.; Pfaendtner, J.; Dauenhauer, P. J. Millisecond Pulsed Films Unify the Mechanisms of Cellulose Fragmentation. *Chem. Mater.* **2016**, *28*, 3108–3114.

(27) Zhu, C.; Krumm, C.; Facas, G. G.; Neurock, M.; Dauenhauer, P. J. Energetics of Cellulose and Cyclodextrin Glycosidic Bond Cleavage. *React. Chem. Eng.* **2017**, *2* (2), 201–214.

(28) Zhang, J.; Nolte, M. W.; Shanks, B. H. Investigation of Primary Reactions and Secondary Effects from the Pyrolysis of Different Celluloses. *ACS Sustain. Chem. Eng.* **2014**, *2* (12), 2820–2830.

(29) Mukarakate, C.; Mittal, A.; Ciesielski, P. N.; Budhi, S.; Thompson, L.; Iisa, K.; Nimlos, M. R.; Donohoe, B. S. Influence of Crystal Allomorph and Crystallinity on the Products and Behavior of Cellulose during Fast Pyrolysis. *ACS Sustain. Chem. Eng.* **2016**, *4* (9), 4662–4674.

(30) Wang, Z.; McDonald, A. G.; Westerhof, R. J. M.; Kersten, S. R. A.; Cuba-Torres, C. M.; Ha, S.; Pecha, B.; Garcia-Perez, M. Effect of Cellulose Crystallinity on the Formation of a Liquid Intermediate and on Product Distribution during Pyrolysis. *J. Anal. Appl. Pyrolysis* **2013**, *100*, 56–66.

(31) Parthasarathi, R.; Bellesia, G.; Chundawat, S. P. S.; Dale, B. E.; Langan, P.; Gnanakaran, S. Insights into Hydrogen Bonding and Stacking Interactions in Cellulose. *J. Phys. Chem. A* **2011**, *115* (49), 14191–14202.

(32) Zhang, X.; Li, J.; Yang, W.; Blasiak, W. Formation Mechanism of Levoglucosan and Formaldehyde during Cellulose Pyrolysis. *Energy & Fuels* **2011**, *25* (8), 3739–3746.

(33) Mayes, H. B.; Broadbelt, L. J. Unraveling the Reactions That Unravel Cellulose. *J. Phys. Chem. A* **2012**, *116* (26), 7098–7106.

(34) Zhang, X.; Yang, W.; Dong, C. Levoglucosan Formation Mechanisms during Cellulose Pyrolysis. *J. Anal. Appl. Pyrolysis* **2013**, *104*, 19–27.

(35) Broido, A.; Yow, H. Resolution of Molecular Weight Distributions in Slightly Pyrolyzed Cellulose Using the Weibull Function. *J. Appl. Polym. Sci.* **1977**, *21* (6), 1677–1685.

(36) Seshadri, V.; Westmoreland, P. R. Concerted Reactions and Mechanism of Glucose Pyrolysis and Implications for Cellulose Kinetics. *J. Phys. Chem. A* **2012**, *116* (49), 11997–12013.

(37) Maliekkal, V.; Maduskar, S.; Saxon, D. J.; Nasiri, M.; Reineke, T. M.; Neurock, M.; Dauenhauer, P. Activation of Cellulose via Cooperative Hydroxyl-Catalyzed Transglycosylation of Glycosidic Bonds. *ACS Catal.* **2019**, 1943–1955.

(38) Burnham, A. K.; Zhou, X.; Broadbelt, L. J. Critical Review of the Global Chemical Kinetics of Cellulose Thermal Decomposition. *Energy & Fuels* **2015**, *29* (5), 2906–2918.

(39) Lynch, B. J.; Fast, P. L.; Harris, M.; Truhlar, D. G. Adiabatic Connection for Kinetics. *J. Phys. Chem. A* **2000**, *104* (21), 4811–4815.

(40) Radlein, D. S.; Grinshpun, A.; Piskorz, J.; Scott, D. S. On the Presence of Anhydro-Oligosaccharides in the Sirups from the Fast Pyrolysis of Cellulose. *J. Anal. Appl. Pyrolysis* **1987**, *12* (1), 39–49.

(41) Meyer, R.; Köhler, J.; Homberg, A. *Explosives*, 6th ed.; Wiley-VCH, 2007.

CHAPTER 4 STRUCTURAL AND CHEMICAL CHANGES IN PLANT CELL WALLS DURING EARLY STAGES OF THERMAL DECONSTRUCTION

Jake K. Lindstrom,[a] Chad A. Peterson,[a] Peter N. Ciesielski,[b] John Ralph,[c] Mingjie Chen,[c] Joseph E. Jakes,[d] Preston A. Gable,[e] Robert C. Brown[a,e]

a- Department of Mechanical Engineering, Iowa State University, Ames, IA 50011, United States of America

b- Biosciences Center and National Bioenergy Center, National Renewable Energy Laboratory, 15013 Denver West Parkway, Golden, Colorado 80401-3393, United States of America

c- Department of Biochemistry, and the Department of Energy's Great Lakes Bioenergy Research Center, the Wisconsin Energy Institute, University of Wisconsin-Madison, 1552 University Ave. Madison, WI 53726-4084, United States of America

d- Forest Biopolymers Science and Engineering, USDA Forest Service, Forest Products Laboratory, One Gifford Pinchot Drive, Madison, WI 53726, United States of America

e- Bioeconomy Institute, Iowa State University, Ames, IA 50011, United States of America

Abstract

Volatile products from lignocellulosic biomass thermal deconstruction processes—combustion, gasification, fast pyrolysis, and solvent liquefaction—have been well characterized, but the solid- and liquid-phase reactions that occur in the early stages of decomposition are largely unknown. Here we analyze the initial solid-phase biomass thermal deconstruction reactions *in situ* and with high particle heating rates, delineating how these processes occur. Using a variety of instrumentation, we quantify the extent and relative rates of deconstruction, demonstrating that biopolymers resist the thermally energetic conditions to differing degrees, even when ensconced in biomass cell walls. Hemicellulose and the more frangible lignin components decompose and volatilize more readily than cellulose; this outcome temporarily enriches biomass with cellulose. These

chemical changes manifest in larger cell wall structural and mechanical property transformations. In all, our investigation concludes that these solid-phase reactions strongly influence the production rates of volatile species and will require additional study before these processes can be modeled precisely to improve product yields.

Introduction

Thermochemical processing, which employs thermal energy at elevated temperatures to achieve rapid deconstruction of feedstocks, is effective in converting recalcitrant lignocellulosic biomass into gaseous, liquid, and solid products.[1] These thermally-driven processes include pyrolysis,[2] gasification,[3] combustion,[4] and solvent liquefaction.[5] Thermochemical processes have been exploited by humankind for thousands of years to convert coal and biomass into energy and chemical products, and yet the incipient reactions common to all four processes are poorly understood.[6] This limited understanding of condensed-phase reactions arises from two sources: the focus of most thermochemical processes is to produce volatile products; and interrogating high temperature reactions of condensed-phase matter is notoriously difficult.

Volatile products include hot flue gas from combustion, synthesis gas from gasification and bio-oil condensed from fast pyrolysis or solubilized during solvent liquefaction. For millennia, humans have used these products for heating,[7] curing pottery,[7] embalming Pharaohs,[8] waterproofing ships,[9] as well as a plethora of other applications.[10–13] Accordingly, researchers have focused on characterizing volatile products released from thermochemical processes, but this approach has created a substantial knowledge gap: condensed-phase reactions that precede volatile product formation.[6]

For several decades, researchers have recognized the importance of condensed-phase reactions in determining the outcome of thermochemical processes but have not had recourse to appropriate instrumentation to enable interrogation of the interior of hot, rapidly reacting biomass particles. Consequently, researchers have resorted to deducing reaction mechanisms from volatile products released from the condensed phase, which is frequently not even time resolved. Several recent studies have leveraged innovative reactor designs to truncate rapid thermal deconstruction prematurely, so the intermediate products can be evaluated;[14–16] however, none of these efforts has analyzed the solid-phase reactions within lignocellulosic biomass.

Herein, we present a comprehensive analysis of the reactions occurring during rapid biomass thermal deconstruction. Our analyses focus on the early stages of thermochemical processing, before subsequent gas-phase reactions. By concentrating solely on the initial solid-phase reactions, our results and conclusions are applicable to most high temperature biomass thermochemical processing methodologies because they primarily differ in the extent and type of secondary gas-phase reactions. An enhanced understanding of these initial reactions can inform subsequent modeling and related efforts to improve these processes.

Thermal deconstruction of biomass particles

We performed so-called "truncated thermal deconstruction" experiments on *Quercus rubra* (red oak) in a free-fall reactor (Figure 4.1) to produce partially-reacted solid particles (Figure 4.2). These partially-reacted samples were subjected to offline analysis using a variety of sophisticated analytical methods to understand incipient reactions in the condensed phase. The continuously-fed biomass fibers (250-850 μm) were entrained

through the pre-heated zone with nitrogen gas; after approximately 0.9 s of reaction time, the exiting particles were quenched with cold nitrogen gas (approximately -196 °C). The Supplemental Material presents additional free-fall modeling. Volatile products were condensed by an electrostatic precipitator (ESP) followed by a water-cooled condenser. By performing experiments at three different reactor temperatures (400, 450, 500 °C), we were able to examine the effect of temperature on product yields and biopolymer composition.

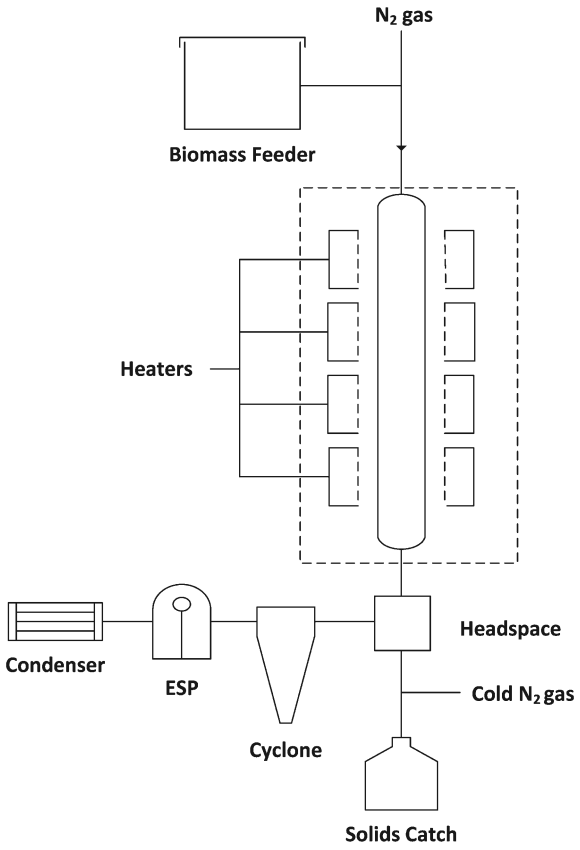

Figure 4.1. Reactor design for incomplete thermal deconstruction. Block flow diagram of the free-fall reactor.

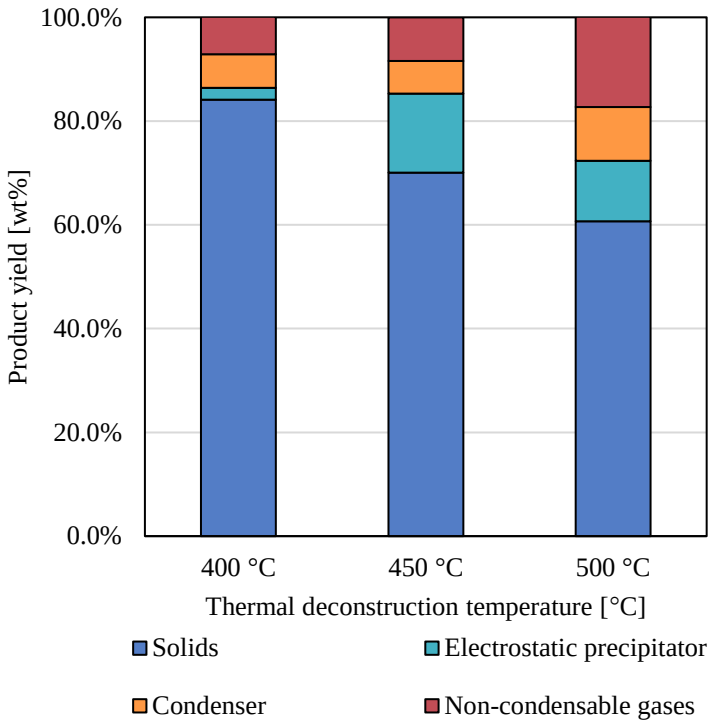

Figure 4.2. Reactor yields from incomplete thermal deconstruction. Product yield dependence on reactor temperature.

We first measured the ash, fixed carbon, and volatiles content of our red oak before partial thermal deconstruction (termed “native”) and also after (labelled according to reactor temperature) to gauge the severity of reaction conditions (Figure 4.3). The volatiles content of the partially deconstructed red oak decreased with increasing reactor temperature compared to native red oak. However, under the most severe reactor conditions, the partially reacted red oak still retained 60% of its initial volatiles content, indicating that the biomass particles were only partially degraded—a significant distinction between previous efforts to probe the early stages of thermal deconstruction.

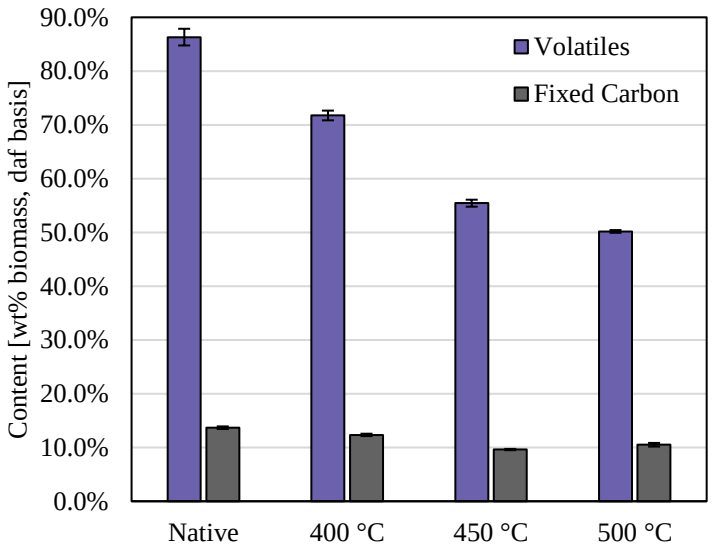

Figure 4.3. Extent of thermal deconstruction. Volatiles decreased as a function of reaction temperature, but fixed carbon remained constant. Error bars represent 95% confidence intervals.

Chemical deconstruction

To analyze basic chemical deconstruction trends, we quantified the elemental composition of native and partially deconstructed red oak. These results reveal that rapid thermochemical processing deconstructs biomass differently than slower methods. In slow thermal deconstruction processes, such as torrefaction or slow pyrolysis, the hemicellulosic fraction of biomass degrades first, which lowers the atomic ratios of oxygen to carbon and hydrogen to carbon.[6,17,18] In our rapid thermochemical experiments, however, these ratios do not change significantly throughout the process (Figure 4.4), indicating that all biopolymers—both polysaccharides and lignin—degraded simultaneously during these truncated thermal deconstruction experiments.

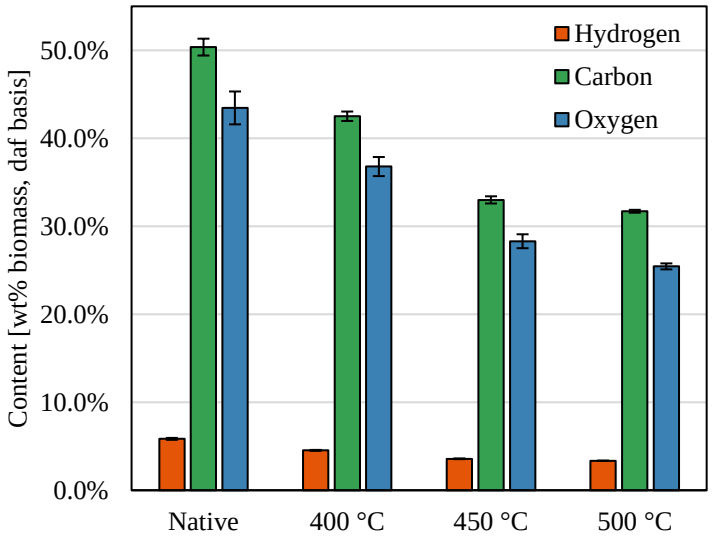

Figure 4.4. Elemental composition of the biomass. The reduction in volatiles content reduced the amount of each element, but the hydrogen to carbon and oxygen to carbon atomic ratios remain similar. Error bars represent 95% confidence intervals.

To investigate how each biopolymer degrades individually, we performed compositional analysis. Except for lignin, these experiments do not quantify biopolymers directly, but measure sub-components that reflect the amounts of biopolymers formed.[19] Cellulose is a polymer composed of glucan monomers, so glucan serves as our cellulose proxy; however, hemicelluloses also contains some glucan, which slightly obscures our glucan-cellulose surrogacy. In addition to glucan, hemicelluloses are composed of xylan, galactan, mannan, and arabinan, as well as hexuronic acids, and may be decorated with pendant acetyl groups.[20] In lignocellulosic biomass, these monosaccharides and the acetyl moiety are only derived from hemicelluloses, so they serve as our hemicellulose indicators. While imperfect, this methodology allows us to investigate changes in biopolymer composition during thermal deconstruction.

Figure 4.5 indicates the extent of solid-phase biopolymer deconstruction. Cellulose (composed of glucan monomers) is more resistant to thermal deconstruction than either lignin or hemicelluloses. Thus, during thermal deconstruction, biomass is enriched

temporarily with cellulose as the relative composition of cellulose rises due to the disproportionate volatilization rates of the other biopolymers. Hemicelluloses, represented by xylan, galactan, arabinan, mannan, and acetyl, decomposes readily during thermal deconstruction. Notably, for hardwoods such as red oak, the galactan, arabinan, and mannan exist primarily within the innermost cell wall layers.[20] The extent to which these components volatilize demonstrates that, during these truncated thermal deconstruction experiments, despite their brevity, reaction occurs within the entire cell wall.

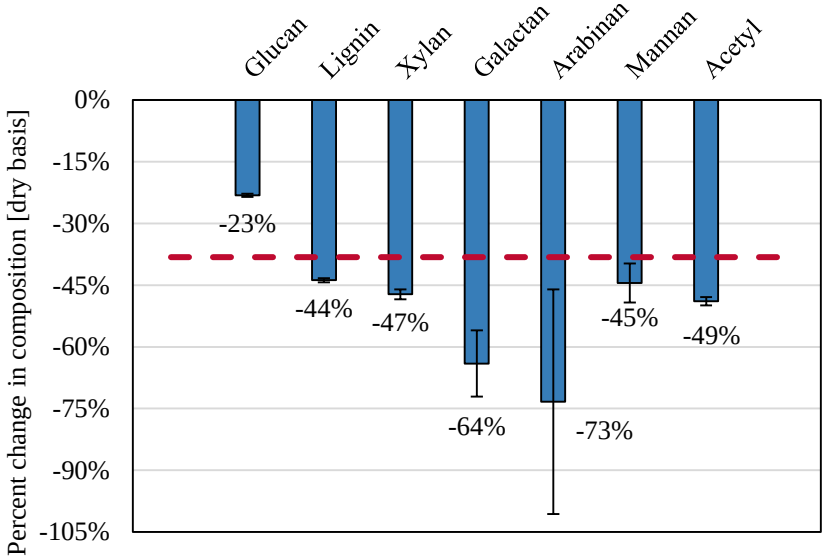

Figure 4.5. Changes in biomass composition. Relative reduction in biomass components after truncated thermal deconstruction at 450 °C after accounting for solids yield. The red dashed line indicates the expected change in biomass components if each component were reduced equally. Error bars represent standard deviation.

We further analyzed native and residual lignin using heteronuclear single-quantum coherence (HSQC) nuclear magnetic resonance (NMR) spectroscopy, which employs ^{1}H and ^{13}C nuclei to determine how the various units decompose and monomers volatilize (Figure 4.6a). Similar experiments have been performed for low temperature biomass pretreatment processes and high temperature *ex situ* lignin analysis,[21–25] but these data are

the first obtained from whole plant cell wall materials from intermediate stages of rapid thermal deconstruction. Our experiments reveal that even during truncated thermal deconstruction the structure of lignin is significantly modified.

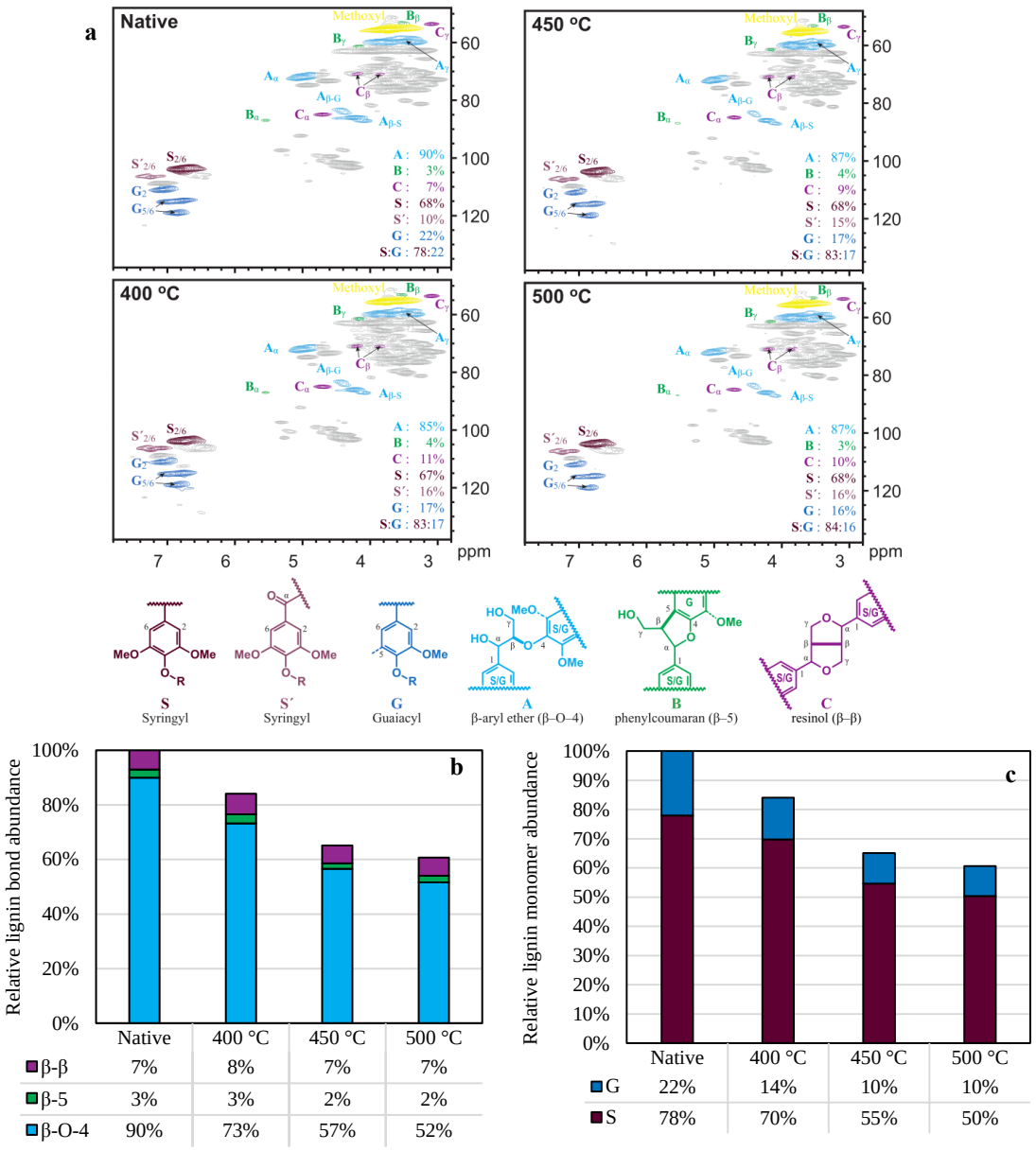

Figure 4.6. Plant lignin thermal deconstruction. a, $^{1}H–^{13}C$ HSQC NMR spectra of red oak before and after truncated thermal deconstruction at different temperatures. **b**, Abundance of major lignin units (with their characteristic inter-unit linkages) as a function of reactor temperature. **c**, Abundance of lignin monomers as a function of reactor temperature.

Figure 4.6b demonstrates how certain lignin units, namely the β-ether unit (with its characteristic β–O–4 bond), decompose readily, while more recalcitrant sections remain unperturbed, including those units linked by β–β and β–5 bonds. This result corroborates prior computational chemistry work that determined lignin bond dissociation energies (BDEs). The BDE of the β–O–4 bond[26] is less than that of either the β–β[26] or β–5.[27] Our work confirms deductions inspired by the results of computational chemistry studies.

Additionally, the data in Figure 4.6c suggests avenues for future study. Guaiacyl and syringyl monomers decreased by at most 53 and 40% respectively; however, α-keto-syringyl units **S´** were not reduced significantly. Two causes may explain this phenomenon. In biological processes, syringyl units **S** can be benzyl-oxidized to **S´** units, and a similar process may occur here, despite reaction in an inert gaseous environment. Regardless of the cause, this result indicates that monomers evolve from biomass at different rates.

Cell wall structural degradation

Using transmission and scanning electron microscopy (denoted TEM and SEM, respectively), we probed alterations to cell wall ultrastructure. Figure 4.7 compares TEM micrographs at two different magnifications of thin sections of native and thermally deconstructed red oak. We subjected samples to identical staining procedures using potassium permanganate ($KMnO_4$), which shows preference for lignin,[28] to enhance contrast. As expected, the staining patterns of native cell walls (Figure 4.7A and B) display a lignin-rich compound middle lamella (CML), which is comprises both middle lamella and both primary cell walls from the adjoining cells, which stained darker than the adjacent layers of secondary cell wall (SCW). The thermally deconstructed samples

(Figure 4.7C and D) exhibit a markedly different staining patterns; the CML region is substantially lighter than the native walls, such that the primary cell walls may be clearly differentiated from the middle lamella. Furthermore, the staining of the SCWs is also lighter than that observed in the native material. The reduction in staining intensity corroborates our compositional analysis, indicating significant delignification that is likely localized to regions of the cell wall that are relatively rich in the more volatile biopolymer components. Additionally, the texture of the thermally deconstructed material exhibits a prominent fibrillar pattern, further signifying lignin and hemicellulose removal.

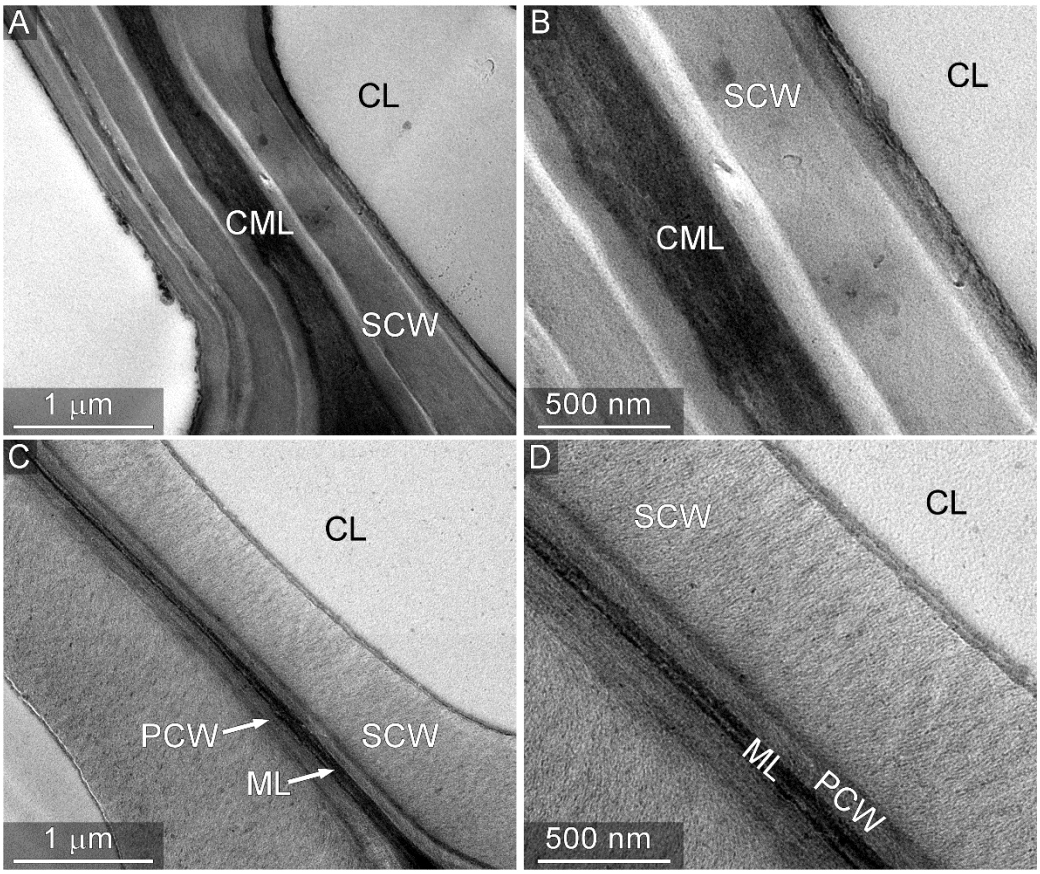

Figure 4.7. Transmission electron microscopy of native (A and B) and thermally deconstructed cell walls (C and D). Micrographs of native cell wall thin sections stained with $KMnO_4$ are shown at two different magnifications in (A) and (B). Micrographs of thermally deconstructed material subjected to identical sample preparation are shown in (C) and (D). The lighter staining of the SCW and middle lamella region indicate a reduction in the lignin content relative to native material. Annotations: CL, cell lumen; CML, compound middle lamella; SCW, secondary cell wall; PCW, primary cell wall; ML, middle lamella.

SEM imaging was employed to provide complimentary structural information about the surface of the cell wall cross sections of the same samples. The morphology of the cleaved surface of native cell walls (Figure 4.8A and B) appears globular, wherein bundles of cellulose fibrils are closely integrated with the cell wall matrix biopolymers, lignin and hemicellulose. In contrast, the morphology of the cleaved surface of the thermally deconstructed cell walls (Figure 4.8C and D) displays a notably more detailed texture; the fibrillar structure of cellulose microfibrils can be clearly observed (particularly in Figure 4.8D). Similar features have been reported previously for the nanostructure of cellulose fibrils in maize SCWs after minor thermochemical pretreatments that remove and relocate lignin.[29,30] In the context of our study, these observations further support the selective removal of the matrixing biopolymers that ensconce the cellulose in the native material, leaving behind the cellulosic component in greater relative abundance and allowing for clearer observation of its fibrillar nanostructure in the images of the thermally deconstructed material.

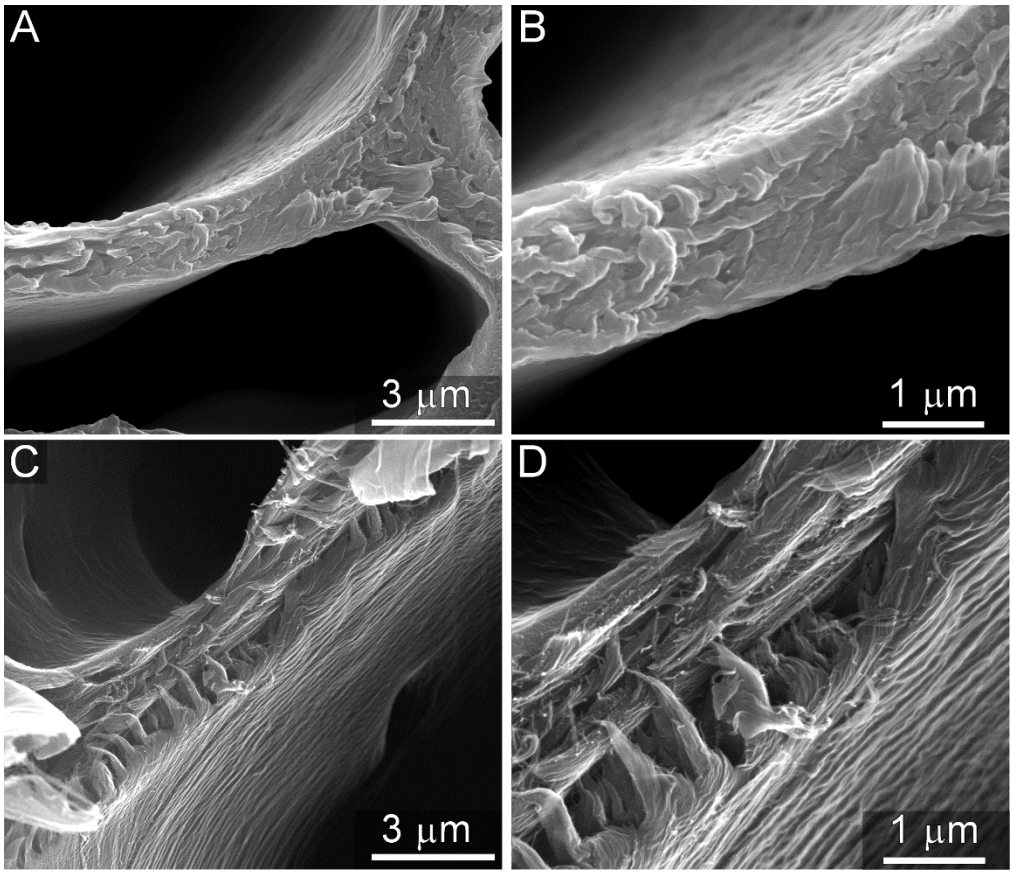

Figure 4.8. Scanning electron microscopy of native (A and B) and thermally deconstructed cell walls (C and D). Micrographs of native cell wall cross sections are shown at two different magnifications in (A) and (B). The cross-sectional surface of the thermally deconstructed material (C and D) displays a more fibrillar texture, which is characteristic of the nanostructure of cellulose microfibrils. This observation further supports the selective removal of the matrixing biopolymers lignin and hemicelluloses by the thermal deconstruction process.

Cell wall mechanical properties

We utilized nanoindentation to test SCW mechanical properties in the wood particles. We chose the anatomical longitudinal plane because the elastic modulus measurements are more sensitive to changes in matrix biopolymers when the elastic stiffness is measured perpendicular to the long axis of the stiff cellulose microfibrils. Nanoindentations were placed in SCWs between compound middle lamella and exposed lumina (Figure 4.9A and B). The obviously smaller residual nanoindentation impressions in the thermally deconstructed specimen serve as a first indication that the thermally

degraded SCWs increased in hardness, which indicates an increase in resistance to plastic deformation. Quantifying the changes in hardness and nanoindentation elastic modus for the native and thermally deconstructed material (Figure 4.9C) shows that thermal degradation modifies the SCWs inside the wood particles, corroborating the TEM and SEM observations (Figure 4.7 and Figure 4.8).

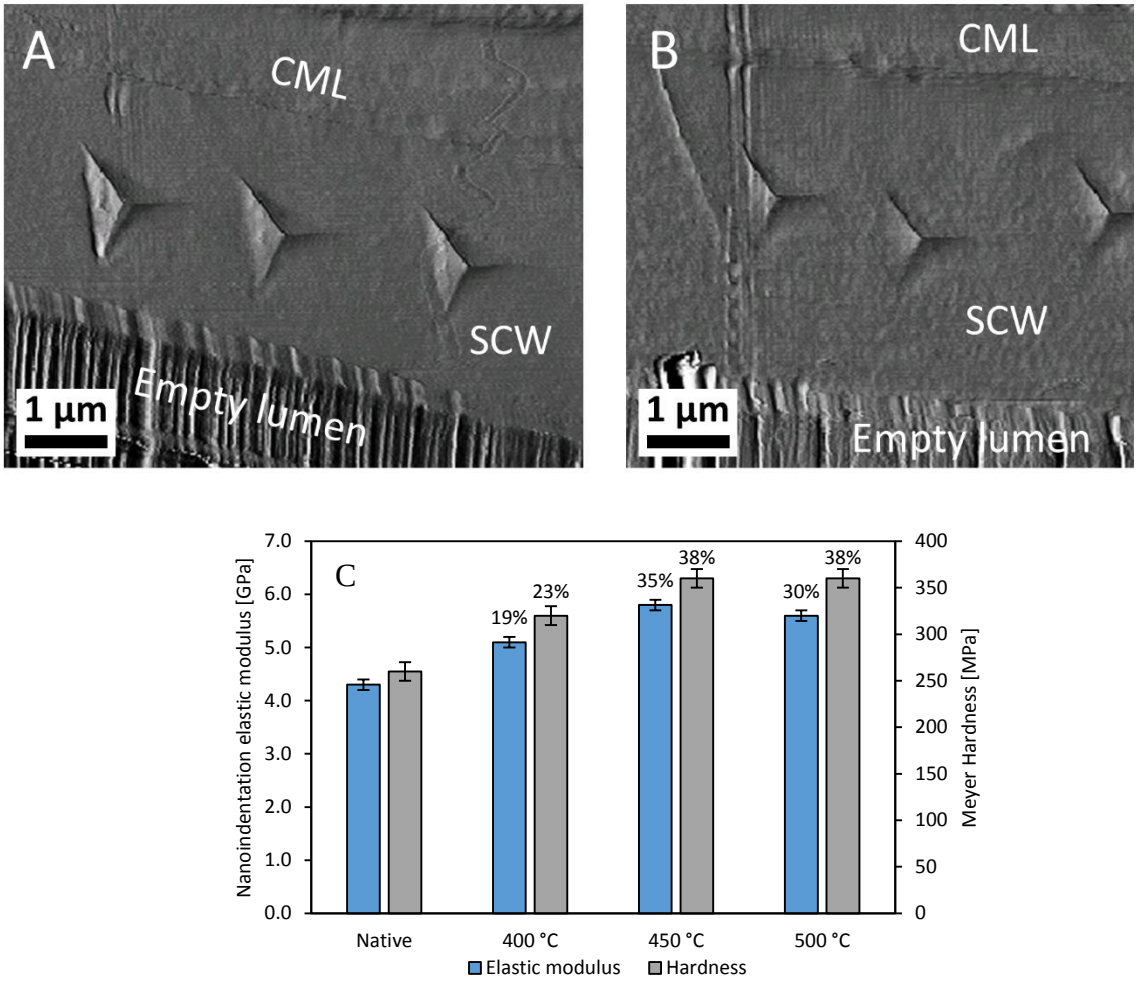

Figure 4.9. Nanoindentations (A and B) and hardness measurements (C) of the SCW. The atomic force microscopy images of the native (A) and thermally deconstructed material (B) at 500 °C demonstrate how we used nanoindentation to determine elastic modulus and Meyer Hardness (C) across the different processing temperatures and their percent change relative to those of native red oak. Annotations: CML, compound middle lamella; SCW, secondary cell wall. Error bars represent standard error.

The nanoindentation elastic modulus and hardness of the SCWs inside the particles increased after thermal deconstruction. The experiments were performed under

50% relative humidity conditions, and the increased mechanical strength is likely caused by a reduction in water sorption capacity. Water acts as a plasticizer in SCWs, and nanoindentation measurements of mechanical properties in the transverse[31,32] and longitudinal planes[33] of the SCW generally decrease with increasing amounts of absorbed water. Water sorption into hemicelluloses accounts for the majority of water sorption in SCWs. Therefore, the increases in SCW mechanical properties with temperature support that hemicelluloses are being modified or removed from the thermally deconstructed specimens. In previous nanoindentation experiments on the transverse wood plane, SCW hardness also increased in wood that underwent slow pyrolysis.[34,35] Collectively, these results suggest that, although matrix biopolymers are being removed during thermal degradation, any potential formation of a porous structure is not sufficient to decrease the mechanical properties of the SCW.

Conclusions

By interrogating the solid-phase reactions that occur during biomass thermal deconstruction, we have been able to more directly measure what previous studies could only deduce. Our work corroborates some prior theories but also adds substantial new insights. Primarily, our experiments indicate significant multiscale degradation stemming from underlying chemical transformations.

Cellulose, due to its insular microfibrils, resists initial thermal deconstruction more than does either hemicellulose or lignin. These microfibrils are more intact than the surrounding hemicellulose and lignin, which has the effect of enriching biomass with cellulose temporarily—a phenomenon not previously anticipated or detected.

Hemicelluloses, the other main class of biomass polysaccharides, rapidly decompose as expected. Even under the brief reaction conditions we studied, biomass hardness increased as hemicellulose was removed, corroborating related studies with substantially longer reaction durations.[34,35]

Lignin contains bonds that vary in both strength and abundance, and these aspects greatly influence its deconstruction rate and products. In particular, lignin monomers will volatilize at differing rates that relate to the initial composition of the lignin.

Our results foray into directly analyzing the solid-phase reactions occurring throughout rapid biomass thermal deconstruction. This multiscale investigation demonstrates that small chemical transformations can affect larger physical structure and mechanical properties. Each length-scale is worth studying in whole plant cell wall materials, as many of our observations would not be possible by using only extracted biopolymers. Overall, the rarely studied solid-phase reactions within biomass thermochemical processing are more varied than previously known, challenging models and theories to account for these phenomena.

Methods

Free-fall reactor

A free-fall reactor was used to generate thermally deconstructed red oak as described by Gable and Brown.[36] Biomass was fed into a 3.05 m tall reactor tube made of 316L stainless steel (internal diameter of 0.035 m) heated by ceramic Watlow heaters. Three reactor temperatures were used: 400, 450, and 500 °C. The 450 °C test was performed twice to collect sufficient solids for analysis. After approximately 0.9 s of residence time,

the reacting biomass particles exited the reactor tube and were rapidly quenched with gaseous nitrogen at approximately -196 °C, stopping all reactions promptly.

This method allows the effect of different temperatures to be compared directly by only changing the thermal profile experienced by the particles. (Final particle temperatures and residence times predicted by computational fluid dynamics are contained in Supplemental Material.) The vapor or aerosol products were collected by an electrostatic precipitator and then a condenser. The non-condensable gas yield was determined by difference.

All analyses were performed on unmodified red oak and red oak thermally deconstructed in the free-fall reactor.

Ultimate, Proximate, and Compositional analyses

A Mettler Toledo thermogravimetric analyzer (TGA)/differential scanning calorimeter (DSC) was used to determine the amount of moisture, volatiles, fixed carbon, and ash in each substrate using a 20 ± 0.5 mg sample. These tests were conducted in duplicate. The temperature profile used was developed by Johnston.[37]

An Elementar vario MICRO cube elemental analyzer was used to quantify chemical elements. Carbon, hydrogen, nitrogen, and sulfur content was determined, whereas oxygen was calculated by difference.[37] These tests were conducted in duplicate.

The compositional analysis was performed at the National Renewable Energy Laboratory using standard laboratory analysis procedures for ash,[38] lignin,[19] structural carbohydrates,[19] and extractives content.

HSQC NMR

Gel-state whole-cell-wall HSQC was performed on a Bruker Biospin AVANCE-III 700 MHz spectrometer following the procedure described by Kim and Ralph.[39] Briefly, the biomass (0.5 g) was ball-milled using a Fritsch Planetary micro mill Pulverisette 7 vibrating at 600 rpm for 4 h. The ball-milled sample (50 mg) was dissolved into DMSO-d_6/pyridine-d_5 (0.6 ml, 4:1, v/v) and subjected to HSQC studies. Bruker's Topspin 3.5 pl 7 (Mac) software was used to process spectra. The central DMSO solvent peak was used as internal reference (δ_C 39.5, δ_H 2.49 ppm).

Transmission Electron Microscopy

Samples were dehydrated by treating with increasing concentrations of ethanol in a Pelco laboratory microwave oven. Samples were then infiltrated with LR White (London Resin Company) at room temperature overnight. The infiltrated samples were polymerized in an oven in a nitrogen environment at 60 °C overnight. Samples were sectioned to ~80 nm and collected on polyvinyl formal coated copper slot grids (SPI Supplies, West Chester, PA). Grids were post-stained for 1 min with 1% aqueous $KMnO_4$. Images were captured with a four-megapixel Gatan UltraScan 1000 CCD camera (Gatan, Pleasanton, CA) using FEI Tecnai G2 20 Twin LaB6 TEM operated at 200 kV accelerating voltage (FEI, Hillsboro, OR).

Scanning Electron Microscopy

Samples were hand-sectioned to reveal cross sections of xylem tissue. The sections were freeze-dried prior to imaging to avoid dehydration artifacts and then mounted on aluminum stubs using carbon tape. The mounted samples were sputter-coated with 8 nm

of iridium. Imaging was performed at beam accelerating voltages from 15 to 20 keV with a FEI Quanta 400 FEG scanning electron microscope (FEI, Hillsboro, OR).

Nanoindentation

For the native and thermally deconstructed red oak, a representative wood particle was chosen. Nanoindentation surfaces were prepared in the longitudinal plane of unembedded wood following previously established procedures.[40–42] Quasi-static, multiload nanoindentation experiments were performed using a Bruker-Hysitron (Minneapolis, Minnesota, USA) TriboIndenter® equipped with a Berkovich probe. The relative humidity (RH) inside of the nanoindentation enclosure was maintained at 50% using an InstruQuest (Coconut Creek, Florida, USA) HumiSys^{TM} HF RH generator. Prepared specimens were placed inside of the nanoindenter enclosure at least 60 hours before experiment commencement, and the RH was maintained during the experiments. In each specimen, five to eight nanoindentations were performed in three different cell walls. The multiload nanoindentations were analyzed using the structural compliance method to correct for any potential edge effects and specimen-scale flexing.[40,43] Elastic modulus and Meyer hardness values were then calculated. A Quesant (Agoura Hills, California, USA) atomic force microscope (AFM) incorporated in the TriboIndenter was used for high resolution imaging or residual nanoindentations. The AFM was operated in contact mode and calibrated in lateral directions using an Advanced Surface Microscopy (Indianapolis, Indiana, USA) calibration standard as described previously.[40]

Acknowledgments

The authors gratefully acknowledge funding from the National Science Foundation (grant number 1630404), U.S. Department of Energy's (DOE) Office of Energy

Efficiency & Renewable Energy (award number: DE-EE0008326), and DOE Great Lakes Bioenergy Research Center (DOE Office of Science DE-SC0018409). Additionally, the authors would like to acknowledge Sean Rollag for error analysis assistance and Juan Proano-Aviles for initial free fall modeling work.

Data availability

The datasets generated and/or analyzed during the current study are available from the corresponding author on reasonable request.

References

(1) Zhang, X.; Brown, R. C. Introduction to Thermochemical Processing of Biomass into Fuels, Chemicals, and Power. In *Thermochemical Processing of Biomass: Conversion into Fuels, Chemicals and Power*; Brown, R. C., Ed.; John Wiley and Sons, 2019; pp 1–16.

(2) Bridgwater, A. V. Review of Fast Pyrolysis of Biomass and Product Upgrading. *Biomass and Bioenergy* **2012**, *38*, 68–94.

(3) Sikarwar, V. S.; Zhao, M.; Clough, P.; Yao, J.; Zhong, X.; Memon, M. Z.; Shah, N.; Anthony, E. J.; Fennell, P. S. An Overview of Advances in Biomass Gasification. *Energy Environ. Sci.* **2016**, *9* (10), 2939–2977.

(4) Mandø, M. Direct Combustion of Biomass. In *Biomass Combustion Science, Technology and Engineering*; Woodhead Publishing Limited, 2013; pp 61–83.

(5) Ghosh, A.; Haverly, M. R. Solvent Liquefaction. In *Thermochemical Processing of Biomass: Conversion into Fuels, Chemicals and Power*; Brown, R. C., Ed.; John Wiley and Sons, 2019; pp 257–306.

(6) Lindstrom, J. K.; Shaw, A.; Zhang, X.; Brown, R. C. Condensed Phase Reactions during Thermal Deconstruction. In *Thermochemical Processing of Biomass: Conversion into Fuels, Chemicals and Power*; Brown, R. C., Ed.; John Wiley and Sons, 2019; pp 17–48.

(7) Gowlett, J. A. J. The Discovery of Fire by Humans: A Long and Convoluted Process. *Philos. Trans. R. Soc. B Biol. Sci.* **2016**, *371* (1696), 20150164.

(8) Koller, J.; Baumer, U.; Kaup, Y.; Weser, U. Herodotus' and Pliny's Embalming Materials Identified on Ancient Egyptian Mummies. *Archaeometry* **2005**, *47* (3), 609–628.

(9) Evershed, R. P.; Jerman, K.; Eglinton, G. Pine Wood Origin for Pitch from the Mary Rose. *Nature* **1985**, *314* (6011), 528–530.

(10) Breault, R. W. Gasification Processes Old and New: A Basic Review of the Major Technologies. *Energies* **2010**, *3* (2), 216–240.

(11) Lillebø, A. H.; Holmen, A.; Enger, B. C.; Blekkan, E. A. Fischer-Tropsch Conversion of Biomass-Derived Synthesis Gas to Liquid Fuels. *Wiley Interdiscip. Rev. Energy Environ.* **2013**, *2* (5), 507–524.

(12) Iisa, K.; Robichaud, D. J.; Watson, M. J.; ten Dam, J.; Dutta, A.; Mukarakate, C.; Kim, S.; Nimlos, M. R.; Baldwin, R. M. Improving Biomass Pyrolysis Economics by Integrating Vapor and Liquid Phase Upgrading. *Green Chem.* **2018**, *20* (3), 567–582.

(13) Shanks, B. H.; Keeling, P. L. Bioprivileged Molecules: Creating Value from Biomass. *Green Chem.* **2017**, *19* (14), 3177–3185.

(14) Zhu, C.; Krumm, C.; Facas, G. G.; Neurock, M.; Dauenhauer, P. J. Energetics of Cellulose and Cyclodextrin Glycosidic Bond Cleavage. *React. Chem. Eng.* **2017**, *2* (2), 201–214.

(15) Lindstrom, J. K.; Proano-Aviles, J.; Johnston, P. A.; Peterson, C. A.; Stansell, J. S.; Brown, R. C. Competing Reactions Limit Levoglucosan Yield during Fast Pyrolysis of Cellulose. *Green Chem.* **2019**, *21* (1), 178–186.

(16) Thompson, L. C.; Ciesielski, P. N.; Jarvis, M. W.; Mukarakate, C.; Nimlos, M. R.; Donohoe, B. S. Estimating the Temperature Experienced by Biomass Particles during Fast Pyrolysis Using Microscopic Analysis of Biochars. *Energy & Fuels* **2017**, *31* (8), 8193–8201.

(17) Tumuluru, J. S.; Sokhansanj, S.; Hess, J. R.; Wright, C. T.; Boardman, R. D. A Review on Biomass Torrefaction Process and Product Properties for Energy Applications. *Ind. Biotechnol.* **2011**, *7* (5), 384–401.

(18) Weber, K.; Quicker, P. Properties of Biochar. *Fuel* **2018**, *217*, 240–261.

(19) Sluiter, A.; Hames, B.; Ruiz, R.; Scarlata, C.; Sluiter, J.; Templeton, D.; Crocker, D. *Determination of Structural Carbohydrates and Lignin in Biomass*; Golden, CO, 2012.

(20) Holtzapple, M. T. Hemicelluloses. In *Encyclopedia of Food Sciences and Nutrition*; Caballero, B., Ed.; Elsevier, 2003; pp 3060–3071.

(21) Yelle, D. J.; Kaparaju, P.; Hunt, C. G.; Hirth, K.; Kim, H.; Ralph, J.; Felby, C. Two-Dimensional NMR Evidence for Cleavage of Lignin and Xylan Substituents in Wheat Straw through Hydrothermal Pretreatment and Enzymatic Hydrolysis. *BioEnergy Res.* **2013**, *6* (1), 211–221.

(22) Kim, J. Y.; Oh, S.; Hwang, H.; Kim, U. J.; Choi, J. W. Structural Features and Thermal Degradation Properties of Various Lignin Macromolecules Obtained from Poplar Wood (Populus Albaglandulosa). *Polym. Degrad. Stab.* **2013**, *98* (9), 1671–1678.

(23) Kim, J.-Y.; Hwang, H.; Oh, S.; Kim, Y.-S.; Kim, U.-J.; Choi, J. W. Investigation of Structural Modification and Thermal Characteristics of Lignin after Heat Treatment. *Int. J. Biol. Macromol.* **2014**, *66*, 57–65.

(24) Mittal, A.; Katahira, R.; Donohoe, B. S.; Black, B. A.; Pattathil, S.; Stringer, J. M.; Beckham, G. T. Alkaline Peroxide Delignification of Corn Stover. *ACS Sustain. Chem. Eng.* **2017**, *5* (7), 6310–6321.

(25) Mittal, A.; Katahira, R.; Donohoe, B. S.; Pattathil, S.; Kandemkavil, S.; Reed, M. L.; Biddy, M. J.; Beckham, G. T. Ammonia Pretreatment of Corn Stover Enables Facile Lignin Extraction. *ACS Sustain. Chem. Eng.* **2017**, *5* (3), 2544–2561.

(26) Parthasarathi, R.; Romero, R. A.; Redondo, A.; Gnanakaran, S. Theoretical Study of the Remarkably Diverse Linkages in Lignin. *J. Phys. Chem. Lett.* **2011**, *2*, 2660–2666.

(27) Elder, T. Bond Dissociation Enthalpies of a Pinoresinol Lignin Model Compound. *Energy & Fuels* **2014**, *28*, 1175–1182.

(28) Donohoe, B. S.; Ciesielski, P. N.; Vinzant, T. B. Preservation and Preparation of Lignocellulosic Biomass Samples for Multi-Scale Microscopy Analysis. In *Biomass Conversion*; Humana Press: Totowa, NJ, 2012; pp 31–47.

(29) Ciesielski, P. N.; Matthews, J. F.; Tucker, M. P.; Beckham, G. T.; Crowley, M. F.; Himmel, M. E.; Donohoe, B. S. 3D Electron Tomography of Pretreated Biomass Informs Atomic Modeling of Cellulose Microfibrils. *ACS Nano* **2013**, *7* (9), 8011–8019.

(30) Ciesielski, P. N.; Wang, W.; Chen, X.; Vinzant, T. B.; Tucker, M. P.; Decker, S. R.; Himmel, M. E.; Johnson, D. K.; Donohoe, B. S. Effect of Mechanical Disruption on the Effectiveness of Three Reactors Used for Dilute Acid Pretreatment of Corn Stover Part 2: Morphological and Structural Substrate Analysis. *Biotechnol. Biofuels* **2014**, *7* (1), 47.

(31) Bertinetti, L.; Hangen, U. D.; Eder, M.; Leibner, P.; Fratzl, P.; Zlotnikov, I. Characterizing Moisture-Dependent Mechanical Properties of Organic Materials: Humidity-Controlled Static and Dynamic Nanoindentation of Wood Cell Walls. *Philos. Mag.* **2015**, *95* (16–18), 1992–1998.

(32) Yu, Y.; Fei, B.; Wang, H.; Tian, G. Longitudinal Mechanical Properties of Cell Wall of Masson Pine (Pinus Massoniana Lamb) as Related to Moisture Content: A Nanoindentation Study. *Holzforschung* **2011**, *65* (1), 121–126.

(33) Youssefian, S.; Jakes, J. E.; Rahbar, N. Variation of Nanostructures, Molecular Interactions, and Anisotropic Elastic Moduli of Lignocellulosic Cell Walls with Moisture. *Sci. Rep.* **2017**, *7* (1), 2054.

(34) Zickler, G. A.; Schöberl, T.; Paris, O. Mechanical Properties of Pyrolysed Wood: A Nanoindentation Study. *Philos. Mag.* **2006**, *86* (10), 1373–1386.

(35) Stanzl-Tschegg, S.; Beikircher, W.; Loidl, D. Comparison of Mechanical Properties of Thermally Modified Wood at Growth Ring and Cell Wall Level by Means of Instrumented Indentation Tests. *Holzforschung* **2009**, *63* (4), 443–448.

(36) Gable, P.; Brown, R. C. Effect of Biomass Heating Time on Bio-Oil Yields in a Free Fall Fast Pyrolysis Reactor. *Fuel* **2016**, *166*, 361–366.

(37) Johnston, P. A. Thermochemical Methylation of Lignin to Produce High Value Aromatic Compounds, Iowa State University, 2017.

(38) Sluiter, A.; Hames, B.; Ruiz, R.; Scarlata, C.; Sluiter, J.; Templeton, D. *Determination of Ash in Biomass*; Golden, CO, 2005.

(39) Kim, H.; Ralph, J. Solution-State 2D NMR of Ball-Milled Plant Cell Wall Gels DMSO-D6/Pyridine-D5. *Org. Biomol. Chem.* **2010**, *8* (3), 576–591.

(40) Jakes, J. E.; Frihart, C. R.; Beecher, J. F.; Moon, R. J.; Stone, D. S. Experimental Method to Account for Structural Compliance in Nanoindentation Measurements. *J. Mater. Res.* **2008**, *23* (4), 1113–1127.

(41) Jakes, J. E.; Yelle, D. J.; Beecher, J. F.; Frihart, C. R.; Stone, D. S. Characterizing Polymeric Methylene Diphenyl Diisocyanate Reactions with Wood: 2 . Nanoindentation. In *International Conference on Wood Adhesives*; Frihart, C. R., Hunt, C. G., Moon, R. J., Eds.; Forest Products Society: Lake Tahoe, Nevada, USA, 2009; pp 366–374.

(42) Jakes, J. E.; Hunt, C. G.; Yelle, D. J.; Lorenz, L.; Hirth, K.; Gleber, S.-C.; Vogt, S.; Grigsby, W.; Frihart, C. R. Synchrotron-Based X-Ray Fluorescence Microscopy in Conjunction with Nanoindentation to Study Molecular-Scale Interactions of Phenol–formaldehyde in Wood Cell Walls. *ACS Appl. Mater. Interfaces* **2015**, *7* (12), 6584–6589.

(43) Jakes, J. E.; Frihart, C. R.; Beecher, J. F.; Moon, R. J.; Resto, P. J.; Melgarejo, Z. H.; Suárez, O. M.; Baumgart, H.; Elmustafa, A. A.; Stone, D. S. Nanoindentation near the Edge. *J. Mater. Res.* **2009**, *24* (3), 1016–1031.

CHAPTER 5 OVERSIGHTS IN THE ANALYSIS OF BIOMASS THERMAL DECONSTRUCTION

Jake K. Lindstrom,[a] Brent H. Shanks,[b,c] Robert C. Brown[a,d]

a- Department of Mechanical Engineering, Iowa State University, Ames, IA 50011, USA

b- Department of Chemical and Biological Engineering, Iowa State University, Ames, IA 50011, USA

c- Center for Biorenewable Chemicals (CBiRC), Iowa State University, Ames, IA 50011, USA

d- Bioeconomy Institute, Iowa State University, Ames, IA 50011, USA

Abstract

Modeling and improving biomass thermochemical processing methodologies, such as fast pyrolysis or combustion, requires understanding the fundamentals of biomass thermal deconstruction. These processes pose significant analytical challenges, therefore strategic concessions are often employed to ease analysis. While sometimes necessary, these compromises have created large oversights, misrepresenting some aspects of the chemical and physical decomposition occurring. With the aim of suggesting methodologies to avoid future errors, this perspective discusses known areas of analytic compromise that may appear to be benign approximations, but instead have led to significant oversights in the field.

Introduction

Interest in biofuels and biobased chemicals has increased in recent decades,[1,2] driven by governmental policies to promote domestic production of transportation fuels[3–5] and growing concern about anthropogenic emissions of greenhouse gases.[6] Early success in biorenewables has come from processing sugar and starch feedstocks like sugar cane and corn grain into fermentation substrates. Extraction and conversion of the polysaccharides in lignocellulosic feedstocks like corn stover and wood has proved more challenging.[7,8] Despite advances in biomass pretreatments, enzyme production and

fermentation technologies, biochemical production of "cellulosic biofuels" represents a minor contribution to commercial biofuels production.[8,9]

Thermochemical routes to cellulosic and lignin-based biofuels have also been slow to commercialize, but have the potential for lower capital and operating costs than processing based on enzymatic hydrolysis.[7,10–13] Progress in thermal deconstruction of biomass is hampered by incomplete understanding of relevant physical and chemical phenomena, which has shown relatively modest advances in the last 40 years compared to biochemical routes. High temperatures and fast reaction rates makes it difficult to interrogate biomass during thermal deconstruction. As a result, most experimental studies have focused on the volatile products of thermal deconstruction rather than the condensed phase reactions that are key to understanding reaction rates and product distributions.

Modeling thermal deconstruction processes suffers from an incomplete set of key relevant experimental data, leading modelers to fill in the gaps with educated guesses. These omissions, we will demonstrate, have resulted in oversights in understanding the fundamental phenomena of thermal deconstruction. To these ends, we highlight three deficiencies in experimental studies of thermal deconstruction: overuse of proxies for real biomass; insufficient time resolution to capture reaction dynamics; and lack of data on condensed-phase species.

Overuse of proxies for real biomass

Researchers often use extracted biopolymers and small model compounds as surrogates for real lignocellulosic biomass, with the goal of simplifying experiments and analysis. For example, nuclear magnetic resonance (NMR) spectroscopy of extracted lignin is much easier than of lignin in biomass due to solubility and interference

challenges.[14–16] Nevertheless, these simplifications can quickly become over simplifications, obscuring important interactions among plant components or involving cell wall structures, as detailed subsequently.

Extracted biopolymers as proxies

Biopolymers extracted from lignocellulose have their place in experimentation, but two major issues can limit their usefulness: harsh extraction procedures, and failing to account for the biopolymer's location within the biomass.

Harsh extraction alters polymer chemistry, making the isolated version a poor surrogate for its *in situ* counterpart. In particular, extraction often leads to depolymerization and non-representative samples. Of the three main biopolymers, cellulose is the least susceptible to these issues. Ensconced in its microfibrils, cellulose can be extracted without significantly modifying its DP, although it will be reduced if care is not taken.[17] Hemicellulose presents additional challenges because it is defined as biopolymers that can be extracted from lignocellulosic biomass with a mild sodium hydroxide solution.[18] Identifying a biomass component by its ability to be extracted—not inherent chemical structure—complicates making a representative sample and ensuring the DP is not lowered during extraction. Similarly, lignin must be extracted with care, such as by a milled wood lignin (MWL)[19,20] or ionic liquid[21,22] procedure, to prevent DP reduction.[23,24] Figure 5.1A shows how harsh extraction can depolymerize lignin.

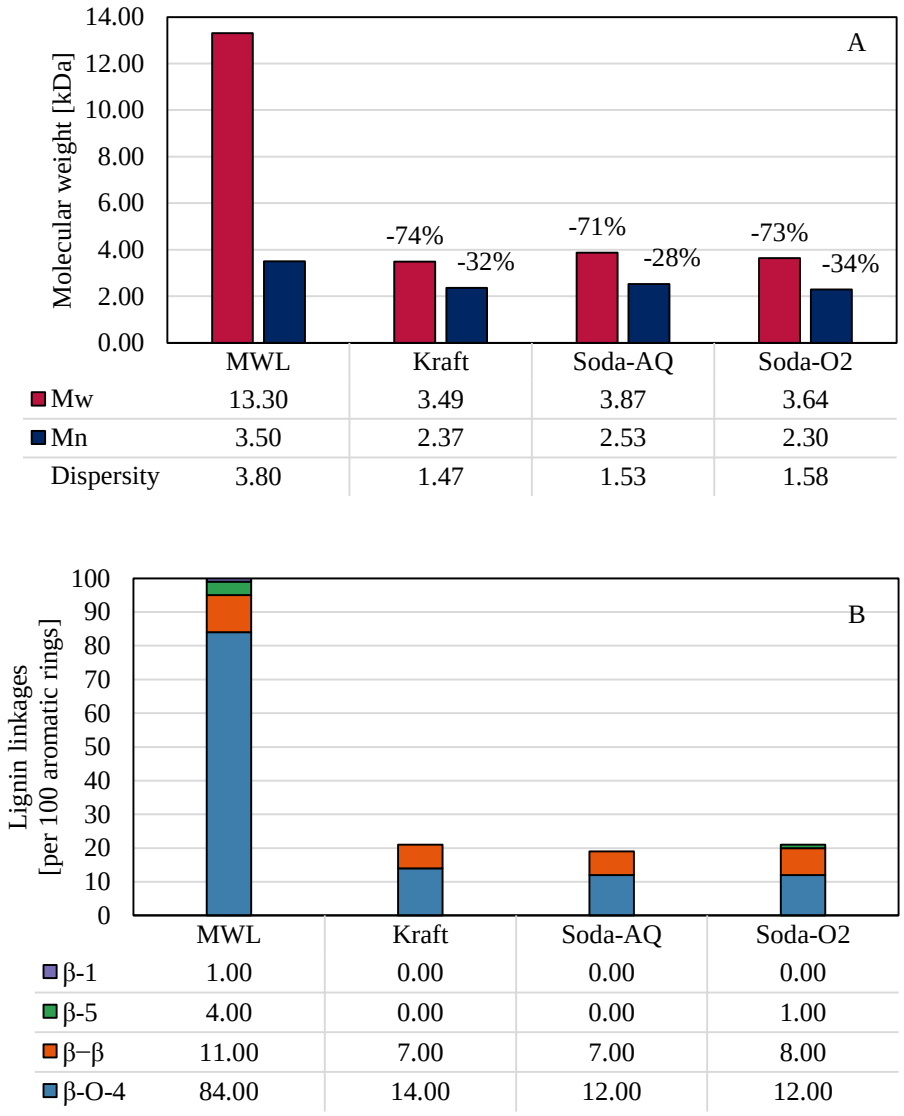

Figure 5.1. Harsh lignin extraction techniques can dramatically reduce the average molecular weight (A) by breaking lignin linkages (B). The lignin extraction procedures performed on eucalyptus are: milled wood lignin (MWL), Kraft cooking, Soda-anthraquinone (Soda-AQ), and Soda-oxygen (Soda-O2). Figure produced using data from Prinsen *et al.*[25]

Even if depolymerization is minor during extraction, the resulting sample may still not be representative.[26] Lignin contains different bond types with varying strengths,[27,28] and depolymerization can preferentially break weaker bonds (such as β-O-4’ alkyl-aryl ether) over stronger bonds (such as β-β’ resinol), leading to a skewed understanding of lignin pyrolysis, as demonstrated by Figure 5.1B. Furthermore, other

intrinsic parameters can be altered, such as lignin monomer ratios and functional group prevalence like aliphatic hydroxyl moieties.[25,27]

Regardless of the method, if the goal is to apply results obtained from extracted biopolymers to their source environment, then the conclusions need to make sense within biomass generally. Overreliance on extracted biopolymers—particularly related to physical, not chemical, phenomena—can lead to erroneous conclusions. For example, non-volatile oligomers from cellulose, hemicellulose, and lignin are often found within bio-oil.[29–35] These relatively large molecules exit the reactor as aerosols that could have formed via secondary gas phase combination reactions or been thermally ejected from the reacting biomass, but thermal ejection has not been directly detected when using biomass.[34] The first step of thermal ejection, liquid formation, has been demonstrated to lead to aerosol ejection from extracted cellulose,[32,35] hemicellulose,[30] and lignin;[32–34] however, the lignocellulosic matrix appears to prevent the liquid coalescence observed with extracted biopolymers, inhibiting aerosol thermal ejection. Aerosols may still be formed via thermal ejection, but so far the evidence is insufficient as it solely relies on extracted biopolymers.

As these examples show, *ex situ* polymers can react differently than their *in situ* counterparts, both chemically and physically. Conclusions from a surrogate material are by their nature imperfect, so care must be taken to confirm whether they can apply to their original source.

Model compounds as proxies

Furthering the extracted biopolymer issue, model compounds are often utilized to examine specific aspects of biopolymer thermal deconstruction without nonessential

components interfering with observations. Small molecules can support detailed analysis of a particular chemical bond or moiety, just as extracted biopolymers are often used as surrogates for their *in situ* counterparts. These techniques can be employed to produce useful results, but the model compound must represent what is being investigated in appropriate ways.

This notion has two aspects. The simple aspect only deals with whether the model compound has the desired moieties, functional groups, or bonds. The more complicated aspect relates to whether the compound can properly mimic the intricacies of the mimicked component of biomass.

For example, α-cyclodextrin has been used as a small molecule surrogate for extracted cellulose;[36–38] however, α-cyclodextrin is a cyclic oligosaccharide of six glucan monomers connected via α-1,4 glycosidic bonds. In contrast, cellulose is a linear polysaccharide composed of thousands of glucan monomers connected by β-1,4 glycosidic bonds.[17] These differences are not trivial and raise serious questions. Can an α bond represent a β bond? Is a small cyclic molecule a good surrogate for a large linear polymer?

The primary argument for α-cyclodextrin's ability to represent cellulose during pyrolysis rests on product yields. Mettler *et al*.[36] found α-cyclodextrin and cellulose produce similar yields only when pyrolyzed as thin films, which generate substantially lower levoglucosan yields—the primary product—than when they are pyrolyzed in powder form. Subsequent work has demonstrated that lumpy thin films, such as those employed in the aforementioned study,[36] result in low yields; whereas smooth thin films produce high yields identical to those from powdered cellulose.[39] Therefore, using α-

cyclodextrin to stand in for cellulose adds layers of uncertainty that are intrinsically coupled to its dissimilar chemical structure. The effects caused by a cyclic instead of a linear compound, α not β bonds, low not high degree of polymerization, and lumpy not smooth thin films, all limit its usefulness as a reliable proxy for cellulose. These results, nonetheless, have been utilized for drawing conclusions disputing other results obtained directly from cellulose, such as proposing that cellulose thermal depolymerization abruptly changes from one reaction to another at 467 °C.[37,38]

Lastly, certain chemicals could be considered either an extracted biopolymer or a model compound. Xylan, for instance, is extracted from lignocellulosic biomass and sold as a hemicellulose surrogate. Hemicellulose includes every polysaccharide present in lignocellulosic biomass except for cellulose and pectin,[18] and xylan, which is mostly composed of xylose, does not encompass this varied array of monosaccharides, hexuronic acids, and acetyl groups.[18] Additionally, the use of sodium hydroxide[18] to extract hemicellulose dopes the resulting polysaccharides with sodium ions. As discussed in *Lack of data on condensed-phase species*, inclusion of AAEM—such as sodium—results in different product yields than what would be expected when using an unadulterated feedstock.[40] In this case, the extraction process of this model compound leads to flawed results.

Model compounds, whether larger polymers or small monomers and dimers, need to reflect the natural conditions within biomass, or they can skew findings even if the desired moiety is present in the chemical compound. These proxies must mimic the desired chemical structure and their broader environment to have a chance of being reliably applicable to lignocellulosic biomass.

Insufficient time resolution

The initial stages of combustion, gasification, and fast pyrolysis can all be reasonably described as the "rapid thermal decomposition of organic compounds," although it is not clear what constitutes "rapid."[41] Few studies explicitly address the time scale of biomass depolymerization, which precedes devolatilization and subsequent gas phase reactions. Thermogravimetric analyzers (TGAs) have frequently been used to generate time series data on mass loss during pyrolysis. However, the heating rates in TGAs do not typically exceed 50 °C min^{-1},[42,43] which is much lower than is typical for fast pyrolysis (greater than 100 °C s^{-1}). Although most early kinetic models of fast pyrolysis were based on TGA rate data, it is now widely recognized that regardless of their conceptual value, these models are of limited usefulness in predicting the time evolution of fast pyrolysis.

For example, Figure 5.2 compares the atomic ratios of oxygen to carbon and hydrogen to carbon from slow and rapid biomass thermal deconstruction using similar temperatures. With a ten minute reaction time, slow deconstruction carbonizes biomass into a coal-like elemental composition. On the other hand, with a one second reaction time, rapid deconstruction degrades all biopolymers concurrently and incompletely, albeit to different degrees. The similar temperatures produce incongruous results because the reaction times and heating rates differ. Comparing low temperature, slow processes with high temperature, rapid reactions can lead to erroneous conclusions, so reactor design must provide the desired thermal and temporal environment.

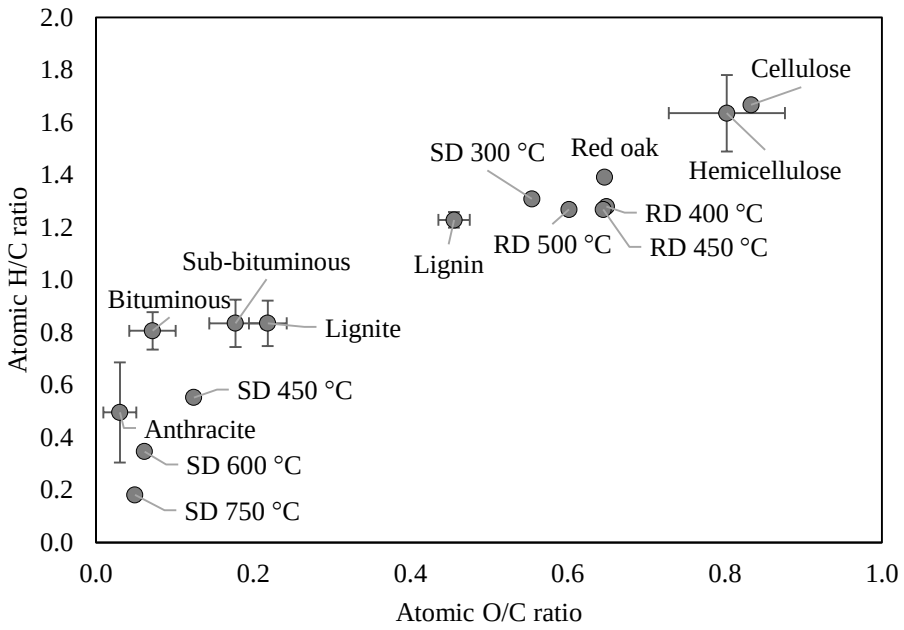

Figure 5.2. The van Krevelen diagram illustrates how slow deconstruction (SD) for ten minutes modifies biomass differently than rapid deconstruction (RD) performed for one second despite the similar temperatures, adapted from reference 41,[44–46] and supplemented with data from Ronsse *et al*.[47] and Lindstrom *et al.*[48]

Time resolution sufficiently useful for fundamental studies of rapid reactions has only been performed by taking frequent measurements throughout the reactions[49–56] or truncating the reactions prematurely and then analyzing the products generated so far. The latter method, described further in the section *Capturing condensed phase intermediates*, requires specialized reactors. For the frequent measurements approach, discussed here, the main hurdle is applying sufficiently rapid instrumentation to batch reactors.

High temperature thermochemical reactions are complete before most standard instrumentation is able to complete a single measurement. For example, micropyrolysis (py)-gas chromatography (GC) pyrolyzes a sample and starts the GC simultaneously, not subsequently, because the pyrolysis duration is negligible compared to GC analysis time, typically 30-60 minutes.[40,57,58] Gas analysis for gasification and combustion takes

seconds to minutes,[56,59] which is still too long to capture chemical dynamics of these processes. Some instruments, however, provide volatile product analysis with sufficiently high time resolution to be useful in kinetic analysis. Examples include Raman spectroscopy,[56] Fourier transform infrared (FTIR) spectroscopy,[50,56] and mass spectrometry.[51–54,56]

Hutchinson *et al*.[54] used a micropyrolyzer connected to a time-of-flight mass spectrometer (TOF MS) with atmospheric pressure chemical ionization (APCI) to perform real-time analysis of volatile pyrolysis products from various carbohydrate feedstocks, including cellulose. The APCI TOF MS monitored multiple chemical species throughout pyrolysis without fragmentation during ionization, which aided analysis. For the most part, the products developed with similar time profiles. Although this result is somewhat unexpected considering the wide range of reactions thought to occur during thermal deconstruction of lignocellulosic biomass, it is consistent with measurements made in the condensed phase, as subsequently discussed in the section *Lack of data on condensed-phase species*.

This study and other recent works have validated the widely held assumption that pyrolysis is complete in a few seconds,[37,54,55,60] contradicting predictions of some pyrolysis models. Notably, these models were developed before experimental techniques were available to obtain time-resolved data from pyrolysis experiments. For example, the cellulose pyrolysis model from Broadbelt *et al*.[61–63] relies on final product yields from micropyrolysis studies[57,62] and computational chemistry.[62,64] The biopolymer and biomass model from Ranzi *et al*.[65,66] used TGAs, resulting in temperature-resolved data, but no time resolution.

Without the benefit of time-resolved data, these models must extrapolate based on kinetic expressions and final product yields. For example, Figure 5.3 demonstrates that the Ranzi model[65,66] predicts that biomass fast pyrolysis durations vary by orders of magnitude across different temperatures. Separately, the Broadbelt model[61–63] predicts large temperature-time stratification for cellulose.[67] However, experiments have found only minor differences in reaction duration from 400-500 °C.[37,54,55,60]

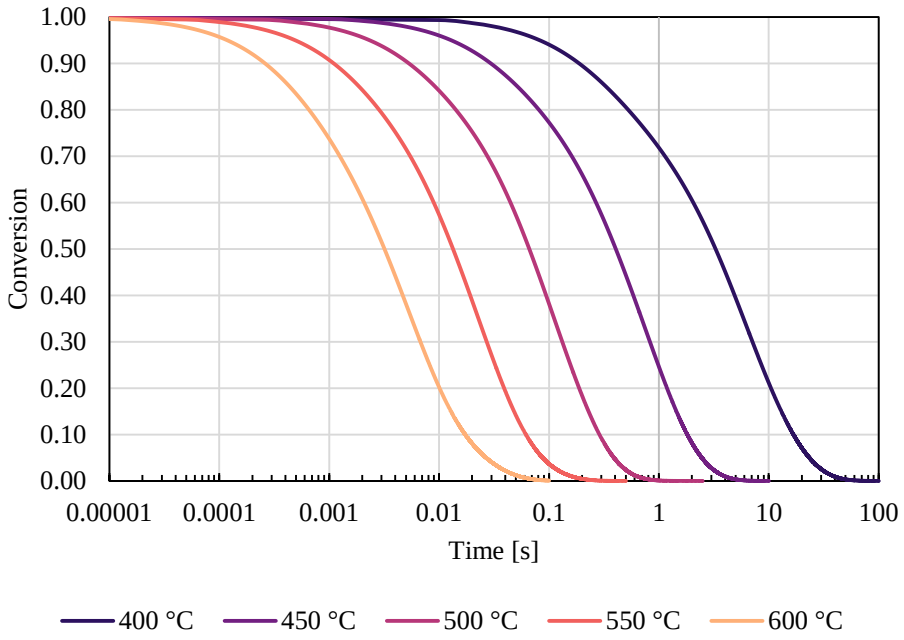

Figure 5.3. Predicted fast pyrolysis conversion using kinetics from Ranzi *et al.*[65,66] shows unrealistic reaction durations using kinetics. Calculations performed in Python[68] with each biopolymer weighted to typical woody biomass composition.[69]

The high apparent activation energies measured experimentally[65,67,70] and calculated computationally[64,71] cause this large time stratification with different computational pyrolysis temperatures. These kinetic parameters lead to reasonable estimates at 500 °C, perhaps their intended purpose, but very long durations below this temperature, which do not match experiments.[54,55,60] The short durations predicted at higher temperatures are more challenging to verify experimentally because heat and mass transfer limitations begin to obscure reaction duration. Nevertheless, despite increasing

model complexity, this fundamental modeling issue remains unresolved and diminishes predictive power, especially with non-isothermal models, in part because the lack of time-resolved data prevents comparison.

These examples show that time resolution is essential for understanding biomass thermal deconstruction, yet the almost complete lack of time-resolved data limits our ability to identify additional oversights. This area presents ample opportunities for experimentalists to rectify this omission. When remedied, new or updated models can improve predictive power, and experimentalists can look for new methods to guide deconstruction reactions toward desired products. Time resolution, however, is not the only omission. Understanding biomass thermal deconstruction completely requires analyzing the condensed phase intermediates as well.

Lack of data on condensed-phase species

The most important reactions of biomass thermal deconstruction occur in the condensed phase (as both solids and liquids). The high molecular weights of cellulose,[17,39,72] lignin,[73,74] and all but the shortest hemicellulose chains[75,76] require almost complete depolymerization before products are small enough to volatilize and escape the condensed phase. Thus, experimental methods are required that directly interrogate the condensed phase of thermally degrading biomass to identify the intermediate and often transient products of biopolymer deconstruction. Measuring only volatile products can be useful in validating models, but without measuring condensed phase species, major oversights in devising models seem inevitable.

For example, Broadbelt *et al*.[61–63] developed a computational model of cellulose pyrolysis before reliable experimental data was available on condensed phase species.

They postulated the existence of thermohydrolysis in the condensed phase, the reaction of water with a terminal glycosidic bond of cellodextrins and anhydro-cellodextrins to form glucose during pyrolysis. According to the model, this reaction occurs up to twice as fast as other reactions and theoretically yields approximately 18 wt% glucose at its maximum extent.[62] Many products, including the purported glucose, suffer from low volatility and may not volatilize readily due to their low vapor pressure.[77] Instead, this high temporary yield of glucose was held to decompose into light oxygenates as the single largest factor controlling final product yields in the model.

Broadbelt *et al*.[78] predicted a similar trend for hemicellulose pyrolysis. Although very few experimental studies to date have analyzed condensed phase products of cellulose pyrolysis, none has verified that thermohydrolysis occurs to any significant extent.[55,79–82] Lindstrom *et al*.[55] specifically analyzed for glucose along with other suspected depolymerization products but did not detect even a trace at any point during the process. Considering the paucity of experimental data on the chain-breaking reactions of thermal deconstruction of polysaccharides, postulating thermohydrolysis to explain anhydrosugar yields that are only 60% of the theoretical, might seem eminently reasonable. However, this example illustrates that it is possible to predict the final products but with incorrect intermediates. Efforts to guide reactions toward improved desired product yields are unlikely to succeed when they rely on models that cannot predict all aspects of a process.

One of the best examples of improving desired product yields comes from understanding the effects of alkali and alkaline earth metals (AAEM) that are naturally present in biomass. Ash content, as AAEM content is often termed, confounded

developing accurate models for cellulose pyrolysis, leading to a multitude of incompatible theories.[83,84] These researchers were interested in producing biofuels, so focused almost exclusively on gas- and vapor-phase products. In contrast, the textiles industry sought to produce less flammable cotton-based fabrics, so they concentrated on physical and chemical changes within textile fibers—the condensed phase. As a result of these different emphases, textiles scientists[85,86] discovered the deleterious effect of ash content on sugar production long before biofuels researchers.[87–89] Broido and Kilzer[83] noted that this oversight "raise[s] questions about all previous work in which the presence of such small amounts of ash was not considered."

As noted in more recent studies, AAEM catalyze many sugar degradation reactions via ion-dipole forces.[90–93] This action can be prevented by washing the biomass to remove AAEM or via passivation of the AAEM catalytic activity using dilute mineral or carboxylic acids.[40,85,92,94–96] In the latter approach, the acid's conjugate base binds to the AAEM to form thermally stable salts. Both pretreatments increase sugars yields several-fold (Figure 5.4). An earlier focus on condensed phase reactions by pyrolysis researchers may have advanced the field of pyrolytic sugar production more quickly.

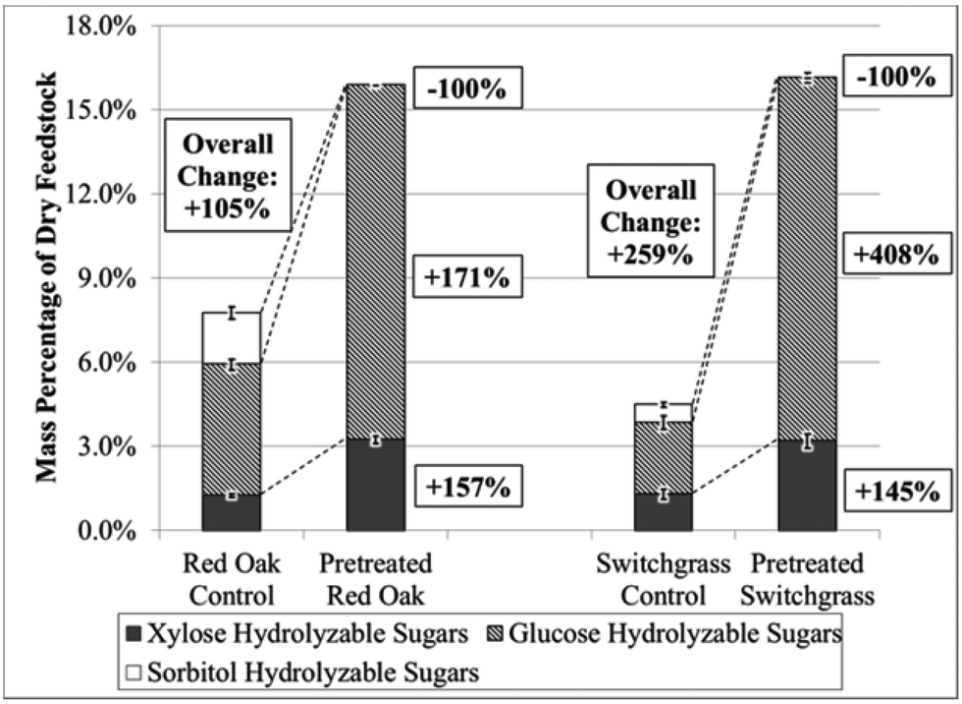

Figure 5.4. Pretreating red oak and switchgrass with dilute sulfuric acid significantly improved sugar yields from fast pyrolysis. Figure reprinted from reference 95 with permission from the Royal Society of Chemistry.

This substantial improvement exploited knowledge of the condensed phase; however, the role of AAEM is still not fully understood. The chemical effects on sugars are now well documented but, curiously, AAEM mineral acid passivation often leads to significant agglomeration during thermal deconstruction.[95,97] AAEM hurts sugar yields but also might assist other deconstruction reactions. This conundrum cannot be overlooked if acid passivation of AAEM is to be used for pyrolytic sugar production.[7] As this problem clearly originates in the condensed phase, further analysis will surely be necessary to understand and then overcome this insufficiently understood area.

Condensed phase analysis should inform the study of every thermal deconstruction process. This work is challenging but is important to get an accurate picture of what occurs in reality.

Capturing condensed phase intermediates

Ideally, *in situ* measurements of condensed phased intermediates would be developed to directly follow the progression of biomass deconstruction. In the absence of *in situ* physical or optical probes, the most promising alternative is rapid cooling of reacting biomass to quench chemical reactions before the reactions are complete and then performing *ex situ* analysis. This hybrid approach combines *ex situ* analysis with time resolution, and allows scientists to use analytical techniques not suited for rapid *in situ* analysis, such as chromatography or nuclear magnetic resonance (NMR) spectroscopy.[37,48,55,98–102] Unencumbered by *in situ* instrumentation requirements, the biomass can be subjected to realistic heating environments followed by rapid cooling after a desired reaction period using relatively simple reactors, albeit with limitations.

Resistively heated strips[34] offer high heating rates and can quench reactions with coolant flowing underneath, such as the Pulse-Heated Analysis of Solid Reactions (PHASR) from Dauenhauer *et al*.[37] However, these reactors do not provide three dimensional heating, which may lead to overestimated heat transfer, especially if a phase transition occurs. Concentrated radiation, as employed by Lédé,[99–101] can provide high heat flux by briefly exposing a small sample to the focal point of an intense reflected light source, such as a xenon lamp, but this type of system relies on relatively slow gaseous convective cooling to quench the samples, which unintentionally increases reaction duration. Both these systems present further issues for condensed and volatile phase product analysis. The unheated gas surrounding or flowing over the sample may cause volatile products to condense prematurely before analysis.[34] Additionally, relying on

intense heat transfer to small samples limits the condensed phase analysis techniques possible after thermal processing.

Slightly larger systems, while imperfect, can overcome these issues, utilize a wider array of analytical methods, and run multiple dissimilar experiments on each produced sample. Lindstrom *et al*.[55] describes a reactor, termed Controlled Pyrolysis Duration (CPD)-Quench, that lowers a sample into a preheated vertical tube furnace[103] and subsequently drops the sample further out the bottom and into a quench vessel containing cold solvent after the desired reactions time. Vapor products are separately collected in a condenser. Together, these product collection systems can examine both the volatile and condensed phase products with time-resolution.[55] Taking advantage of longer reaction times for solvent liquefaction, Ghosh *et al*.[104,105] placed small closed reactors into a preheated fluidized sand bath for the desired reaction duration, and then removed and quenched them in cool water. Both of these systems cannot track thermal history, but instead users can determine the thermal profile *a posteriori* and then apply it to the samples.[103,105]

Even continuous systems are possible, creating gram or kilogram quantities of condensed phase material to analyze, not merely micrograms or milligrams. Plug flow reactors, such as entrained flow reactors at the University of Waterloo[106] and National Renewable Energy Laboratory,[107] can rapidly heat samples within the reactor; however, only some systems have implemented condensed phase product quenching, such as Iowa State University's free fall reactor.[48,102,108] In these cases, thermal history is even more challenging to measure, and modeling is often used *in lieu* of measurements.[48,102]

These reactors require unusual designs and are often only suited to perform these particular experiments, which likely contributes to their scarcity. Utilizing these specialized reactors, however, has provided key insights unobtainable through other means. Additional reactor designs and experimentation will surely continue this trend.

Conclusions

Biomass thermal deconstruction analysis is rapidly improving commensurate with the need for advanced biorenewable technologies, but this field has blind spots. Particularly, the lack of experimentation probing time resolved and condensed phase intermediate products limit future advances. Furthermore, overreliance on simple model compounds, instead of lignocellulosic biomass, can further skew findings and lead to misinterpretations.

Success stories have been spotlighted to show the benefits of improving biomass thermal deconstruction analysis techniques, not just in increasing accuracy of predictions, but in remedying fundamental misunderstandings of the reactions involved. Conversely, missteps were discussed with the aim to prevent their repetition or related manifestations. Better understanding the fundamental reactions can present opportunities to exploit them to improve desired product yields or reactor operability.

Conflicts of interest

There are no conflicts to declare.

Acknowledgements

The financial support from the Gary and Donna Hoover Endowment and National Science Foundation Engineering Research Center for Biorenewable Chemicals (CBiRC) (award number: EEC-0813570) is appreciated. Chad A. Peterson assisted with the Python

modeling for Figure 5.3. Sean Rollag brought several relevant papers to our attention. John Ralph provided insight into NMR methodology. The authors graciously acknowledge Carolyn P. Hutchinson, D. Paul Cole, Erica A. Dalluge, Evan A. Larson, and Young Jin Lee for giving us access to original experimental data useful to our analyses.[54] Lastly, we appreciate Theodore Heindel's suggestion that we reassess "known knowns" in the field before exploring the unknowns.

References

(1) Langholtz, M. H.; Stokes, B. J.; Eaton, L. M. *2016 Billion-Ton Report: Advancing Domestic Resources for a Thriving Bioeconomy*; Oak Ridge National Laboratory, Oak Ridge, TN, 2016; Vol. I.

(2) Lynd, L. R. The Grand Challenge of Cellulosic Biofuels. *Nat. Biotechnol.* **2017**, *35* (10), 912–915.

(3) United States Congress. *The Energy Policy Act 2005*; Government Printing Office: United States of America, 2005; p 550.

(4) United States Congress. *Energy Information and Security Act of 2007*; Government Printing Office: United States of America, 2007; p 310.

(5) *California Global Warming Solutions Act of 2006*; California Legislative Information: California, United States of America, 2006; p 13.

(6) Allen, M.; Dube, O. P.; Solecki, W.; Aragón-Durand, F.; Cramer, W.; Humphreys, S.; Kainuma, M.; Kala, J.; Mahowald, N.; Mulugetta, Y.; et al. Framing and Context. In *Global warming of 1.5°C. An IPCC Special Report on the impacts of global warming of 1.5°C above pre-industrial levels and related global greenhouse gas emission pathways, in the context of strengthening the global response to the threat of climate change*,; Masson-Delmotte, V., Zhai, P., Pörtner, H. O., Roberts, D., Skea, J., Shukla, P. R., Pirani, A., Moufouma-Okia, W., Péan, C., Pidcock, R., et al., Eds.; 2018; pp 49–91.

(7) Lindstrom, J. K.; Ghosh, A.; Rollag, S.; Brown, R. C. Production of Sugars from Lignocellulosic Biomass: A Critical Review of Biological and Thermochemical Routes. *Green Chem.* **2019**, *In prep.*

(8) Haldar, D.; Sen, D.; Gayen, K. A Review on the Production of Fermentable Sugars from Lignocellulosic Biomass through Conventional and Enzymatic Route—a Comparison. *Int. J. Green Energy* **2016**, *13* (12), 1232–1253.

(9) Dutta, S.; Wu, K. C.-W. Enzymatic Breakdown of Biomass: Enzyme Active Sites, Immobilization, and Biofuel Production. *Green Chem.* **2014**, *16* (11), 4615–4626.

(10) Zhang, Y.; Brown, T. R.; Hu, G.; Brown, R. C. Techno-Economic Analysis of Monosaccharide Production via Fast Pyrolysis of Lignocellulose. *Bioresour. Technol.* **2013**, *127*, 358–365.

(11) Oudenhoven, S. R. G.; van der Ham, A. G. J.; van den Berg, H.; Westerhof, R. J. M.; Kersten, S. R. A. Using Pyrolytic Acid Leaching as a Pretreatment Step in a Biomass Fast Pyrolysis Plant: Process Design and Economic Evaluation. *Biomass and Bioenergy* **2016**, *95*, 388–404.

(12) Li, W.; Ghosh, A.; Bbosa, D.; Brown, R.; Wright, M. M. Comparative Techno-Economic, Uncertainty and Life Cycle Analysis of Lignocellulosic Biomass Solvent Liquefaction and Sugar Fermentation to Ethanol. *ACS Sustain. Chem. Eng.* **2018**, *6* (12), 16515–16524.

(13) Griffin, M. B.; Iisa, K.; Wang, H.; Dutta, A.; Orton, K. A.; French, R. J.; Santosa, D. M.; Wilson, N.; Christensen, E.; Nash, C.; et al. Driving towards Cost-Competitive Biofuels through Catalytic Fast Pyrolysis by Rethinking Catalyst Selection and Reactor Configuration. *Energy Environ. Sci.* **2018**, *11* (10), 2904–2918.

(14) Mansfield, S. D.; Kim, H.; Lu, F.; Ralph, J. Whole Plant Cell Wall Characterization Using Solution-State 2D NMR. *Nat. Protoc.* **2012**, *7* (9), 1579–1589.

(15) Foston, M.; Samuel, R.; He, J.; Ragauskas, A. J. A Review of Whole Cell Wall NMR by the Direct-Dissolution of Biomass. *Green Chem.* **2016**, *18* (3), 608–621.

(16) Lange, H.; Giannì, P.; Crestini, C. Lignin Analytics. In *Lignin Valorization: Emerging Approaches*; Beckham, G. T., Ed.; Royal Society of Chemistry: London, U.K., 2018; pp 413–476.

(17) Hallac, B. B.; Ragauskas, A. J. Analyzing Cellulose Degree of Polymerization and Its Relevancy to Cellulosic Ethanol. *Biofuels, Bioprod. Biorefining* **2011**, *5*, 215–225.

(18) Holtzapple, M. T. Hemicelluloses. In *Encyclopedia of Food Sciences and Nutrition*; Caballero, B., Ed.; Elsevier, 2003; pp 3060–3071.

(19) Björkman, A. Isolation of Lignin from Finely Divided Wood with Neutral Solvents. *Nature* **1954**, *174* (4440), 1057–1058.

(20) Björkman, A. Studies on Finely Divided Wood. Part I. Extraction of Lignin with Neutral Solvents. *Sven. Papperstidning* **1956**, *59*, 477–485.

(21) Pu, Y.; Jiang, N.; Ragauskas, A. J. Ionic Liquid as a Green Solvent for Lignin. *J. Wood Chem. Technol.* **2007**, *27* (1), 23–33.

(22) Zhu, X.; Peng, C.; Chen, H.; Chen, Q.; Zhao, Z. K.; Zheng, Q.; Xie, H. Opportunities of Ionic Liquids for Lignin Utilization from Biorefinery. *ChemistrySelect* **2018**, *3* (27), 7945–7962.

(23) Zhang, J.; Kim, K. H.; Choi, Y. S.; Motagamwala, A. H.; Dumesic, J. A.; Brown, R. C.; Shanks, B. H. Comparison of Fast Pyrolysis Behavior of Cornstover Lignins Isolated by Different Methods. *ACS Sustain. Chem. Eng.* **2017**, *5* (7), 5657–5661.

(24) Bozell, J. J.; Chmely, S. E.; Hartwig, W.; Key, R.; Labbé, N.; Venugopal, P.; Zuleta, E. Lignin Isolation Methodology for Biorefining, Pretreatment and Analysis. In *Lignin Valorization: Emerging Approaches*; Beckham, G. T., Ed.; Royal Society of Chemistry: London, UK, 2018; pp 21–61.

(25) Prinsen, P.; Rencoret, J.; Gutiérrez, A.; Liitiä, T.; Tamminen, T.; Colodette, J. L.; Berbis, M. Á.; Jiménez-Barbero, J.; Martínez, Á. T.; del Río, J. C. Modification of the Lignin Structure during Alkaline Delignification of Eucalyptus Wood by Kraft, Soda-AQ, and Soda-O2 Cooking. *Ind. Eng. Chem. Res.* **2013**, *52* (45), 15702–15712.

(26) Constant, S.; Wienk, H. L. J.; Frissen, A. E.; Peinder, P. de; Boelens, R.; Van Es, D. S.; Grisel, R. J. H.; Weckhuysen, B. M.; Huijgen, W. J. J.; Gosselink, R. J. A.; et al. New Insights into the Structure and Composition of Technical Lignins: A Comparative Characterisation Study. *Green Chem.* **2016**, *18* (9), 2651–2665.

(27) Lupoi, J. S.; Singh, S.; Parthasarathi, R.; Simmons, B. A.; Henry, R. J. Recent Innovations in Analytical Methods for the Qualitative and Quantitative Assessment of Lignin. *Renew. Sustain. Energy Rev.* **2015**, *49*, 871–906.

(28) Parthasarathi, R.; Romero, R. A.; Redondo, A.; Gnanakaran, S. Theoretical Study of the Remarkably Diverse Linkages in Lignin. *J. Phys. Chem. Lett.* **2011**, *2*, 2660–2666.

(29) Pecha, M. B.; Montoya, J. I.; Chejne, F.; Garcia-Perez, M. Effect of a Vacuum on the Fast Pyrolysis of Cellulose: Nature of Secondary Reactions in a Liquid Intermediate. *Ind. Eng. Chem. Res.* **2017**, *56* (15), 4288–4301.

(30) Montoya, J.; Pecha, B.; Janna, F. C.; Garcia-Perez, M. Methodology for Estimation of Thermal Ejection Droplet Size Distribution and Intensity during the Pyrolysis of Sugarcane Bagasse and Model Compounds. *J. Anal. Appl. Pyrolysis* **2017**, *125* (November 2016), 69–82.

(31) Montoya, J.; Pecha, B.; Janna, F. C.; Garcia-Perez, M. Single Particle Model for Biomass Pyrolysis with Bubble Formation Dynamics inside the Liquid Intermediate and Its Contribution to Aerosol Formation by Thermal Ejection. *J. Anal. Appl. Pyrolysis* **2017**, *124*, 204–218.

(32) Teixeira, A. R.; Mooney, K. G.; Kruger, J. S.; Williams, C. L.; Suszynski, W. J.; Schmidt, L. D.; Schmidt, D. P.; Dauenhauer, P. J. Aerosol Generation by Reactive Boiling Ejection of Molten Cellulose. *Energy Environ. Sci.* **2011**, *4*, 4306.

(33) Dedic, C.; Tiarks, J. A.; Sanderson, P. D.; Brown, R. C.; Michael, J. B.; Meyer, T. R. Optical Diagnostic Techniques for Investigation of Biomass Pyrolysis. In *Fourth International Conference on Thermochemical Biomass Conversion Science*; Chicago, IL, 2015.

(34) Tiarks, J. A. Investigation of Fundamental Transport and Physicochemical Phenomena in Lignocellulosic Fast Pyrolysis, Iowa State University, 2018.

(35) Teixeira, A. R.; Krumm, C.; Vinter, K. P.; Paulsen, A. D.; Zhu, C.; Maduskar, S.; Joseph, K. E.; Greco, K.; Stelatto, M.; Davis, E.; et al. Reactive Liftoff of Crystalline Cellulose Particles. *Sci. Rep.* **2015**, *5* (JUNE), 11238.

(36) Mettler, M. S.; Mushrif, S. H.; Paulsen, A. D.; Javadekar, A. D.; Vlachos, D. G.; Dauenhauer, P. J. Revealing Pyrolysis Chemistry for Biofuels Production: Conversion of Cellulose to Furans and Small Oxygenates. *Energy Environ. Sci.* **2012**, *5* (1), 5414–5424.

(37) Krumm, C.; Pfaendtner, J.; Dauenhauer, P. J. Millisecond Pulsed Films Unify the Mechanisms of Cellulose Fragmentation. *Chem. Mater.* **2016**, *28*, 3108–3114.

(38) Zhu, C.; Krumm, C.; Facas, G. G.; Neurock, M.; Dauenhauer, P. J. Energetics of Cellulose and Cyclodextrin Glycosidic Bond Cleavage. *React. Chem. Eng.* **2017**, *2* (2), 201–214.

(39) Zhang, J.; Nolte, M. W.; Shanks, B. H. Investigation of Primary Reactions and Secondary Effects from the Pyrolysis of Different Celluloses. *ACS Sustain. Chem. Eng.* **2014**, *2* (12), 2820–2830.

(40) Patwardhan, P. R.; Brown, R. C.; Shanks, B. H. Product Distribution from the Fast Pyrolysis of Hemicellulose. *ChemSusChem* **2011**, *4* (5), 636–643.

(41) Lindstrom, J. K.; Shaw, A.; Zhang, X.; Brown, R. C. Condensed Phase Reactions during Thermal Deconstruction. In *Thermochemical Processing of Biomass: Conversion into Fuels, Chemicals and Power*; Brown, R. C., Ed.; John Wiley and Sons, 2019; pp 17–48.

(42) Friedman, H. L.; Rogers, F. E. Kinetics of Cellulose Pyrolysis in Nitrogen and Steam. *Combust. Sci. Technol.* **1980**, *21* (3–4), 141–152.

(43) Grønli, M.; Antal, M. J.; Várhegyi, G. A Round-Robin Study of Cellulose Pyrolysis Kinetics by Thermogravimetry. *Ind. Eng. Chem. Res.* **1999**, *38* (6), 2238–2244.

(44) Palmer, C. A.; Oman, C. L.; Park, A. J.; Luppens, J. A. The U.S. Geological Survey Coal Quality (COALQUAL) Database Version 3.0. *United States Geol. Surv. Data Ser.* **2015**, *975*, 1–43.

(45) Egüés, I.; Sanchez, C.; Mondragon, I.; Labidi, J. Separation and Purification of Hemicellulose by Ultrafiltration. *Ind. Eng. Chem. Res.* **2012**, *51* (1), 523–530.

(46) Li, P.; Liu, Y.; Lu, J.; Yang, R.; Li, H.; Wang, H. Structural Characterization and Effect on Enzymatic Hydrolysis of Milled Wood Lignin Isolated from Reed Straw and Corn Stover Pretreated with Liquid Hot Water. *BioResources* **2016**, *11* (4), 8777–8790.

(47) Ronsse, F.; van Hecke, S.; Dickinson, D.; Prins, W. Production and Characterization of Slow Pyrolysis Biochar: Influence of Feedstock Type and Pyrolysis Conditions. *GCB Bioenergy* **2013**, *5* (2), 104–115.

(48) Lindstrom, J. K.; Peterson, C. A.; Ciesielski, P. N.; Ralph, J.; Chen, M.; Jakes, J. E.; Gable, P.; Brown, R. C. Structural and Chemical Changes of Plant Cell Walls during Early Stages of Thermal Deconstruction. *In prep.*

(49) Shin, E. J.; Nimlos, M. R.; Evans, R. J. Kinetic Analysis of the Gas-Phase Pyrolysis of Carbohydrates. *Fuel* **2001**, *80* (12), 1697–1709.

(50) Ojha, D. K.; Viju, D.; Vinu, R. Fast Pyrolysis Kinetics of Alkali Lignin: Evaluation of Apparent Rate Parameters and Product Time Evolution. *Bioresour. Technol.* **2017**, *241*, 142–151.

(51) Jarvis, M. W.; Haas, T. J.; Donohoe, B. S.; Daily, J. W.; Gaston, K. R.; Frederick, W. J.; Nimlos, M. R. Elucidation of Biomass Pyrolysis Products Using a Laminar Entrained Flow Reactor and Char Particle Imaging. *Energy & Fuels* **2011**, *25* (1), 324–336.

(52) Hurt, M. R.; Degenstein, J. C.; Gawecki, P.; Borton II, D. J.; Vinueza, N. R.; Yang, L.; Agrawal, R.; Delgass, W. N.; Ribeiro, F. H.; Kenttämaa, H. I. On-Line Mass Spectrometric Methods for the Determination of the Primary Products of Fast Pyrolysis of Carbohydrates and for Their Gas-Phase Manipulation. *Anal. Chem.* **2013**, *85* (22), 10927–10934.

(53) Hutchinson, C. P.; Lee, Y. J. Evaluation of Primary Reaction Pathways in Thin-Film Pyrolysis of Glucose Using 13C Labeling and Real-Time Monitoring. *ACS Sustain. Chem. Eng.* **2017**, *5* (10), 8796–8803.

(54) Hutchinson, C. P.; Cole, D. P.; Dalluge, E. A.; Larson, E. A.; Lee, Y. J. Novel Instrumentation for Tracking Molecular Products in Fast Pyrolysis of Carbohydrates with Sub-Second Temporal Resolution. *J. Anal. Appl. Pyrolysis* **2018**, *136* (October), 107–114.

(55) Lindstrom, J. K.; Proano-Aviles, J.; Johnston, P. A.; Peterson, C. A.; Stansell, J. S.; Brown, R. C. Competing Reactions Limit Levoglucosan Yield during Fast Pyrolysis of Cellulose. *Green Chem.* **2019**, *21* (1), 178–186.

(56) Bahng, M.-K.; Mukarakate, C.; Robichaud, D. J.; Nimlos, M. R. Current Technologies for Analysis of Biomass Thermochemical Processing: A Review. *Anal. Chim. Acta* **2009**, *651* (2), 117–138.

(57) Patwardhan, P. R.; Satrio, J. A.; Brown, R. C.; Shanks, B. H. Product Distribution from Fast Pyrolysis of Glucose-Based Carbohydrates. *J. Anal. Appl. Pyrolysis* **2009**, *86* (2), 323–330.

(58) Patwardhan, P. R.; Brown, R. C.; Shanks, B. H. Understanding the Fast Pyrolysis of Lignin. *ChemSusChem* **2011**, *4* (11), 1629–1636.

(59) Abdoulmoumine, N.; Kulkarni, A.; Adhikari, S. Effects of Temperature and Equivalence Ratio on Pine Syngas Primary Gases and Contaminants in a Bench-Scale Fluidized Bed Gasifier. *Ind. Eng. Chem. Res.* **2014**, *53* (14), 5767–5777.

(60) Maduskar, S.; Facas, G. G.; Papageorgiou, C.; Williams, C. L.; Dauenhauer, P. J. Five Rules for Measuring Biomass Pyrolysis Rates: Pulse-Heated Analysis of Solid Reaction Kinetics of Lignocellulosic Biomass. *ACS Sustain. Chem. Eng.* **2018**, *6* (1), 1387–1399.

(61) Vinu, R.; Broadbelt, L. J. A Mechanistic Model of Fast Pyrolysis of Glucose-Based Carbohydrates to Predict Bio-Oil Composition. *Energy Environ. Sci.* **2012**, *5* (12), 9808–9826.

(62) Zhou, X.; Nolte, M. W.; Mayes, H. B.; Shanks, B. H.; Broadbelt, L. J. Experimental and Mechanistic Modeling of Fast Pyrolysis of Neat Glucose-Based Carbohydrates. 1. Experiments and Development of a Detailed Mechanistic Model. *Ind. Eng. Chem. Res.* **2014**, *53* (34), 13274–13289.

(63) Zhou, X.; Nolte, M. W.; Shanks, B. H.; Broadbelt, L. J. Experimental and Mechanistic Modeling of Fast Pyrolysis of Neat Glucose-Based Carbohydrates. 2. Validation and Evaluation of the Mechanistic Model. *Ind. Eng. Chem. Res.* **2014**, *53* (34), 13290–13301.

(64) Mayes, H. B.; Broadbelt, L. J. Unraveling the Reactions That Unravel Cellulose. *J. Phys. Chem. A* **2012**, *116* (26), 7098–7106.

(65) Ranzi, E.; Debiagi, P. E. A.; Frassoldati, A. Mathematical Modeling of Fast Biomass Pyrolysis and Bio-Oil Formation. Note I: Kinetic Mechanism of Biomass Pyrolysis. *ACS Sustain. Chem. Eng.* **2017**, *5* (4), 2867–2881.

(66) Ranzi, E.; Debiagi, P. E. A.; Frassoldati, A. Mathematical Modeling of Fast Biomass Pyrolysis and Bio-Oil Formation. Note II: Secondary Gas-Phase Reactions and Bio-Oil Formation. *ACS Sustain. Chem. Eng.* **2017**, *5* (4), 2882–2896.

(67) Burnham, A. K.; Zhou, X.; Broadbelt, L. J. Critical Review of the Global Chemical Kinetics of Cellulose Thermal Decomposition. *Energy & Fuels* **2015**, *29* (5), 2906–2918.

(68) Wiggins, G. M. GitHub https://github.com/wigging.

(69) Williams, C. L.; Emerson, R. M.; Tumuluru, J. S. Biomass Compositional Analysis for Conversion to Renewable Fuels and Chemicals. In *Biomass Volume Estimation and Valorization for Energy*; Tumuluru, J. S., Ed.; INTECH, 2017; Vol. 3, pp 251–270.

(70) Reynolds, J. G.; Burnham, A. K. Pyrolysis Decomposition Kinetics of Cellulose-Based Materials by Constant Heating Rate Micropyrolysis. *Energy & Fuels* **1997**, *11*, 88–97.

(71) Zhang, X.; Yang, W.; Dong, C. Levoglucosan Formation Mechanisms during Cellulose Pyrolysis. *J. Anal. Appl. Pyrolysis* **2013**, *104*, 19–27.

(72) Yamamoto, M.; Kuramae, R.; Yanagisawa, M.; Ishii, D.; Isogai, A. Light-Scattering Analysis of Native Wood Holocelluloses Totally Dissolved in LiCl-DMI Solutions: High Probability of Branched Structures in Inherent Cellulose. *Biomacromolecules* **2011**, *12* (11), 3982–3988.

(73) Kim, J. Y.; Shin, E. J.; Eom, I. Y.; Won, K.; Kim, Y. H.; Choi, D.; Choi, I. G.; Choi, J. W. Structural Features of Lignin Macromolecules Extracted with Ionic Liquid from Poplar Wood. *Bioresour. Technol.* **2011**, *102* (19), 9020–9025.

(74) Kim, J. Y.; Oh, S.; Hwang, H.; Kim, U. J.; Choi, J. W. Structural Features and Thermal Degradation Properties of Various Lignin Macromolecules Obtained from Poplar Wood (Populus Albaglandulosa). *Polym. Degrad. Stab.* **2013**, *98* (9), 1671–1678.

(75) Bikova, T.; Treimanis, A. Solubility and Molecular Weight of Hemicelluloses from Alnus Incana and Alnus Glutinosa. Effect of Tree Age. *Plant Physiol. Biochem.* **2002**, *40* (4), 347–353.

(76) Zhou, X.; Li, W.; Mabon, R.; Broadbelt, L. J. A Critical Review on Hemicellulose Pyrolysis. *Energy Technol.* **2017**, *5* (1), 216.

(77) Oja, V.; Suuberg, E. M. Vapor Pressures and Enthalpies of Sublimation of D-Glucose, d-Xylose, Cellobiose, and Levoglucosan. *J. Chem. Eng. Data* **1999**, *44* (1), 26–29.

(78) Zhou, X.; Li, W.; Mabon, R.; Broadbelt, L. J. A Mechanistic Model of Fast Pyrolysis of Hemicellulose. *Energy Environ. Sci.* **2018**, *11* (5), 1240–1260.

(79) Radlein, D. S.; Grinshpun, A.; Piskorz, J.; Scott, D. S. On the Presence of Anhydro-Oligosaccharides in the Sirups from the Fast Pyrolysis of Cellulose. *J. Anal. Appl. Pyrolysis* **1987**, *12* (1), 39–49.

(80) Liu, D.; Yu, Y.; Wu, H. Evolution of Water-Soluble and Water-Insoluble Portions in the Solid Products from Fast Pyrolysis of Amorphous Cellulose. *Ind. Eng. Chem. Res.* **2013**, *52* (36), 12785–12793.

(81) Wooten, J. B.; Seeman, J. I.; Hajaligol, M. R. Observation and Characterization of Cellulose Pyrolysis Intermediates by 13C CPMAS NMR. A New Mechanistic Model. *Energy & Fuels* **2004**, *18* (1), 1–15.

(82) Gong, X.; Yu, Y.; Gao, X.; Qiao, Y.; Xu, M.; Wu, H. Formation of Anhydro-Sugars in the Primary Volatiles and Solid Residues from Cellulose Fast Pyrolysis in a Wire-Mesh Reactor. *Energy & Fuels* **2014**, *28* (8), 5204–5211.

(83) Broido, A.; Kilzer, F. J. A Critique of the Present State of Knowledge of The Mechanism of Cellulose Pyrolysis. *Fire Res. Abstr. Rev.* **1963**, *5* (2), 157–161.

(84) Golova, O. P. Chemical Effects of Heat on Cellulose. *Russ. Chem. Rev.* **1975**, *44*, 687–697.

(85) Venn, H. J. P. The Yield of β-Glucosane Obtained from Low-Pressure Distillation of Cellulose. *J. Text. Inst. Trans.* **1924**, *15* (8), T414–T418.

(86) Madorsky, S. L.; Hart, V. E.; Straus, S. Pyrolysis of Cellulose in a Vacuum. *J. Res. Natl. Bur. Stand. (1934).* **1956**, *56* (6), 343–354.

(87) Golova, O. P.; Krylova, R. G. Thermal Depolymerization of Cellulose. *Dokl. Akad. Nauk SSSR* **1960**, *135* (6), 1391–1394.

(88) Golova, O. P.; Epshtein, V.; Durynina, L. I. Effect of Inorganic Components on C-C Cleavage during Thermal Degradation of Cellulose. *Vysokomol. Soedin.* **1961**, *3*, 536–540.

(89) Broido, A. Thermogravimetric and Differential Thermal Analysis of Potassium Bicarbonate Contaminated Cellulose. *Pyrodynamics* **1966**, *4* (3), 243–251.

(90) Nimlos, M. R.; Blanksby, S. J.; Ellison, G. B.; Evans, R. J. Enhancement of 1,2-Dehydration of Alcohols by Alkali Cations and Protons: A Model for Dehydration of Carbohydrates. *J. Anal. Appl. Pyrolysis* **2003**, *66* (1–2), 3–27.

(91) Patwardhan, P. R.; Satrio, J. A.; Brown, R. C.; Shanks, B. H. Influence of Inorganic Salts on the Primary Pyrolysis Products of Cellulose. *Bioresour. Technol.* **2010**, *101* (12), 4646–4655.

(92) Kuzhiyil, N.; Dalluge, D.; Bai, X.; Kim, K. H.; Brown, R. C. Pyrolytic Sugars from Cellulosic Biomass. *ChemSusChem* **2012**, *5* (11), 2228–2236.

(93) Mayes, H. B.; Nolte, M. W.; Beckham, G. T.; Shanks, B. H.; Broadbelt, L. J. The Alpha-Bet(a) of Salty Glucose Pyrolysis: Computational Investigations Reveal Carbohydrate Pyrolysis Catalytic Action by Sodium Ions. *ACS Catal.* **2015**, *5* (1), 192–202.

(94) Scott, D. S.; Piskorz, J.; Radlein, D.; Majerski, P. Process for the Production of Anhydrosugars from Lignin and Cellulose Containing Biomass by Pyrolysis. 5,395,455, 1995.

(95) Dalluge, D. L.; Daugaard, T.; Johnston, P.; Kuzhiyil, N.; Wright, M. M.; Brown, R. C. Continuous Production of Sugars from Pyrolysis of Acid-Infused Lignocellulosic Biomass. *Green Chem.* **2014**, 4144–4155.

(96) Oudenhoven, S. R. G.; Westerhof, R. J. M.; Kersten, S. R. A. Fast Pyrolysis of Organic Acid Leached Wood, Straw, Hay and Bagasse: Improved Oil and Sugar Yields. *J. Anal. Appl. Pyrolysis* **2015**, *116*, 253–262.

(97) Oudenhoven, S. R. G.; Lievens, C.; Westerhof, R. J. M.; Kersten, S. R. A. Effect of Temperature on the Fast Pyrolysis of Organic-Acid Leached Pinewood; the Potential of Low Temperature Pyrolysis. *Biomass and Bioenergy* **2016**, *89*, 78–90.

(98) Hao, N.; Ben, H.; Yoo, C. G.; Adhikari, S.; Ragauskas, A. J. Review of NMR Characterization of Pyrolysis Oils. *Energy & Fuels* **2016**, *30* (9), 6863–6880.

(99) Boutin, O.; Ferrer, M.; Lédé, J. Radiant Flash Pyrolysis of Cellulose—Evidence for the Formation of Short Life Time Intermediate Liquid Species. *J. Anal. Appl. Pyrolysis* **1998**, *47* (1), 13–31.

(100) Lédé, J.; Blanchard, F.; Boutin, O. Radiant Flash Pyrolysis of Cellulose Pellets: Products and Mechanisms Involved in Transient and Steady State Conditions. *Fuel* **2002**, *81* (10), 1269–1279.

(101) Boutin, O.; Ferrer, M.; Lédé, J. Flash Pyrolysis of Cellulose Pellets Submitted to a Concentrated Radiation: Experiments and Modelling. *Chem. Eng. Sci.* **2002**, *57*, 15–25.

(102) Lindstrom, J. K.; Peterson, C. A.; Johnston, P. A.; Gable, P.; Brown, R. C. Cellulose Solid Phase Thermal Depolymerization. *In prep.*

(103) Proano-Aviles, J.; Lindstrom, J. K.; Johnston, P. A.; Brown, R. C. Heat and Mass Transfer Effects in a Furnace-Based Micropyrolyzer. *Energy Technol.* **2017**, *5* (1), 189–195.

(104) Ghosh, A.; Brown, R. C.; Bai, X. Production of Solubilized Carbohydrate from Cellulose Using Non-Catalytic, Supercritical Depolymerization in Polar Aprotic Solvents. *Green Chem.* **2016**, *18* (4), 1023–1031.

(105) Ghosh, A.; Bai, X.; Brown, R. C. Solubilized Carbohydrate Production by Acid-Catalyzed Depolymerization of Cellulose in Polar Aprotic Solvents. *ChemistrySelect* **2018**, *3* (17), 4777–4785.

(106) Piskorz, J.; Majerski, P.; Radlein, D.; Vladars-Usas, A.; Scott, D. S. Flash Pyrolysis of Cellulose for Production of Anhydro-Oligomers. *J. Anal. Appl. Pyrolysis* **2000**, *56* (2), 145–166.

(107) Thompson, L. C.; Ciesielski, P. N.; Jarvis, M. W.; Mukarakate, C.; Nimlos, M. R.; Donohoe, B. S. Estimating the Temperature Experienced by Biomass Particles during Fast Pyrolysis Using Microscopic Analysis of Biochars. *Energy & Fuels* **2017**, *31* (8), 8193–8201.

(108) Gable, P.; Brown, R. C. Effect of Biomass Heating Time on Bio-Oil Yields in a Free Fall Fast Pyrolysis Reactor. *Fuel* **2016**, *166*, 361–366.

CHAPTER 6 SUMMARY AND PROPOSED FUTURE WORK

Summary

This dissertation serves as the most detailed investigation of the condensed phase reactions during biomass thermal deconstruction to date. The initial goal was to explore improving sugar yields from biomass fast pyrolysis. This problem was approached by trying to understand how biomass and its main sugar component, cellulose, thermally deconstruct. All laboratory research efforts described here were performed with respect to this problem. This dissertation is not the first publication to examine condensed phase reactions, although it does so in the most detail to date. Each chapter is briefly outlined subsequently.

Chapter 1

This chapter summarizes the thermochemical processes, similarities they share, and condensed phase reactions that occur. The chapter serves as a thorough examination of the specific reactions and overarching themes of thermochemical processing of biomass. In particular similarities between thermochemical processing methodologies are presented. The main differences between these techniques are reaction temperature and equivalence ratio; however, condensed phase reactions are only affected by temperature.

Chapter 2

Starting the laboratory research, this chapter presents the first experimental examination of cellulose fast pyrolysis with time-resolved analysis of the volatile and condensed phases. The results demonstrate that cellulose cracks rapidly into anhydro-oligosaccharides which continue to crack into progressively smaller versions. From these anhydro-oligosaccharides, levoglucosan and light oxygenates drive inexorably toward particular certain product yields based on their relative reaction rates, limiting potential

sugar yield improvement. There are several important results that challenge, at the time, accepted literature.

Pyrolytic depolymerization always begins with rapid cracking reactions, regardless of pyrolysis temperature, that reduce the degree of polymerization (DP) of cellulose. This contradicts a prior theory that cracking reactions only occur above 467 °C.

The partially depolymerized cellulose (specifically, anhydro-oligosaccharides) are much larger than previously thought. We can detect anhydro-oligosaccharides up to approximately DP 60—over triple the highest previously reported DP. More importantly, we have discovered that even larger anhydro-oligosaccharides exist but are insoluble in water, the solvent used in most common analytical methodologies to measure oligosaccharides.

The intermediate products of cellulose fast pyrolysis only include anhydro-oligosaccharides and the anhydro-monosaccharide levoglucosan. Importantly, glucose was not among the depolymerization products, which calls in doubt previous studies that suggest its production and subsequent decomposition explain the experimentally observed limits to levoglucosan production during pyrolysis.

Levoglucosan and less desirable products form concurrently throughout pyrolysis from the progressively depolymerizing anhydro-oligosaccharides. The concurrent, unavoidable competition between producing levoglucosan and less desirable chemicals from anhydro-oligosaccharides precludes improving levoglucosan yields beyond approximately 60 wt%.

Chapter 3

This research delves into the large, water-insoluble anhydro-oligosaccharides detected in chapter two. Cellulose underwent brief and incomplete thermal deconstruction in a free fall reactor and the product were quenched as soon as they exited the reactor. This process probes the earliest stages of cellulose thermal deconstruction, so the reactions investigated all occur in the solid phase. This work led to three main conclusions:

Anhydro-oligosaccharides, nearly as large as the initial cellulose polymer, are formed by rapid cracking reactions. These anhydro-oligosaccharides are 20 times larger than we could detect in our previous paper and 70 times larger than the next highest reported DP.

Cellulose decrystallization appears independent from depolymerization reactions.

Given the similar kinetic rates of mid- and end-chain depolymerization reactions, DP controls depolymerization much more than minor differences in kinetic rates.

Chapter 4

Instead of focusing on one biopolymer, chapter four examines red oak thermal deconstruction. The same brief and incomplete thermal deconstruction from chapter three was applied to red oak. This method created partially deconstructed biomass for further examination. With this starting point, this study is the first to focus solely on *in situ* condensed phase intermediate products during rapid, high temperature thermal deconstruction. As a corollary, all analyses performed on the thermally deconstructed biomass were the first of their kind. They are detailed subsequently.

All biopolymers within biomass are affected, but to different extents. Lignin and hemicellulose both greatly degrade, but cellulose presents slight resistance. This variation led to cellulose being momentarily enriched within the biomass.

Lignin depolymerization follows computational chemistry-derived bond dissociation energies and bond type natural abundance.

Electron microscopy corroborates preferential lignin and hemicellulose removal compared to cellulose. Atomic force validates hemicellulose removal and quantifies increasing secondary cell wall hardness. Both analyses demonstrate that chemical transformations lead to structural and mechanical changes.

Chapter 5

Switching from research to perspective, chapter five details omissions and oversights in how biomass thermal deconstruction is analyzed. In particular, the perils of excessive reliance on model compounds, and general lack of time resolution and condensed phase analysis are detailed. Furthermore, it showcases examples of these lapses can affect pyrolysis models and theory negatively. The most important two conclusions are presented:

Models almost certainly lack predictive power that is sufficient to improve a process if they cannot accurately describe the condensed phase reactions and product evolution over time. Experimental studies are required to provide this information to modelers.

Understanding how these fundamental condensed phase reactions occur can lead to opportunities to exploit them. The best example is the effect of alkali and alkaline earth metals (AAEM). Only by understanding how these metals influenced the condensed

phase reactions were researchers able to develop methods to prevent them from undesirably degrading sugar monomers.

Proposed Future Work

The analysis of the condensed phase products and reactions within biomass thermal deconstruction in this dissertation is extensive but not exhaustive. Many offshoots of this work are possible; for example, a similar version of chapter two or three could be performed on hemicelluloses or extracted lignin. Chapter four could be repeated using different biomass species or after various pretreatments. Despite this assortment of possibilities, I believe the main takeaway from this section should not be the proposed "what" but the "how." This field lacks many studies focusing on either condensed phase reactions, time-resolution, or most often both. Given the challenges, this omission is understandable; however, this dissertation hopefully serves as an example for how to study them and what the field has to gain through their analysis (as discussed in chapter five.) Instead of suggesting specific experiments, I urge researchers to find knowledge gaps and then ways to eliminate them.

APPENDIX A SUPPLEMENTAL MATERIAL FOR CHAPTER 3

Cellulose dissolution procedure

We wrote and used the following procedures, based on McCormick,[1] to dissolve cellulose, thermally deconstructed cellulose, and Pullulan polysaccharide standards. Despite the heating in this dissolution method, no degradation was detected, as expected based on Dawsey and McCormick.[2] Additionally, if degradation had occurred, it would have been clearly detectable with size-exclusion chromatography. Solvent exchange procedures make dissolution easier,[2] but were not used due to low quantities of the polysaccharide standards.

Solvent preparation

Fill a 500 mL volumetric flask with high performance liquid chromatography (HPLC) grade dimethylacetamide (DMAc). Weigh 2.34 g of 99% lithium chloride (LiCl) for the mobile phase solution or 37.48 g of LiCl for the dissolving solution into a 500 mL glass media bottle. Add a stir bar and then the DMAc to the bottle. Close the bottle securely, as moisture will inhibit dissolution. Stir overnight or until dissolved. Keep closed and refrigerated when not in use.

Dissolution

Suspend 30 mg of cellulose in 2.00 mL of DMAc containing 8% lithium chloride in a sealable container that can withstand moderate pressure (such as a Grace Davison Discovery Science Maxi-Vial with a phenolic/vinyl cap and polytetrafluoroethylene septum.) Heat the containers in an oil bath from room temperature to 150 °C over 60-90 minutes with stirring, and then maintain at 140-150 °C for 10-20 minutes. Turn off heat and let it cool to room temperature slowly while stirring. The polysaccharides should be

dissolved. If the polysaccharides have not dissolved, try holding the system at 140-150 °C for a longer time or sparging with dry nitrogen prior to dissolution.[2]

References

(1) McCormick, C. L. Novel Cellulose Solutions. 4,278,790, 1981.

(2) Dawsey, T. R.; McCormick, C. L. The Lithium Chloride/Dimethylacetamide Solvent for Cellulose: A Literature Review. *J. Macromol. Sci. Part C* **1990**, *30* (3–4), 405–440.

APPENDIX B SUPPLEMENTAL MATERIAL FOR CHAPTER 4

Modeling free fall reactor particle temperatures and residence times

The free fall successfully isolated reaction temperature as the only independent variable for our truncated thermal deconstruction process (Figure A.1). Our modeling predicted the red oak particles does not reach the wall temperatures, but the different final particle temperatures vary significantly between the free fall experiments. Importantly, the particle residence times do not significantly change among different free fall temperatures.

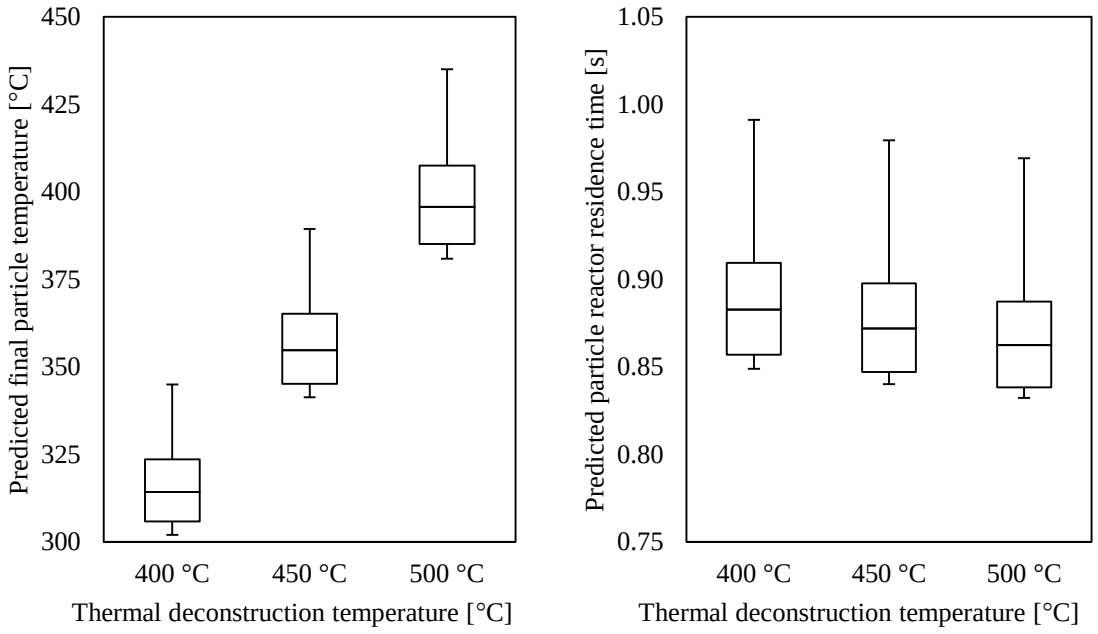

Figure A.1. The model of the free fall reactor predicts final particle temperatures will be significantly different for each reactor temperature. The final temperature is unlikely to equal the reactor temperature, which is less important than the temperature stratification. The model of the free fall reactor predicts essentially the same particle residence time for each reactor temperature.

These simulations demonstrate that the free fall reactor with product quenching serves as an excellent test reactor. The free fall produces partially deconstructed biomass

that allows for examining how temperature influences biomass deconstruction without interference from other variables.

Nanoindentation

For the native and thermally deconstructed red oak, a larger, representative particle was chosen. A longitudinal plane of the particle was bonded to a 12 mm steel AFM puck using five-minute epoxy with care taken to ensure the epoxy did not get near the cells used for nanoindentation. Surfaces were prepared in the longitudinal plane of unembedded wood following previously established procedures.[1–3] In brief, a hand razor was used to carefully trim a pyramid with an apex in the region of interest about 100-200 microns from the original particle surface. Then the specimens were fitted into a Leica EM UC7 ultramicrotome (Wetzlar, Germany) equipped with a diamond knife. Surfaces were prepared by removing 200 nm thick sections from the apex until an appropriately sized surface was prepared, typically about 100 microns on a side.

A Bruker-Hysitron (Minneapolis, Minnesota, USA) TriboIndenter® equipped with a Berkovich probe was used. The machine compliance, probe area function, and tip roundness effects were determined from a series of 80 nanoindents in a fused silica standard using the load function and the procedures in Jakes[4] and Stone et al. [5] Following the calibration reporting procedure prescribed in Jakes:[4] values for the square root of the Joslin-Oliver parameter of 1.199 ± 0.002 $\mu m/N^{1/2}$, elastic modulus of 72.0 ± 0.3 GPa, and Meyer's hardness of 8.9 ± 0.1 GPa (uncertainties are standard errors) were assessed for fused silica calibration nanoindentations. Using contact depths between 57 and 200 nm, no systematic variations of machine compliance or Joslin-Oliver parameter were observed in the systematic SYS plot analysis over this range of contact depths.

The inside of the nanoindentation enclosure was maintained at 50% relative humidity using an InstruQuest (Coconut Creek, Florida, USA) HumiSys^{TM} HF RH generator. Prepared specimens were placed inside of the nanoindenter enclosure at least 60 hours before experiment commencement and the humidity was maintained during the experiments. Nanoindentations were placed inside of a secondary cell wall between a compound middle lamella and exposed lumen. In each specimen, five to eight nanoindentations were performed in three different cell walls. From scanning probe microscopy images of residual nanoindentations, any nanoindentation that was not completely contained within the secondary cell wall was excluded from analysis. The multiload load function described by Youssefian[6] was used in this study. The maximum load for all specimens was 0.2 to 0.35 mN. The structural compliance method[1,7] was employed to remove artifacts caused by edge effects and specimen-scale flexing at each nanoindentation location. Unloading segments with contact depths less than 57 nm, which were those found to be affected by tip roundness effects in the fused silica calibrations, were excluded from the structural compliance analysis. After correcting the data for structural compliance, the Meyer hardness (H) was calculated using

$$H = \frac{P_0}{A_0} \tag{1}$$

where P_0 and A_0 are, respectively, the maximum load and contact area calculated using the probe area function immediately prior to each unloading segment. The effective modulus (E_{eff}) of contact was calculated using

$$E_{\text{eff}} = \frac{S}{A_0^{1/2}} \tag{2}$$

where S is the contact stiffness calculated by fitting the Oliver–Pharr[8] power law function to 40-95% of the maximum load of each unloading segment. We accounted for

the diamond probe contributions to E_{eff} and assessed the nanoindentation elastic modulus E_s^{NI} using

$$\frac{1}{E_{\mathrm{eff}}} = \frac{1}{\beta}\frac{\pi^{1/2}}{2}\left(\frac{1-\upsilon_{\mathrm{s}}^2}{E_{\mathrm{s}}} + \frac{1-\upsilon_{\mathrm{d}}^2}{E_{\mathrm{d}}}\right) \quad (3)$$

where E_d is the Young's modulus of diamond (1137 GPa), v_d is the Poisson's ratio of diamond (0.07), and v_s is the Poisson's ratio assumed for the S2 cell wall layer (0.45).[9] The numerical factor β was assumed to be 1. The material isotropy assumption implicit in Equation 3 is violated in secondary cell wall nanoindents because the cellulose microfibrils cause orientation effects.[10] We include the "NI" superscript to indicate that the elastic modulus assessed here is not the Young's modulus typically calculated with Equation 3. The H and E_s^{NI} were calculated for each unloading segment in the multiload nanoindentations. Results from unloading segments affecting by tip roundness effects (contact depths less than 57 nm) were excluded. After excluding data affected by tip roundness, no data exhibited any systematic size dependence; therefore, for each specimen, all results from the remaining unloading slopes were averaged and used to calculate standard error.

A Quesant (Agoura Hills, California, USA) atomic force microscope (AFM) incorporated in a TriboIndenter was used for high resolution imaging of residual nanoindentation impressions. The AFM was operated in contact mode and calibrated in the lateral directions using an Advanced Surface Microscopy (Indianapolis, Indiana, USA) calibration standard as described previously.[1]

References

(1) Jakes, J. E.; Frihart, C. R.; Beecher, J. F.; Moon, R. J.; Stone, D. S. Experimental Method to Account for Structural Compliance in Nanoindentation Measurements. *J. Mater. Res.* **2008**, *23* (4), 1113–1127.

(2) Jakes, J. E.; Yelle, D. J.; Beecher, J. F.; Frihart, C. R.; Stone, D. S. Characterizing Polymeric Methylene Diphenyl Diisocyanate Reactions with Wood: 2 . Nanoindentation. In *International Conference on Wood Adhesives*; Frihart, C. R., Hunt, C. G., Moon, R. J., Eds.; Forest Products Society: Lake Tahoe, Nevada, USA, 2009; pp 366–374.

(3) Jakes, J. E.; Hunt, C. G.; Yelle, D. J.; Lorenz, L.; Hirth, K.; Gleber, S.-C.; Vogt, S.; Grigsby, W.; Frihart, C. R. Synchrotron-Based X-Ray Fluorescence Microscopy in Conjunction with Nanoindentation to Study Molecular-Scale Interactions of Phenol–Formaldehyde in Wood Cell Walls. *ACS Appl. Mater. Interfaces* **2015**, *7* (12), 6584–6589.

(4) Jakes, J. E. Improved Methods for Nanoindentation Berkovich Probe Calibrations Using Fused Silica. *J. Mater. Sci.* **2018**, *53* (7), 4814–4827.

(5) Stone, D. S.; Yoder, K. B.; Sproul, W. D. Hardness and Elastic Modulus of TiN Based on Continuous Indentation Technique and New Correlation. *J. Vac. Sci. Technol. A Vacuum, Surfaces, Film.* **1991**, *9* (4), 2543–2547.

(6) Youssefian, S.; Jakes, J. E.; Rahbar, N. Variation of Nanostructures, Molecular Interactions, and Anisotropic Elastic Moduli of Lignocellulosic Cell Walls with Moisture. *Sci. Rep.* **2017**, *7* (1), 2054.

(7) Jakes, J. E.; Frihart, C. R.; Beecher, J. F.; Moon, R. J.; Resto, P. J.; Melgarejo, Z. H.; Suárez, O. M.; Baumgart, H.; Elmustafa, A. A.; Stone, D. S. Nanoindentation near the Edge. *J. Mater. Res.* **2009**, *24* (3), 1016–1031.

(8) Oliver, W. C.; Pharr, G. M. An Improved Technique for Determining Hardness and Elastic Modulus Using Load and Displacement Sensing Indentation Experiments. *J. Mater. Res.* **1992**, *7* (6), 1564–1583.

(9) Wimmer, R.; Lucas, B. N.; Oliver, W. C.; Tsui, T. Y. Longitudinal Hardness and Young's Modulus of Spruce Tracheid Secondary Walls Using Nanoindentation Technique. *Wood Sci. Technol.* **1997**, *31* (2), 131–141.

(10) Jäger, A.; Bader, T.; Hofstetter, K.; Eberhardsteiner, J. The Relation between Indentation Modulus, Microfibril Angle, and Elastic Properties of Wood Cell Walls. *Compos. Part A Appl. Sci. Manuf.* **2011**, *42* (6), 677–685.